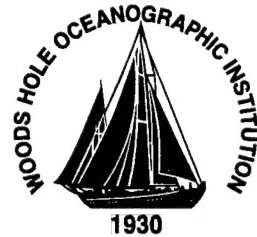# Massachusetts Institute of Technology
Woods Hole Oceanographic Institution

Joint Program
in Oceanography/
Applied Ocean Science
and Engineering

1930

DOCTORAL DISSERTATION

*Mechanisms and Variability of Salt Transport in
Partially-Stratified Estuaries*

by

Melissa Marie Bowen

February 2000

20000802 107

MIT/WHOI

00-04

Mechanisms and Variability of Salt Transport in Partially-Stratified Estuaries

by

Melissa Marie Bowen

Massachusetts Institute of Technology
Cambridge, Massachusetts 02139

and

Woods Hole Oceanographic Institution
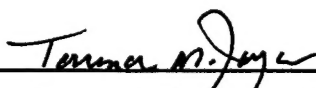Woods Hole, Massachusetts 02543

February 2000
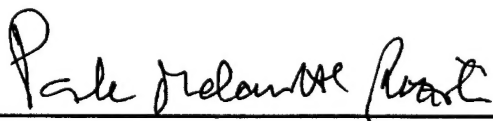
DOCTORAL DISSERTATION

Approved for publication; distribution unlimited.

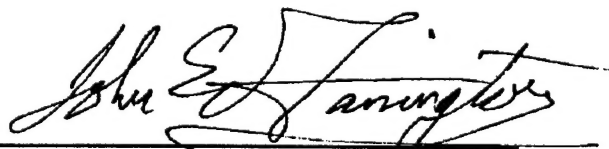**Approved for Distribution:**

_____
Terrence M. Joyce, Chair
Department of Physical Oceanography

_____
Paola Malanotte-Rizzoli
MIT Director of Joint Program

_____
John W. Farrington
WHOI Dean of Graduate Studies

Mechanisms and Variability of Salt Transport in Partially-Stratified Estuaries

by

Melissa Marie Bowen

B.S. Stanford University
(1991)
M.S. Stanford University
(1993)

Submitted in partial fulfillment of the
requirements for the degree of

DOCTOR OF PHILOSOPHY

at the

MASSACHUSETTS INSTITUTE OF TECHNOLOGY

and the

WOODS HOLE OCEANOGRAPHIC INSTITUTION

February 2000

© Melissa Marie Bowen

Signature of Author .... *Melissa M. Bowen* ....

Joint Program in Physical Oceanography
Massachusetts Institute of Technology
Woods Hole Oceanographic Institution
September 15, 1999

Certified by.............. *W. Rockwell Geyer* ....

W. Rockwell Geyer
Associate Scientist
Thesis Supervisor

Certified by.......... *Steven J. Lentz* ....

Steven J. Lentz
Associate Scientist
Thesis Supervisor

Accepted by .... *W. Brechner Owens* ....

W. Brechner Owens
Chairman, Joint Committee for Physical Oceanography
Massachusetts Institute of Technology
Woods Hole Oceanographic Institution

Mechanisms and Variability of Salt Transport in Partially-Stratified Estuaries

by

Melissa Marie Bowen

Submitted to the Woods Hole Oceanographic Institution / Massachusetts Institute of Technology Joint Program in Physical Oceanography in September, 1999 in partial fulfillment of the requirements for the degree of Doctor of Philosophy.

ABSTRACT

The variability of salt transport determines the variation of the length of the salinity intrusion and the large-scale density gradient in an estuary. This thesis contains three studies that address salt transport and the salt balance. The variation of salt transport with the depth, the along-channel salinity gradient, and the amplitude of the tidal velocity is investigated with analytic and numerical models. The results indicate that salt transport increases dramatically during stratified periods when vertical mixing is weak. Analysis of salt transport from observations in the Hudson Estuary show that stratified periods with elevated estuarine salt transport occur in five-day intervals once a month during apogean neap tides. Oscillatory salt transport, which is hypothesized to be primarily caused by lateral exchange and mixing of salt, appears to play a more minor role in the salt balance of the estuary. The salt balance of the estuary adjusts very little to the spring-neap modulation of salt transport but adjusts rapidly to pulses of freshwater flow. A simple model is used to investigate the process and time scales of adjustment of the salt balance by connecting variations of salt transport to the variations of freshwater flow and vertical mixing. The results show the length of the salinity intrusion adjust via advection to rapid and large increases in freshwater flow. The salinity intrusion adjusts more rapidly to the spring-neap cycle of tidal mixing the higher the freshwater flow.

Thesis Supervisor: W. Rockwell Geyer, Associate Scientist, WHOI

Acknowledgements

This thesis would never have been accomplished without the guidance and support of many people. First, thanks to my advisor, Rocky Geyer, for setting me off on a fruitful research topic and for sharing his ideas at every step. I am also very grateful to my thesis committee, Steve Lentz (a gracious co-advisor), John Trowbridge, Karl Helfrich, Heidi Nepf, and Carl Wunsch. Each of them provided mentorship and advice at critical moments. Ronni Schwartz at MIT and the WHOI Education Office provided a warm and human side to my experience here.

Second, the numerous conversations with other students, scientific or otherwise, have been my greatest education over the last six years. Thanks to Bill Williams, Lyn Harris, François Primeau, and Brian Racine for all the great conversions. And thanks to the Woods Hole Gang–Jay Austin, Jamie Pringle, Miles Sundermeyer, and Derek Fong–for your friendship, enthusiasm, and encouragement over the years. Not to mention great cooking! A special thank you to all the members of my own "class": Michael Chechelnitsky, Dan Goldner, Steve Jayne, Misha Soloviev, Richard Wardle, Sandra Werner, and Jubao Zhang. The comradery during the first two years of classes and generals was wonderful. I am grateful to several students for opening doors in learning about other disciplines of oceanography: Örjan Gustafsson, Mak Saito, Liz Mann, and Liz Minor. And thanks to my officemates Steve Fries, Bill Shaw, and Jon Woodruff for sharing the daily student experience with extraordinary humor and optimism.

Family and friends have provided the most important source of everyday laughter and wisdom. My parents deserve honorary degrees in psychology after simultaneously counseling two daughters through doctorate programs. Nina Shapley has shared every step of the way. I've benefited from her wonderful sense of humor and boundless energy over thousands of cups of tea. Thanks also to other MIT friends I always look forward to seeing: Ginger, Hrund, Liz and Lana. And, of course, thanks to Ingo Pecher, who taught me to look forward, but not too far forward.

Table of Contents

Chapter 1

Introduction

Estuaries, in their most common form, are arms of the coastal ocean where fresh water and ocean water meet and mix. They are extremely productive regions due to the high flux of nutrients from the land and serve as breeding and nursery grounds for many species (Ketchum 1983; Neilson and Cronin 1981). Because many major cites are located next to estuaries, the impact of anthropogenic activity on the estuarine environment is a frequent concern (Kennish 1986; Dyer 1973). Assessing these impacts requires an understanding of the variability of circulation and stratification in the estuary.

The circulation and stratification of estuaries are a result of the interactions of the tides, the river outflow, the density difference between the river and the ocean, the coastal sea level fluctuations, the winds and the bathymetry (Dyer 1973; Fischer et al. 1979) (Figure 1.1). Generally, the tidal wave drives the strongest flows in an estuary (Fischer et al. 1979). These are often on the order of 1 m s^{-1} and are principally semidiurnal and diurnal and modulated at fortnightly and monthly periods. Flows driven by along-channel salinity gradients, winds, coastal sea level fluctuations, and rectification of tidal flows cover a wide range of frequencies and are typically on the order of 0.1 m s^{-1} (Wang and Elliott 1978; Fischer et al. 1979; Zimmerman 1978b; Jay and Musiak 1996). River discharge produces a seaward-directed flow that can vary from near zero to near 1 m s^{-1}, usually exhibiting a seasonal variation and shorter term fluctuations due to precipitation events. Mean circulation and circulation at frequencies lower than the semidiurnal and diurnal tides are often collectively called the residual circulation (Lewis and Lewis 1983; Jay and Musiak 1996) since they are the residual of a time average over the principal tidal periods. The vertical and lateral deviations of the residual circulation from the cross-sectional average are usually defined as the estuarine circulation (Fischer, 1976) (Figure 1.1).

The stratification in an estuary is a result of shears straining the along-channel

12
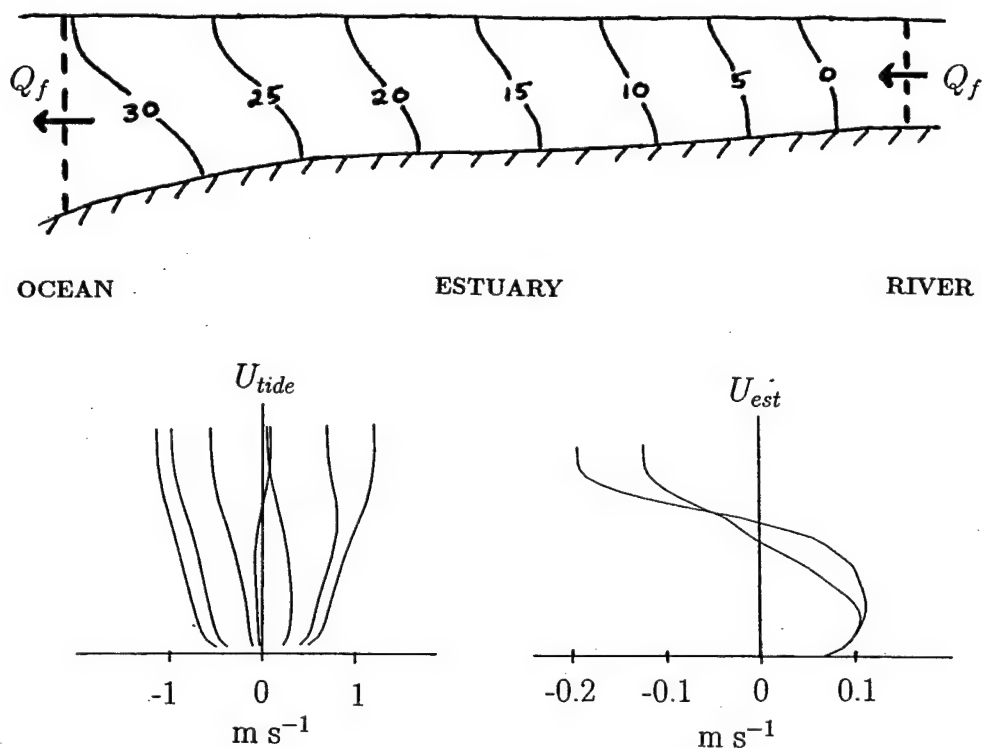
Figure 1.1: Schematic of an estuary. The tidal pressure gradient drives the oscillatory tidal flow, U_{tide}. At time scales longer than the semidiurnal and diurnal tides there is a residual circulation comprised of the net flow through a cross section, Q_f, and spatial deviations of the flow, U_{est}. The net flow through the estuary, Q_f, is equal to the river flow. The length of the salinity intrusion and the density difference between the ocean and the river provide a scale for the longitudinal density gradient.

salinity gradient and mixing from tides, winds, and waves (Simpson et al. 1990; Dyer 1973). In general, the residual shear and the ebb tidal shear both increase the vertical stratification; flood tidal shear and mixing decrease the stratification (Simpson et al. 1990; Nunes Vaz 1990). Vertical and lateral velocities, commonly referred to as secondary circulation, also modify the stratification (Nepf and Geyer 1996; Scott 1994; Nunes and Simpson 1985).

The velocity and salinity determine the salt transport. The net outflow continually removes salt from the estuary. Generally salt is brought back in by the "estuarine salt transport" (i.e. the vertical and lateral variations of tidally-averaged velocity and salinity) and "tidal dispersion" (i.e., the tidal correlations of velocity and salinity) (Fischer 1976). The magnitude of salt transport and the processes that produce it depend on the bathymetry of the estuary and on the strength of the physical forcing (e.g., tides, freshwater flow). In highly-stratified estuaries, salt transport is predominantly due to advection by the net flow and the estuarine salt transport (Knudsen 1900; Hansen and Rattray 1966). Conversely, in well-mixed estuaries, which are weakly stratified, tidal dispersion plays a larger role in the salt balance (Smith 1980). The stratification of partially-stratified (also known as partially-mixed) estuaries varies between these extremes (Haas 1977), and the mechanisms of salt transport should vary accordingly. The remainder of this chapter reviews previous work concerning salt transport in and the salt balance of partially-stratified estuaries.

1.1   Previous work

Much of the framework for describing salt transport and the salt balance of estuaries comes from the work of Hansen and Rattray (1965, 1966). Hansen and Rattray (1965) related the strength of the estuarine salt transport in an estuary to the

14

vertical mixing, along-channel salinity gradient, and depth, based on momentum and salt balances developed by Pritchard (1954, 1956). An imbalance between the estuarine salt transport and the salt transport out of the estuary by the net flow was attributed to tidal "diffusion", now interpreted as a collection of processes producing tidal dispersion (Fischer, 1972). Although their study provided a useful way of classifying estuaries (Hansen and Rattray 1966), their analysis did not consider the connection between vertical mixing and the forcing conditions nor the variations of vertical mixing within the tidal cycle. In addition, their study did not provide any insight into the processes of tidal dispersion.

Studies since Hansen and Rattray (1965) have shown that the modulation of vertical mixing due to tidal and spring-neap cycles is critical in determining the magnitude of residual circulation and stratification. Observations (Nunes and Lennon 1987; Geyer and Cannon 1982), laboratory experiments (Linden and Simpson 1988), and simple models (Simpson et al. 1990; Nunes Vaz et al. 1989) show that longitudinal mass exchange is elevated during neap tides when vertical mixing is suppressed. Numerical models with more sophisticated parameterizations of vertical mixing demonstrate that variations in vertical mixing within a tidal cycle also play a role in determining the magnitude of the residual circulation (Stacey 1996; Monismith et al. 1996; Nunes Vaz and Simpson 1994). In addition, observations indicate that the magnitude of the residual circulation in an estuary may in part be determined by the magnitude of tidal variations of mixing and shear (Jay and Musiak 1996; Geyer et al. 1999), rather than the magnitude of the baroclinic pressure gradient. These studies suggest that the variations of vertical mixing over the spring-neap cycle and within a tidal cycle must be included in order to understand the dependence of salt transport mechanisms on the forcing parameters.

Many studies have sought to quantify the magnitude of tidal dispersion produced by tidal flow and variations of bathymetry (Schijf and Schönfeld 1953; Okubo 1973;

Zimmerman 1978a; Geyer and Signell 1992; Smith 1980). Several authors have investigated the variation of oscillatory shear dispersion in simple geometries with constant eddy coefficients (Smith 1980; Young et al. 1982; Larsen 1977; Ou et al. 1999). Smith (1980) provided solutions for estuarine and oscillatory salt transport in a well-mixed estuary. The variation of both the estuarine and oscillatory salt transport in estuaries over the range of stratification in a partially-stratified estuary has not been investigated.

Advancing the understanding of salt transport through observational studies has proved difficult. Moored observations provide the long time series necessary to separate higher-frequency fluctuations from lower frequencies, but they do not resolve the cross-channel structure necessary to determine net salt transport (Fischer, 1972; Jay and Smith, 1990). Shipboard observations provide the spatial structure of the semidiurnal tidal velocity and salinity fields, but are rarely long enough to determine the lower frequency fields (Dronkers and van de Kreeke 1986; Oey et al. 1985; Jay et al. 1997). Difficulties in obtaining direct measurements of salt transport have led many authors to estimate the magnitude of landward salt flux by assuming it balances the salt transport due to the net flow through the estuary acting on the along-channel salinity distribution (Fischer et al. 1979; Posmentier and Raymont 1979; Uncles and Radford 1980; van de Kreeke 1990), an estimate that is erroneous when the salt balance is unsteady (Fischer et al. 1979; Uncles and Radford 1980).

The salt balance of an estuary is unsteady while adjusting to the spring-neap cycle and changing freshwater flow. Some authors have observed this adjustment process and made qualitative links between variations of forcing, salt transport, and the length of the salinity intrusion (Jay and Smith 1990; Uncles and Radford 1980; Lewis and Lewis 1983). Others have noted the high variability of tidal velocity, freshwater flow, and mouth salinity in real systems, and constructed numerical models of the salt balance in individual estuaries to simulate the temporal response

16

of the salinity intrusion (Godfrey 1980; Thatcher and Harlemann 1981; Park and Kuo 1996). Analytic approaches have also been used to predict the adjustment of the salt balance for more general bathymetries and variations of forcing (Kranenburg 1986; MacCready 1999). Comparisons with numerical model results suggest that the partially-stratified estuaries are highly sensitive to changes in forcing and poorly represented by analytic time scales (MacCready 1999).

1.2   Thesis outline

Several questions concerning the variability of salt transport in partially-stratified estuaries and the consequences for the salt balance remain unanswered. The variation of both estuarine and oscillatory salt transport over the range of stratification found in a partially-stratified estuary has not been investigated. The variation of each mechanism and its role in the salt balance has not been quantified with a long time series of observations. In addition the adjustment of the length of the salinity intrusion in a partially-stratified estuary to variations of the freshwater flow and spring-neap tidal amplitude has not been addressed.

This thesis addresses these issues. In Chapter 2, the role of vertical mixing in determining the variation and relative contributions of estuarine and oscillatory salt transport is examined. The mechanisms and variability of salt transport measurements at a section of the Hudson Estuary and the role of these mechanisms in the salt balance are discussed in Chapter 3. Examples of the adjustment of the salinity intrusion to variable freshwater flow and the spring-neap cycle using a simple model are presented in Chapter 4. The key results of the thesis are summarized in Chapter 5.

Chapter 2

The role of vertical mixing in longitudinal salt transport

2.1 Introduction

The magnitude and variability of salt transport along the channel of an estuary provide insights for predicting the dispersal of other substances and the extent of saline intrusion (Monismith et al. 1996; Wells and Young 1992). Salt transport is generally divided into a seaward advection of salt due to the net outflow and two mechanisms of landward salt transport, the estuarine salt transport (i.e., the vertical and lateral variations of tidally averaged, or "residual", velocity and salinity) and tidal dispersion (i.e., the tidal correlations of velocity and salinity) (Fischer 1976), also referred to as "oscillatory salt transport". Numerous studies have attempted to quantify the dependence of these salt transport mechanisms on the tidal flow, bathymetry, and along-channel salinity gradient.

Estuarine salt transport in stratified and partially-stratified estuaries is due primarily to vertical variations of shear and stratification (Knudsen 1900; Pritchard 1956; Hansen and Rattray 1965; Nunes Vaz et al. 1989) rather than transverse variations that dominate in less stratified systems (Fischer 1972; Wong 1994). Hansen and Rattray (1965) developed the first analytical description of estuarine salt transport due to vertical variations based on Pritchard's (1956) formulation of the main terms in the tidally-averaged momentum and salt balances. Hansen and Rattray (1965) assumed a steady salt balance, attributing the difference between the estuarine salt transport and the salt transport from the net, riverine outflow to tidal "diffusion", a collection of mechanisms producing tidal dispersion (Fischer 1976). The ratio of tidal dispersion to the total landward salt transport defined the "diffusive fraction", ν, indicating the character of salt transport in an estuary and forming the basis for their estuarine classification scheme (Hansen and Rattray 1966).

There are, however, two problematic assumptions in Hansen and Rattray's (1965) analysis. First, in order to find analytic solutions, the tidally-averaged turbulent

transfer of momentum and salt are parameterized with a constant eddy coefficient acting on the residual shear and stratification. Recent studies have observed considerable variation of vertical mixing in estuaries both over the course of the tidal cycle and with depth (Peters 1997; Stacey 1996). Second, Hansen and Rattray (1965) did not provide any insight into the physics of tidal dispersion. Studies since have suggested that oscillatory salt transport has its own variation with bathymetry, tidal velocity, mixing, and along-channel salinity gradient (Smith 1980; Okubo 1973; Zimmerman 1978).

Several studies have also considered the vertical shear and stratification, as did Hansen and Rattray (1965), but incorporated the variation of vertical mixing over the spring-neap cycle and within the tidal cycle (Nunes Vaz et al. 1989; Simpson et al. 1990; Nunes Vaz and Simpson 1994). Nunes Vaz et al. (1989) argued that long periods of weakened mixing during neap tides produced the most significant salt transport in estuaries. Several one-dimensional modeling studies have shown that the variation of vertical mixing within the tidal cycle leads to periodic pulses of circulation (Monismith et al. 1996) and stratification (Nunes Vaz et al. 1989; Simpson et al. 1990; Nunes Vaz and Simpson 1994).

Two observational studies have also suggested that the residual circulation in estuaries may be due in part to "tidal asymmetry", a mechanism in which the magnitude of residual shear is determined by the magnitude of tidal variations of vertical mixing and shear within the tidal cycle (Jay and Musiak 1996; Geyer et al. 1999) rather than by the magnitude of the baroclinic pressure gradient (Hansen and Rattray 1965). Jay and Musiak (1996) estimated that about half the residual shear in a set of observations from the Columbia Estuary was associated with tidal asymmetry, suggesting that this mechanism is as important as the baroclinic pressure gradient in creating residual flow. Geyer et al. (1999) provided another example of tidal asymmetry from estimates of residual stress and shear in the Hudson Estuary.

21

Although observations from these two estuaries suggest that tidal asymmetry is an important process in determining the residual shear, its influence on salt transport and its variability with tidal amplitude, along-channel salinity gradient, and depth have not been investigated.

A wide variety of processes produce tidal dispersion in estuaries (Stommel and Farmer 1952; Zimmerman 1978; Geyer and Signell 1992; Okubo 1973; Schijf and Schönfeld 1953; Smith 1980). In a uniform channel tidal dispersion is produced by oscillatory shear dispersion, a process in which tidal shear and mixing separate water parcels. Analytical solutions have been derived for the simplest cases of dispersion in an oscillatory shear flow using mixing coefficients that are constant in both time and space (Fischer et al. 1979; Young et al. 1982). Smith (1980) provided a complete analytical framework for determining the oscillatory salt transport in a well-mixed estuary. His solutions described the variations of both vertical and transverse oscillatory shear dispersion with tidal flow, along-channel salinity gradient, and cross-section shape. The solutions, however, are only applicable to the nearly unstratified water column found in well-mixed estuaries. The variation of both estuarine and oscillatory salt transport in the presence of stratification has not been investigated.

The spatial structure of oscillatory salt transport has often been ignored. Most studies have considered either the spatial average of oscillatory salt transport (Young et al. 1982; Smith 1980), or examined only part of the spatial structure (Scott 1994). Using analytic solutions of salt and momentum balances in a tidal boundary layer, Larsen (1977) found that although oscillatory flux was down-gradient in the depth average, counter-gradient transport was present near the bottom of the water column. Hunkins (1981) found counter-gradient oscillatory salt transport from measurements at one cross section in the Hudson Estuary, postulating that the sign might be due to the phase behavior of momentum and salt in a tidal boundary layer.

Recently, Ou et al. (1999) derived the depth variation of the magnitude and sign of temperature flux as a function of the vertical mixing from analytical expressions for temperature and momentum in a tidal boundary layer demonstrating that a regions of counter-gradient flux exist within the flow. They also used numerical simulations of a tidal mixing front to illustrate that similar vertical structures of temperature flux occurred with more realistic variations of vertical mixing.

Numerical models provide a tool for understanding the effects of spatially- and temporally-varying mixing on the estuarine and oscillatory salt transport. One-dimensional vertical numerical models have been used to examine the dominant processes in the momentum and salt balance in stratified estuaries (Monismith et al. 1996; Simpson et al. 1990; Nunes Vaz and Simpson 1994; Stacey 1996). A feature of the model results is the appearance of persistent, increasing, "runaway" stratification (Nunes Vaz et al. 1989), for certain combinations of the forcing conditions (Stacey 1996; Monismith et al. 1996). Comparisons of model results with observations suggest that runaway stratification is, to some degree, a natural phenomenon. One-dimensional model results compare well with the evolution of the stratification in shelf seas (Simpson and Sharples 1991). The onset and duration of stratification have also been predicted successfully in estuaries, provided the along-channel salinity gradient is varied according to observations (Sharples et al. 1994; Uncles et al. 1990).

Sharples et al. (1994) found that a one-dimensional model predicted the vertical extent of stratification in the water column but tended to overpredict stratification during neap tides and underpredict during spring tides. Recently, two studies comparing the Mellor-Yamada level 2.5 turbulence closure scheme (Mellor and Yamada 1982) with observations of turbulent quantities also suggest that this closure scheme underpredicts stratification during times of weak stratification and overpredicts during periods of strong stratification (Simpson et al. 1996; Stacey et al. 1999). Although the one-dimensional modeling studies show some discrepancies between

observed and modeled stratification, the models do predict the main features of stratification in an estuary.

This chapter characterizes the mechanisms of longitudinal salt transport due to tidal flow, an along-channel salinity gradient, and bottom boundary-generated mixing. First, a complete analytical description of salt transport is found by combining existing analytical solutions for estuarine salt transport (Hansen and Rattray 1965) and oscillatory salt transport (Young et al. 1982; Smith 1980). The effects of time- and depth-dependent vertical mixing on the variability and mechanisms of salt transport are described using a vertical, one-dimensional numerical model. Finally, modeled velocity and salinity are compared to observations from the Hudson Estuary to assess the quantitative ability of the one-dimensional model for predicting salt transport.

The governing equations for the momentum and salt balances are described in Section 2.2. In Section 2.3 the analytical expressions for estuarine and oscillatory salt transport are combined and the spatial dependence of oscillatory salt transport discussed. The numerical model description and results are discussed in Section 2.4. A model simulation is compared to observations from the Hudson Estuary in Section 2.5. The results of the chapter are discussed in Section 2.6 and summarized in Section 2.7.

2.2 Governing equations

2.2.1 Momentum balance

A simple description of the momentum balance in an estuary, used in a number of studies (Larsen 1977; Sharples et al. 1994; Uncles et al. 1990; Nunes Vaz and Simpson 1994), contains the interaction of a tidal flow, an along-channel salinity

24

gradient, and vertical mixing,

$$\frac{\partial u}{\partial t} = -\frac{1}{\rho_0}\frac{\partial p}{\partial x} + \frac{\partial}{\partial z}\left(k_m\frac{\partial u}{\partial z}\right),\qquad(2.1)$$

where the shear stress is parameterized by an eddy viscosity, k_m, acting on the shear. The x direction is along the channel of the estuary, positive towards the river. The flow along the channel direction is u. The vertical coordinate is defined so that $z = 0$ at the bottom and $z = h$ at the surface and h does not vary in time.

Averaged over a tidal cycle, the simple momentum balance (Equation 2.1) also contains the terms customarily used to describe the tidally-averaged momentum balance in estuaries (Pritchard 1956; Hansen and Rattray 1965; Chatwin 1976).

The advective and rotation terms in the momentum balance have been ignored. Contributions from the advective terms only become dominant in the balance in estuaries of complex bathymetry (Zimmerman 1978) and in regions of significant local changes in bathymetry (Ianniello 1979). The influence of rotation on the balance is considered where the internal radius of deformation is less than or comparable to the transverse scales (Nunes Vaz and Simpson 1994), a condition not usually found in most estuaries.

The pressure gradient in the momentum balance consists of the along-channel salinity gradient $\left(\frac{\partial S}{\partial x}\right)$ and the sea surface slope $\left(\frac{\partial \eta}{\partial x}\right)$,

$$-\frac{1}{\rho_0}\frac{\partial p}{\partial x} = -g\beta\int_z^h \frac{\partial S}{\partial x}dz - g\frac{\partial \eta'}{\partial x} - g\frac{\partial \overline{\eta}}{\partial x},\qquad(2.2)$$

where β is the coefficient of saline expansion, an overbar is used to denote an average over a semidiurnal tidal cycle,

$$\overline{(\,)} = \frac{1}{\tau_{tide}}\int_t^{t+\tau_{tide}} (\,)\,d\tau,\qquad(2.3)$$

and deviations from the tidal average are denoted by a prime,

$$() ' = () - \overline{()}. \tag{2.4}$$

The sea surface slope is divided into a tidal pressure gradient, $g\frac{\partial \eta'}{\partial x}$, and a tidally-averaged pressure gradient, $g\frac{\partial \overline{\eta}}{\partial x}$, that determines the tidally-averaged transport. The magnitude of $g\frac{\partial \overline{\eta}}{\partial x}$ is usually governed by the baroclinic gradient (Hansen and Rattray 1965).

Boundary conditions on the momentum flux must be specified at the surface and bottom of the water column. For the analytical solutions and most of the numerical model runs there is no stress at the surface as the effects of winds are not the focus of this study. In the numerical model runs, the stress at the bottom is specified using a quadratic drag law (discussed further in the model description section). In the analytical solutions the velocity is set to zero at the bottom, which makes the problem simpler than a stress condition without significantly altering the character of the solution (Officer 1976).

2.2.2   Salt balance

The one-dimensional balance for salt contains the time rate of change of salinity, due to the advection of salt acting on the along-channel salinity gradient, and the divergence of vertical salt flux,

$$\frac{\partial S}{\partial t} = -u\frac{\partial S}{\partial x} + \frac{\partial}{\partial z}\left(k_h\frac{\partial S}{\partial z}\right), \tag{2.5}$$

where vertical salt flux is parameterized by an eddy diffusivity, k_h, acting on the stratification (Larsen 1977; Sharples et al. 1994; Uncles et al. 1990; Nunes Vaz and Simpson 1994).

Salt cannot move through either the surface or bottom of the water column, so stratification must vanish at the boundaries. An evaporative flux would cause an effective salt transport at the surface, but this flux is generally small for mid-latitude estuaries and is not considered here.

The along-channel salinity gradient can be treated as a constant with depth and time and still produce the main characteristics of the estuarine salt and momentum balances (Chatwin 1976). Therefore, the salinity can be divided into a part that varies only with distance along the channel and a part that varies with depth and time,

$$S(x, z, t) = S_1(x) + S_2(z, t) \tag{2.6}$$

Note that $\frac{\partial S}{\partial x} = \frac{dS_1}{dx} = $ constant. The along-channel salinity gradient is assumed to be constant over an along-channel distance of at least a tidal excursion. The along-channel salinity gradient will be written as $\frac{d[\bar{S}]}{dx}$, where the square brackets will be used throughout the chapter to indicate an average over depth,

$$[\,(\,)\,] = \frac{1}{h} \int_0^h (\,) \, d\zeta. \tag{2.7}$$

Deviations from the depth average will be indicated by a tilde,

$$\tilde{(\,)} = (\,) - [\,(\,)\,]. \tag{2.8}$$

2.3 Salt transport with constant eddy coefficients

2.3.1 Estuarine salt transport

The derivation of an analytical expression for estuarine salt transport (also known as salt transport due to the "density driven" or "gravitational" circulation) follows Hansen and Rattray (1965). A shortened version is included here to show the assumptions that underlie the expression for salt transport and the model in Chapter 4.

First, an expression for the residual velocity is found by taking the tidal average of the momentum balance (Equation 2.1). The acceleration of the residual flow is assumed to be small compared to the other terms. The tidally-averaged stress is parameterized by a time- and depth-independent eddy viscosity, k_{m0}, acting on the tidally-averaged shear.

$$0 = -\frac{1}{\rho_0}\frac{\partial \bar{p}}{\partial x} + \frac{\partial}{\partial z}\left(k_{m0}\frac{\partial \bar{u}}{\partial z}\right) \tag{2.9}$$

The pressure gradient consists of the along-channel salinity gradient and the tidally-averaged sea surface slope.

$$-\frac{1}{\rho_0}\frac{\partial \bar{p}}{\partial x} = -g\beta\int_z^h \frac{d[\bar{S}]}{dx}d\zeta - g\frac{\partial \bar{\eta}}{\partial x} \tag{2.10}$$

The residual circulation can be found by integrating Equation 2.9 twice with depth and applying boundary conditions of no flow at the bottom and no stress at the surface. The tidally-averaged sea surface slope is specified by requiring the depth-averaged residual flow equal to the river flow, u_f. Applying these constraints yields Hansen and Rattray's (1965) expression for velocity.

$$\bar{u} = -\beta g \frac{d[\bar{S}]}{dx} \frac{h^3}{k_{m0}} \left(\frac{1}{6} \left(\frac{z}{h} \right)^3 - \frac{5}{16} \left(\frac{z}{h} \right)^2 + \frac{1}{8} \frac{z}{h} \right) + u_f \left(-\frac{3}{2} \left(\frac{z}{h} \right)^2 + 3 \frac{z}{h} \right) \quad (2.11)$$

The tidally-averaged salt balance can be written in the same manner as the tidally-averaged momentum balance using a depth- and time-independent eddy diffusivity, k_{h0}, acting on the tidally-averaged stratification to provide the vertical salt flux.

$$0 = -\bar{u} \frac{d[\bar{S}]}{dx} + \frac{\partial}{\partial z} \left(k_{h0} \frac{\partial \bar{S}}{\partial z} \right) \quad (2.12)$$

Ignoring the net outflow, which is usually small compared to the magnitude of the estuarine circulation, Equation 2.11 can be substituted into Equation 2.12 and the salinity found by integrating Equation 2.12 twice with depth, imposing the boundary conditions of no flux of salt at the surface and bottom.

$$\bar{S} = -g\beta \left(\frac{d[\bar{S}]}{dx} \right)^2 \frac{h^5}{24 k_{m0} k_{h0}} \left(\frac{1}{5} \left(\frac{z}{h} \right)^5 - \frac{5}{8} \left(\frac{z}{h} \right)^4 + \frac{1}{2} \left(\frac{z}{h} \right)^3 - \frac{1}{30} \right) + [\bar{S}](x) \quad (2.13)$$

The estuarine salt transport is the product of the depth-dependent residual velocity and salinity. After multiplying the depth-dependent parts of Equations 2.11 and 2.13 and averaging over depth, the estuarine salt transport is

$$[\tilde{\tilde{u}} \tilde{\bar{S}}] = -C_0 \beta^2 g^2 \left(\frac{d[\bar{S}]}{dx} \right)^3 \frac{h^8}{k_{m0}^2 k_{h0}}, \quad (2.14)$$

where $C_0 = \frac{19}{1451520} \simeq 1.3 \times 10^{-5}$.

The estuarine salt transport (Equation 2.14) can be recognized as an extension of Taylor's (1954) solution for steady shear dispersion. For flow along a pipe, with shear

29

and turbulent mixing across the pipe, Taylor (1954) found the steady state along-pipe dispersion of a substance was proportional to the along-pipe concentration gradient and inversely proportional to the across-pipe diffusivity. In the estuarine example, the shear flow is itself dependent on the along-channel salinity gradient and the vertical eddy viscosity. This adds another two factors of the salinity gradient and eddy coefficient to the classical shear dispersion solution for along-channel mass transport and longitudinal dispersion coefficient.

2.3.2   Oscillatory salt transport

Oscillatory salt transport due to oscillatory shear dispersion occurs in the following manner. As shear in the along-channel flow separates fluid parcels, mixing perpendicular to the shear redistributes them. When the shear reverses, the fluid parcels are not brought back to their original positions. As a result of experiencing different along-channel velocities, the distribution of parcels has dispersed along the channel and the variance has grown.

In the following section, oscillatory salt transport is derived in two dimensions assuming a given along-channel tidal flow (u') with vertical shear $(\frac{\partial u'}{\partial z})$, a vertical diffusivity (k_{h0}) and an along-channel salinity gradient $(\frac{d[\bar{S}]}{dx})$ that are independent of time and depth. These assumptions are consistent with the analytical solution for the estuarine salt transport in the previous section. A similar derivation for the spatial average of oscillatory salt transport can be found in Young et al. (1982). Derivations for the case of a tidal boundary layer can be found in Larsen (1977) and Ou et al. (1999). The solution here provides the general spatial-dependence of oscillatory salt transport.

The solution derived in this section can also be applied to transverse oscillatory shear dispersion, the along-channel dispersion due to transverse shear and the trans-

verse mixing of salt, by choosing a transverse field of shear and an across channel mixing coefficient, k_{trans}. The transverse form of the solution is used in the next chapter.

The tidally-varying salt balance is

$$\frac{\partial S'}{\partial t} - k_{h0}\frac{\partial^2 S'}{\partial z^2} = -u'(z,t)\frac{d[\bar{S}]}{dx}. \qquad (2.15)$$

The along-channel velocity, acting on the along-channel salinity gradient, forces fluctuations in the salinity while the mixing constantly erases vertical gradients. The unforced salt balance can be solved, with the condition of no salt flux through the bottom, $z = 0$, or the surface, $z = h$, of the water column, to yield the homogeneous solution, which consists of a series of decaying exponentials in time and sinusoidal vertical spatial modes,

$$S'_{homog} = \sum_{n=0}^{\infty} A_n e^{-\lambda_n k_{h0}t} cos(n\pi\frac{z}{h}), \qquad (2.16)$$

where $\lambda_n = \frac{n^2\pi^2}{h^2}$ is the square of the vertical spatial wave number.

The forced solution can now be solved by first dividing the velocity profile into the sum of a cosine and a sine at the principle tidal frequency, each with vertical structure (the flow is oscillatory so the sign is arbitrary and has been chosen to be negative to cancel out the negative sign in Equation 2.15),

$$u'(z,t) = -(U_c(z)cos\omega t + U_s(z)sin\omega t). \qquad (2.17)$$

The solution for the salinity is a sum of spatial wave numbers each multiplied by a time-dependent coefficient, $b_n(t)$,

$$S' = \sum_{n=0}^{\infty} b_n(t)cos(n\pi\frac{z}{h}). \tag{2.18}$$

Substituting Equation 2.17 and 2.18 into the salt balance (Equation 2.15) yields the following balance for each vertical wave number,

$$\frac{db_n}{dt} + \lambda_n k_{h0} b_n = (U_{cn}cos\omega t + U_{sn}sin\omega t)\frac{d[\bar{S}]}{dx}, \tag{2.19}$$

where U_{cn} and U_{sn} are the projections of the along-channel velocity on to the vertical modes.

$$U_{cn} = \frac{\int_0^h U_c cos(n\pi\frac{z}{h})dz}{\int_0^h cos^2(n\pi\frac{z}{h})dz} \tag{2.20}$$

$$U_{sn} = \frac{\int_0^h U_s cos(n\pi\frac{z}{h})dz}{\int_0^h cos^2(n\pi\frac{z}{h})dz} \tag{2.21}$$

The oscillatory salinity can be found by substituting $b_n = B_n cos\omega t + C_n sin\omega t$ into Equation 2.19,

$$S' = \sum_{n=0}^{\infty} \frac{1}{\lambda_n^2 k_{h0}^2 + \omega^2}\frac{d[\bar{S}]}{dx}\{(U_{cn}\omega + k_{h0}\lambda_n U_{sn})sin\omega t + (\lambda_n k_{h0} U_{cn} - \omega U_{sn})cos\omega t\}. \tag{2.22}$$

After multiplying S' and u' and integrating over a tidal cycle, only the part of the salinity that has been pulled into phase with the velocity by vertical mixing produces a net salt transport,

$$\overline{u'S'} = \frac{1}{2} \sum_{m=0}^{\infty} U_{cm} cos(m\pi\frac{z}{h}) \sum_{n=0}^{\infty} \frac{\lambda_n U_{cn} k_{h0} - \omega U_{sn}}{\omega^2 + \lambda_n^2 k_{h0}^2} \frac{d[\bar{S}]}{dx} cos(n\pi\frac{z}{h}) +$$

$$\frac{1}{2} \sum_{m=0}^{\infty} U_{sm} cos(m\pi\frac{z}{h}) \sum_{n=0}^{\infty} \frac{U_{cn}\omega + k_{h0}\lambda_n U_{sn}}{\omega^2 + \lambda_n^2 k_{h0}^2} \frac{d[\bar{S}]}{dx} cos(n\pi\frac{z}{h}). \qquad (2.23)$$

This expression contains all the spatial variability of oscillatory salt transport driven by an arbitrary velocity profile with constant vertical diffusivity and a constant along-channel salinity gradient.

Depth-averaged, oscillatory salt transport

The depth-averaged oscillatory salt transport, or oscillatory shear dispersion, can be found by integrating Equation 2.23 over depth and substituting $\lambda_n = \frac{n^2\pi^2}{h^2}$,

$$[\overline{u'S'}] = \frac{1}{4} \frac{d[\bar{S}]}{dx} \sum_{n=0}^{\infty} \frac{k_{h0}\frac{n^2\pi^2}{h^2}}{\omega^2 + \left(k_{h0}\frac{n^2\pi^2}{h^2}\right)^2} (U_{cn}^2 + U_{sn}^2). \qquad (2.24)$$

This expression is identical with the results of Fischer et al. (1979) and Young et al. (1982).

The tidal velocity in an estuary can be described by a series of vertical wavenumbers. The lowest order mode ($n = 0$) has no spatial structure and does not contribute to the dispersion. The dispersion is weighted towards the first terms in the series as the coefficient containing the mixing and tidal time scales depends on $\frac{1}{n^2}$.

For the remainder of the section the tidal velocity is described by the first two terms in the series ($n = 0, 1$). The terms are assumed to be in phase and the amplitudes of both are $\frac{U_t}{2}$, producing a tidal velocity of U_t at the surface and zero at the bottom. The difference between the oscillatory salt transport produced by this

33

approximation of vertical velocity structure and the full analytic solution of velocity in a tidal boundary layer was found to be less than 10% for most of the range of parameters used in this study and less than 30% for the entire range.

The depth-averaged, oscillatory shear dispersion can be found by substituting $U_{c1}^2 + U_{s1}^2 = \frac{U_t^2}{4}$ and rewriting Equation 2.24,

$$[\overline{u'S'}] = \frac{1}{16} \frac{d[\bar{S}]}{dx} \frac{U_t^2}{\omega} \frac{\frac{\pi^2 k_{h0}}{h^2 \omega}}{\left(\frac{\pi^2 k_{h0}}{h^2 \omega}\right)^2 + 1}. \tag{2.25}$$

The oscillatory shear dispersion is proportional to the along-channel salinity gradient, the magnitude of the tidal velocity (U_t), a tidal advection length scale ($\frac{U_t}{\omega}$), and a coefficient that contains the ratio of a tidal time scale (ω^{-1}) and a vertical mixing time scale ($\frac{h^2}{k_{h0}}$).

The amount of along-channel dispersion depends on how quickly mixing occurs, a time scale of $\frac{h^2}{k_{h0}}$, compared to the time scale of the shear oscillations, ω^{-1} (see also the discussion by Fischer et al. (1979) and Young et al. (1982)). If mixing is slow compared to the period of shear reversals, water parcels barely move perpendicular to the flow and, as a result, are brought back to nearly the same initial position at the end of the oscillation. If the mixing is fast compared to the period of shear reversal, vertical stratification and shear are weak, and there is only a small correlation between the velocity and salinity and a small net transport of salt along the channel. At these extremes, the dispersion approaches zero.

The maximum amount of shear dispersion, $[\overline{u'S'}]_{max} = \frac{1}{32} \frac{d[\bar{S}]}{dx} \frac{U_t^2}{\omega}$, occurs between these two extremes when $k_{h0} = \frac{h^2 \omega}{\pi^2}$, or when the tidal and mixing time scales are matched. The maximum dispersion can also be expressed as a maximum longitudinal dispersion coefficient, $K_{H,max} = \frac{1}{32} \frac{U_t^2}{\omega}$, acting on the salinity gradient. The maximum dispersion coefficient is dependent only on the tidal frequency and amplitude

34

of the tidal velocity. For example, a semidiurnal tidal velocity with an amplitude of 1 m s^{-1} produces a maximum dispersion coefficient of $K_{H,max} = 220$ m^{2}s^{-1}.

Depth-dependent, oscillatory salt transport

The spatial structure of oscillatory salt transport must be considered when interpreting the salt transport from observations at a particular location. To illustrate the spatial dependence, consider the vertical structure of tidal flow in an estuary expressed by the first two vertical modes of velocity, the oscillations of the depth-mean and the first vertical sinusoid.

$$u'(z,t) = (U_0 - U_1 cos(\pi \frac{z}{h}))cos\omega t \qquad (2.26)$$

The depth-dependent, oscillatory salt transport is

$$\overline{u'S'} = -\frac{1}{4}\left(cos\left(\pi\frac{z}{h}\right)\frac{d[\bar{S}]}{dx}\frac{U_1}{\omega}\frac{\frac{\pi^2 k}{h^2\omega}}{1+\left(\frac{\pi^2 k}{h^2\omega}\right)}\right)\left(-U_1 cos\left(\pi\frac{z}{h}\right)+U_0\right). \qquad (2.27)$$

Figure 2.1 shows the vertical structure of salt transport for three values of vertical mixing at and around the optimum. In every case, the region near the bottom has counter-gradient salt flux (negative) and the region near the surface has down-gradient flux (positive). The depth-averaged salt transport is down-gradient and given by Equation 2.25. The net flux is greatest for the optimum mixing rate (solid line) and smaller for the higher and lower values of vertical mixing.

The explanation for this structure is as follows. The shear in the oscillating flow acts on the along-channel salinity gradient, creating oscillatory stratification which drives an oscillating vertical exchange of salt. The tidal variations of stratification and vertical salt flux oscillate around a stable, tidal-mean stratification and
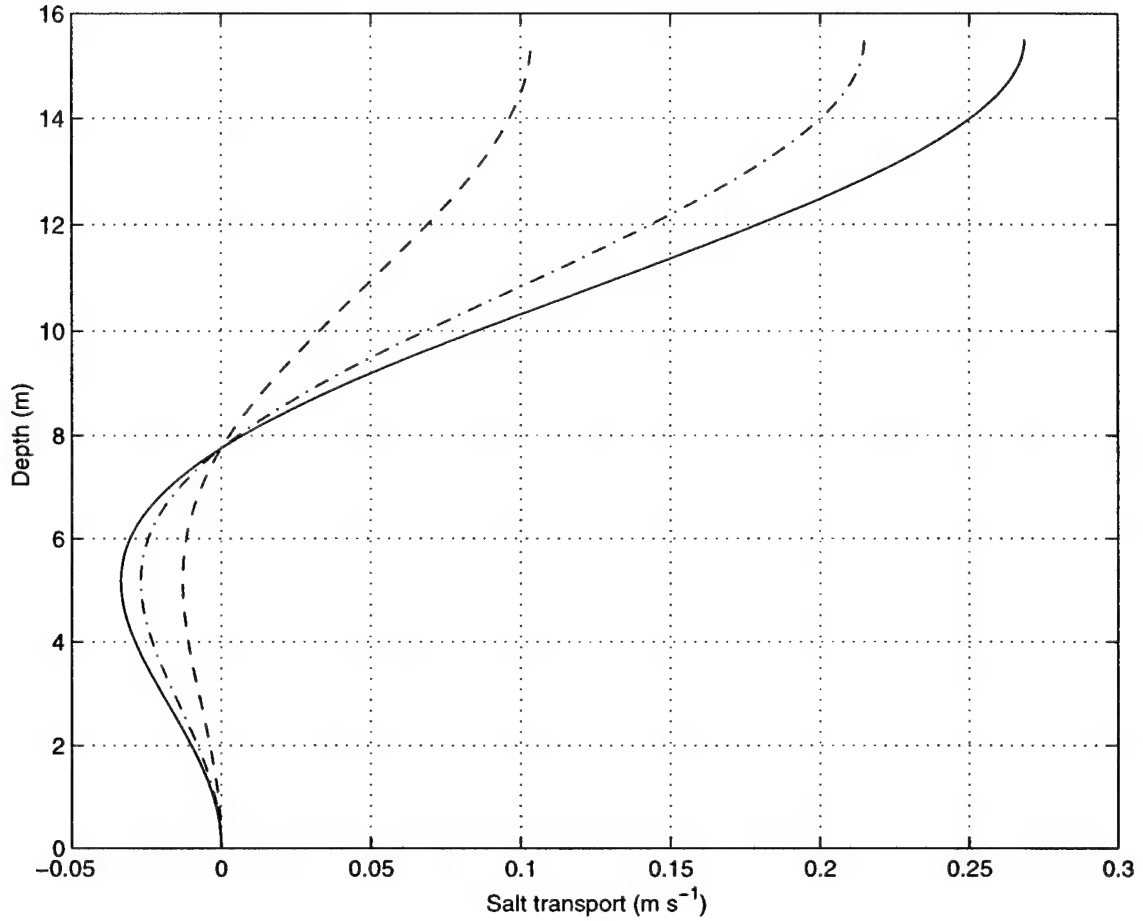
Figure 2.1: Vertical structure of oscillatory salt transport for three values of eddy diffusivity: diffusivity which maximizes the depth-averaged salt transport ($k = 0.0034$ m^{2}s^{-1}, solid line), half this diffusivity ($k = 0.0017$ m^{2}s^{-1}, dash-dotted line), and five times the diffusivity ($k = 0.017$ m^{2}s^{-1}, dashed line).

an upward, tidal-mean vertical salt flux. During the latter part of the ebb and the beginning of the flood, the stratification is greater than the tidal average, and the transfer of salt from the near bottom to near surface is increased. Salinity is advanced in the surface layer and delayed in the lower layer. Towards the end of flood tides and beginning of ebb, the stratification is less than the tidal average and the vertical transfer of salt from the bottom to surface is reduced, which again delays the salinity in the bottom of the water column and advances it near the surface. Therefore, the salinity and velocity have an in-phase component that produces a positive correlation near the surface, where the salinity is advanced, and a negative correlation near the bottom, where the salinity is delayed.

The dispersion is always down-gradient. Intuitively, down-gradient flux occurs because the same amount of salt is transferred vertically between the top and bottom of the water column, but the down-gradient flux happens in the faster surface velocities. From a more mathematical viewpoint, the oscillatory shear dispersion (Equation 2.25) is down-gradient because it is comprised of products of velocity and salinity from identical modes. The products of velocity and salinity from different modes produce regions of counter-gradient salt transport but contribute nothing to the depth-averaged flux.

The example in this section shows that a vertical phase shift in velocity is not required to produce local regions of counter-gradient flux, as other studies have stated (Larsen 1977; Hunkins 1981). Counter-gradient flux requires only a gradient of velocity and mixing of salt perpendicular to the salinity gradient. Ou et al. (1999) provided a thorough derivation for the case of a tidal boundary layer, in which the mixing of salt and momentum are inextricably linked. The spatial dependence of oscillatory salt transport derived here (Equation 2.23) is more general, which allows its application to other dimensions (as will be exploited in the next chapter), and links the results of Ou et al. (1999) with the framework of Young et al. (1982), who

37

considered shear from sources other than tides.

2.3.3   Total salt transport

The analytical expressions for the estuarine salt transport (Equation 2.14) and oscillatory salt transport (Equation 2.25) are combined to show the variation with respect to one another and the variation of their sum. Figure 2.2 shows the two fluxes and their sum as a function of the vertical mixing coefficient, holding depth and along-channel salinity gradient fixed constant at 15 meters and 0.0003 m^{-1}, values representative of partially-stratified estuaries. Estuarine salt transport increases rapidly with decreasing vertical mixing. The magnitude of the first two modes of tidal velocity for the oscillatory salt transport are held constant at 0.4 $m\ s^{-1}$. Oscillatory salt transport increases with increasing vertical mixing, overtakes the estuarine salt transport, reaches a maximum, and then decreases. The point at which the oscillatory and estuarine salt transport are equal marks a transition between a region where the advection of salt by the residual circulation provides most of the landward salt transport and a region where vertical oscillatory shear dispersion is more important. The relative importance of the oscillatory salt transport is illustrated in the second panel: it displays ν, the fraction of the total salt transport provided by the oscillatory salt transport.

Other choices of parameters change the magnitude of each salt transport mechanism. The estuarine salt transport increases with increasing depth and along-channel salinity gradient, playing the larger role in the salt transport as either of those variables increases. The oscillatory salt transport is the larger component for shallower depths and weaker along-channels salinity gradients.

It would be more useful to express salt transport as a function of the tidal velocity rather than a vertical eddy coefficient. One way of doing so is to let the vertical

38

eddy coefficient be proportional to the tidal velocity and the depth, $k = \gamma U_{tide} h$ (Bowden, 1953). The salt transport as a function of U_{tide} is shown in the third panel with $\gamma = 10^{-4}$ used to match a range of eddy coefficients $(0.0006 - 0.002 \ \mathrm{m^2 s^{-1}})$ to a realistic range of tidal velocities. The value of γ is more than an order of magnitude smaller than typical values of drag coefficients (Heathershaw 1979), in order to account for the reduction in mixing due to stratification. The value of γ is consistent with the numerical factor Godfrey (1980) used to match the parameter dependence of estuarine salt transport from the Hansen and Rattray (1965) solutions to observations from the James Estuary.

The estuarine and oscillatory salt transport with the simple closure (Figure 2.2b) have similar behavior to what they did with a constant eddy coefficient. The estuarine salt transport dominates the total salt transport at lower tidal velocities, changing by more than an order of magnitude over the range of tidal velocities shown. The variation is consistent with Nunes Vaz et al. (1989) who suggested that estuarine salt transport can increase dramatically during neap tides when vertical mixing is weak, but is effectively shut down during spring tides when vertical mixing is stronger. The oscillatory salt transport becomes larger than the estuarine at higher tidal velocities. The addition of the simple closure removes the maximum in

Figure 2.2: Top panel shows the analytical expressions for estuarine salt transport (dashed line), oscillatory shear dispersion (dotted line), and their sum (solid line) for a depth of 15.5 meters, along-channel salinity gradient of 0.0003 $\mathrm{m^{-1}}$, and a range of eddy mixing coefficients. A scale for the equivalent along-channel dispersion coefficient, $K_H (\mathrm{m^2 s^{-1}})$, is found by dividing salt transport by the along-channel salinity gradient. The second panel shows the diffusive fraction, ν, the ratio of the oscillatory salt transport to the total landward salt transport as a function of the vertical eddy coefficient. The third panel shows the estuarine and oscillatory salt transport and their sum as a function of tidal velocity, where the vertical mixing rate has been set proportional to tidal velocity, i.e. $k = \gamma U_{tide} h$. The constant, $\gamma = 10^{-4}$, has been chosen to match a range of eddy coefficients from the upper panel with a realistic range of tidal velocities. The fourth panel show the dispersive fraction as a function of tidal velocity.
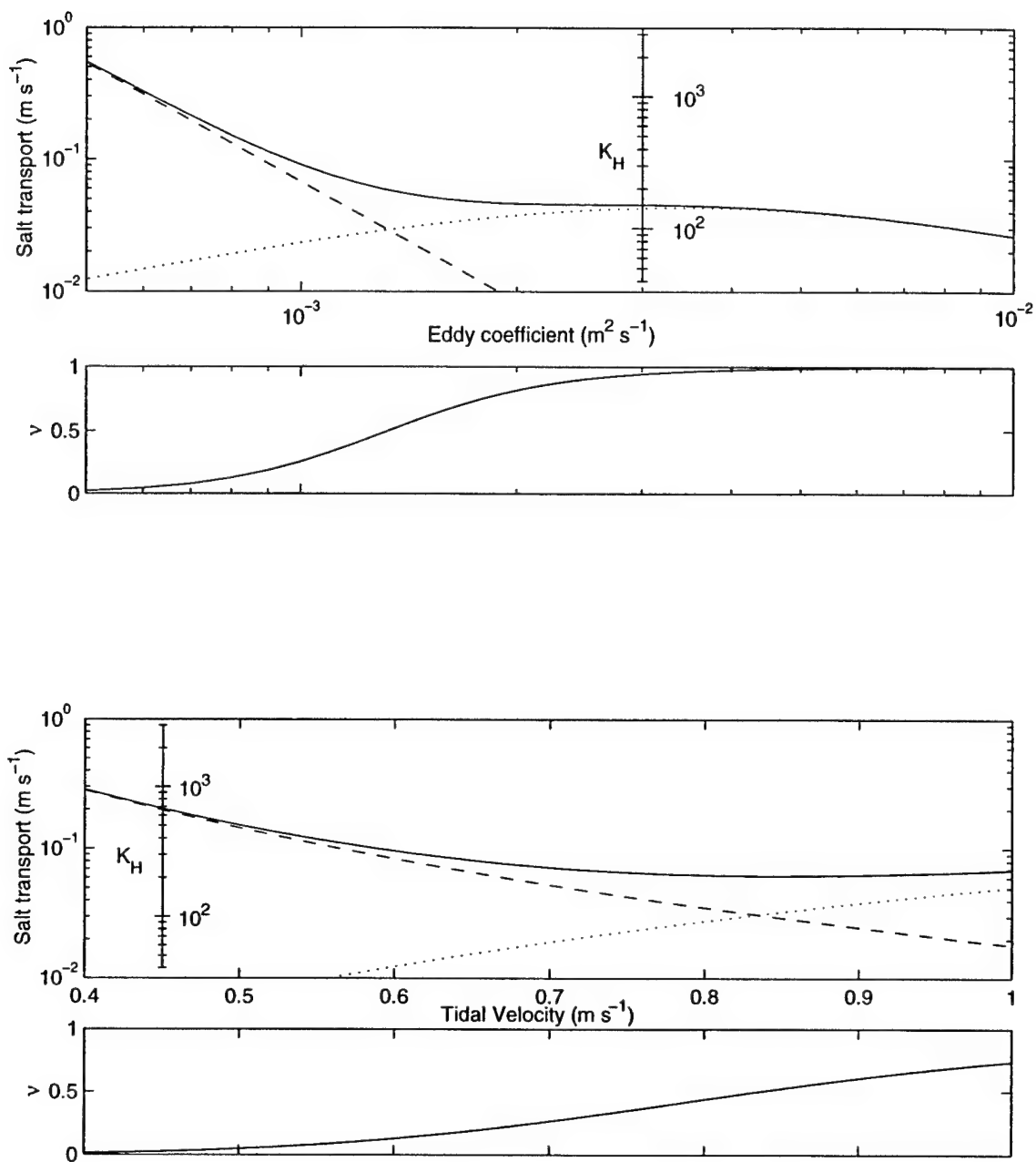
Figure 2.2: Caption on previous page.

oscillatory shear dispersion: oscillatory shear dispersion increases monotonically with increasing amplitude of tidal velocity, asymptoting to a linear increase. At higher tidal velocities, as the estuary becomes more well-mixed, oscillatory shear dispersion due to transverse shear and mixing would be more effective in producing salt transport, eventually exceeding the salt transport produced by the vertical oscillatory shear dispersion (Smith 1980).

2.4 Salt transport with variable eddy coefficients

2.4.1 Model description

A one-dimensional version of the Blumberg and Mellor (1987) Estuarine and Coastal Model (ECOM) was used to determine the effects of turbulence closure on the mechanisms and variation of along-channel salt transport. The one-dimensional ECOM model was chosen because it implements the MY level 2.5 turbulence closure, the current standard used by a large community in the US for modeling coastal and estuarine systems. The numerical model implemented the momentum and salt balances laid out in Section 2.2 (Equations 2.1 and 2.5).

Forcing conditions

The momentum balance was forced by the pressure gradients (Equation 2.2). In the idealized study the along-channel salinity gradient was held constant with depth and with time, consistent with the assumptions for the analytical solutions of Section 2.3. The range of tidal velocities and the along-channel salinity gradients were chosen so that the model salinities remain in a realistic estuarine range between 0 and 32. The depth-averaged, tidally-averaged flow, $[\bar{u}] = u_f$, was kept at zero in order to focus on the salt transport due to the tidal flow and the along-channel salinity gradient. In previous studies the tidally-averaged sea surface slope ($\frac{\partial \bar{\eta}}{\partial x}$) has been

adjusted every tidal cycle until $[\bar{u}] = 0$ (Simpson and Sharples 1991; Monismith et al. 1996), a technique that proved impractical for running over a wide range of tidal amplitudes and salinity gradients. An alternate, more successful method of forcing the model was adopted (R. Chant and W. Geyer, personal communication). In this method, the depth-averaged flow was specified at each time step and the sea surface slope required to drive the flow calculated from the specified, depth-averaged acceleration, the pressure gradient due to the along-channel salinity gradient, and the bottom stress of the previous time step. The momentum balance was stepped forward with the new barotropic pressure gradient, producing the specified sinusoidal depth-averaged tidal flow with a tidal average very near zero.

For the Hudson simulation, the barotropic pressure gradient was specified in the manner more often used in one-dimensional modeling studies. The observed values of the semidiurnal pressure gradient from the Hudson Estuary were used to specify the tidal pressure gradient in the model and $[\bar{u}]$ was kept close to zero by adjusting $\frac{\partial \bar{\eta}}{\partial x}$. This single simulation required repeated runs to find the sequence of $\frac{\partial \bar{\eta}}{\partial x}$ necessary to keep the depth averaged residual flow close to zero. The along-channel salinity gradient was varied according to observations.

Boundary conditions

In all the model runs, the boundary conditions in the numerical model were as outlined in Section 2.2. There was no flux of salt through the top or bottom of the water column and there was no stress at the surface. At the lowest grid cell (z_b), a stress was applied using a quadratic drag law with a drag coefficient (C_D) based on a bottom roughness (z_0):

$$\frac{\tau_b}{\rho_0} = C_D(z_0, z_b)|u(z_b)|u(z_b). \tag{2.28}$$

42

A bottom roughness of 1 cm was used in all the runs, corresponding to a drag coefficient of 0.008 one meter above the bottom.

Initial conditions

Velocity at every depth was initially zero for all runs. Salinity was initially equal to 15 at all depths for the idealized study. For the Hudson simulation, the salinity was initially set to 23 at all depths to agree with the depth-averaged salinity from the observations.

Turbulence closure

The turbulent vertical fluxes of salt and momentum were parameterized using the QETE version (Galperin et al. 1988) of the Mellor-Yamada (MY) turbulence closure scheme (Mellor and Yamada 1982) in which eddy coefficients scale with the turbulent kinetic energy, q, a mixing length scale, l, and exchange coefficients, S_M and S_H,

$$k_m = qlS_M \ , \ k_h = qlS_H. \tag{2.29}$$

The turbulent kinetic energy and the mixing length were determined at each time step from the shear production, buoyancy production, dissipation, and self-diffusion. The exchange coefficients, S_M and S_H, were then found from algebraic expressions containing $G_H = -\left(\frac{l}{q}\right)^2 \beta g \frac{\partial S}{\partial z}$, a ratio of the buoyancy frequency to the frequency of turbulent eddies. For small and negative values of G_H, when the water column is highly turbulent or weakly or unstably stratified, S_M and S_H are large. S_M and S_H decrease rapidly with increasing G_H in response to either a less turbulent or a more stratified water column.

43
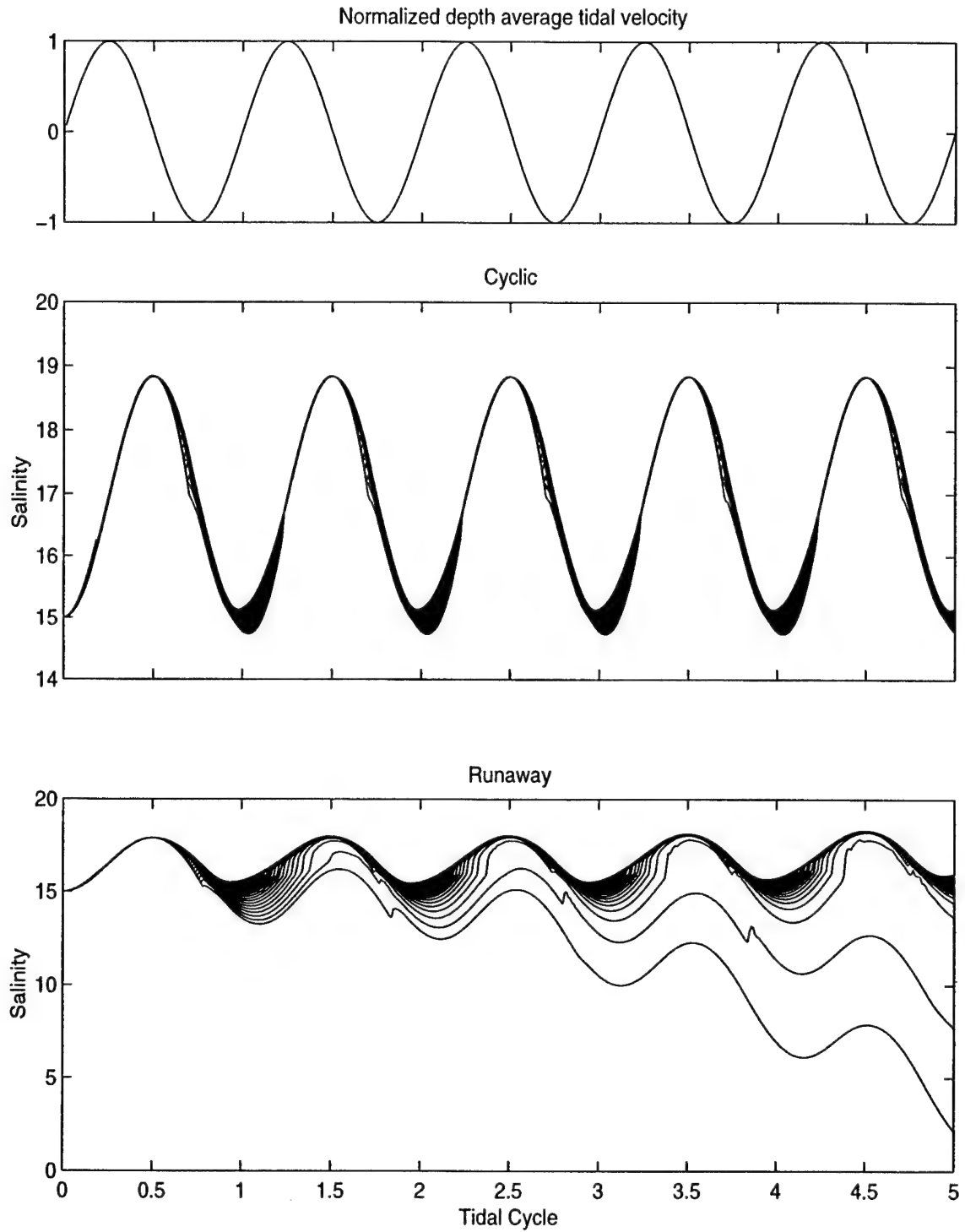
Figure 2.3: Normalized depth-averaged velocity (top panel, positive is flood tide) and salinity every half meter from cyclic (middle panel, $U_{tide} = 0.9$ m s^{-1}) and runaway (bottom panel, $U_{tide} = 0.6$ m s^{-1}) model runs. In both runs the depth is 15.5 meters and the along-channel salinity gradient is 0.0003 m^{-1}.

44

2.4.2 Model behavior

All model runs fall into one of two categories. Either the salinity and velocity fields repeat every tidal cycle ("cyclic", also referred to as "periodic" by Monismith et al. (1996)), or the stratification and circulation increase with every tidal cycle ("runaway" Nunes Vaz and Simpson (1994)). Conditions were found to be cyclic when the vertical mixing is strong enough to remove all of the stratification at some point during the tidal cycle (Figure 2.3, middle panel). Periodic stratification is produced by the ebb tidal shear straining the density field (Simpson et al. 1990). During the flood, stratification is removed by both the flood tidal shear and vertical mixing.

Runaway stratification occurs when mixing near the surface is too weak to erode the stratification produced during the tidal cycle (Figure 2.3, lower panel). This process begins during ebb tide when the tidal shear strains the density field and produces vertical stratification. The stratification is partially removed by the shear and vertical mixing on the subsequent flood, but not entirely, leaving residual shear and stratification at the surface. During the next ebb, tidal straining produces more stratification, extending further down into the water column than on the previous ebb, and again the shear and mixing during the flood tide remove some, but not all, of the newly created stratification. The nearly inviscid layer grows downward from the surface as this process is repeated every tidal cycle. The residual stratification and circulation at the surface increase with every tidal cycle until the surface water is fresh.

Transition point scaling

Whether a run is cyclic or runaway depends on the depth (h), tidal amplitude (U_{tide}), and along-channel salinity gradient ($\frac{d[\bar{S}]}{dx}$). Simpson et al. (1990) derived an

energetics balance that described the point at which the stratification begins to run away. Stacey (1996) followed essentially the same reasoning as Simpson et al. (1990) but took the analysis further to find a non-dimensional parameter that describes the transition. Simpson et al. (1990) and Stacey (1996) developed the scaling by first assuming that runaway stratification should occur when the buoyancy production term in the turbulent kinetic energy balance is some fraction of the shear production term. Stacey (1996) then proceeded to scale the two terms using u_* as a turbulent velocity scale and the tidally-averaged momentum and salt balances to find scales for $\frac{\partial \bar{S}}{\partial z}$ and $\frac{\partial \bar{u}}{\partial z}$. The momentum and salt balances he used are identical to the Hansen and Rattray (1965) expressions (Equations 2.11 and 2.13) with k_{m0} and k_{h0} replaced by $u_* h$. After finding scales for each of the terms, the ratio of buoyant production to shear production becomes what Stacey (1996) calls the horizontal Richardson number, Ri_x.

$$Ri_x = g\beta \frac{d[\bar{S}]}{dx} \frac{h^2}{u_*^2} \qquad (2.30)$$

This quantity can be shown to be related to Fischer's (1972) Estuarine Richardson number (see Appendix A), a quantity that he found to be a good predictor of estuarine stratification.

Stacey (1996) tested Ri_x in a numerical model, identical to the one used in this study, and found the transition occurred near a value of 0.3. Monismith et al. (1996) also arrived at the same parameter, making it more readily applicable to observations by replacing u_*^2 with $C_D U_{max}^2$. They found that the transition point in a one-dimensional vertical model (identical to the one in this study) occurred when $Ri_x \approx 0.25$, using a drag coefficient of 0.002 and the free-stream tidal velocity, $U_{max} = \frac{g}{\omega_{tide}} \frac{\partial \eta_{tide}}{\partial x}$.

The skill of Ri_x in predicting the transition tidal velocity was tested for a range of

along-channel salinity gradients, depths, and tidal frequencies by repeatedly running the model to find the tidal velocities that bracket the transition. Ri_x proved to be an excellent predictor of the transition even for large changes in the along-channel salinity gradient (0.05-0.5 km^{-1}), depth (8.5-22.5 m), and tidal frequency (0.75-2 ω_{M2}). The average transition value was $Ri_x = 0.33$ with deviations of $\pm 3\%$ around this.

2.4.3 Total salt transport

Estuarine and oscillatory salt transport on either side of the Ri_x transition are found by running the model for a range of tidal amplitudes holding depth, along-channel salinity gradient, and tidal frequency constant and equal to the same values used to illustrate salt transport with constant eddy coefficients (Figure 2.4). The variation is similar to the salt transport from the analytical descriptions (Figure 2.2). Estuarine salt transport (crosses) has greater magnitude when tidal velocities are small and decreases with increasing tidal amplitude. Oscillatory salt transport (circles) is much less than the estuarine salt transport for lower tidal amplitudes but eventually becomes greater at higher tidal amplitudes.

Although the trends with variable eddy coefficients are similar to those with constant eddy coefficients, the variability of the eddy coefficients plays a role in the magnitude of the salt transport in the one-dimensional model results. The reasons for the variation of estuarine and oscillatory salt transport above and below the Ri_x transition are discussed in the following sections.

2.4.4 Estuarine salt transport

Estuarine salt transport increases with decreasing tidal amplitude (crosses on Figure 2.4) dominating the total salt transport during runaway conditions and cyclic

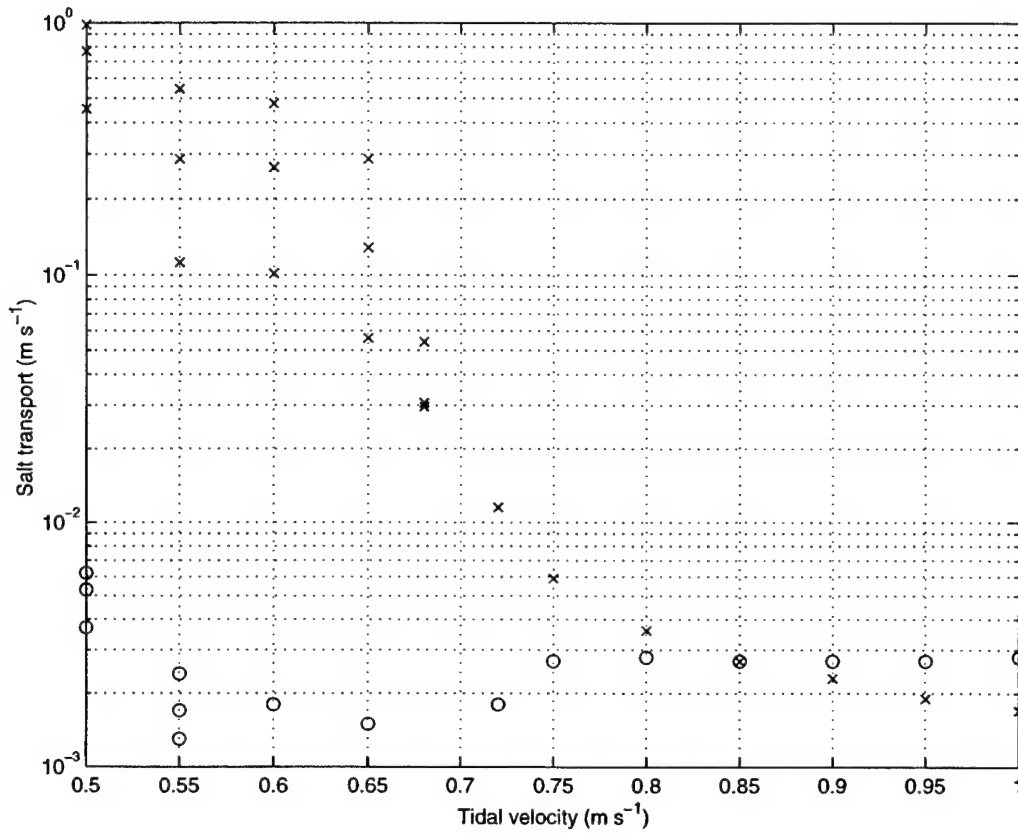Figure 2.4: Estuarine salt transport (x) and oscillatory salt transport (o) for model runs with a depth of 15.5 meters, along-channel salinity gradient of 0.0003 m^{-1}, over a range of tidal velocities. The transition between cyclic and runaway conditions occurs near $U_{tide} = 0.7$ m s^{-1}. Salt transport for runaway runs is plotted for each of the first three tidal cycles into the run.

conditions close to the transition. The trends are similar to the Hansen and Rattray (1965) expressions for estuarine salt transport (Figure 2.2), but the values are much greater when $Ri_x > 0.33$ and much smaller when $Ri_x < 0.33$, mirroring the abrupt change of stratification in the model at $Ri_x = 0.33$.

For runaway cases, estuarine salt transport increases rapidly as the residual circulation and stratification in the upper few meters increase. After the first three tidal cycles, over 80% of the estuarine salt transport is produced by the shear and stratification in the surface layer. The tidally-averaged salt and momentum balances include significant time dependent terms not included in the balances postulated by Hansen and Rattray (1965). As a result, the estuarine salt transport in the numerical model increases by many orders of magnitude across the transition, an effect not captured by the analytical expressions.

For cyclic cases, approximately 90% of the estuarine salt transport is due to the residual circulation and stratification produced by tidal asymmetry, a mechanism discussed in the following sections.

The residual circulation

The mechanisms that produce the residual circulation on either side of the transition in Ri_x can be examined by relating the residual shear to the other terms in the momentum balance. Averaging the momentum balance (Equation 2.1) over a tidal cycle (denoted by an overbar) and splitting the residual stress into two terms produces the following balance.

$$\frac{\partial \bar{u}}{\partial t} = -\frac{1}{\rho_0}\frac{\partial \bar{p}}{\partial x} + \frac{\partial}{\partial z}\left(\overline{k_m \frac{\partial \bar{u}}{\partial z}}\right) + \frac{\partial}{\partial z}\left(\overline{k'_m \frac{\partial u'}{\partial z}}\right) \qquad (2.31)$$

The residual stress consists of a component that depends on the tidally-averaged eddy coefficient and the residual shear $(\overline{k_m \frac{\partial \bar{u}}{\partial z}})$ and a component that depends on the

covariance of the tidal shear and tidal mixing $\left(\overline{k'_m \frac{\partial u'}{\partial z}}\right)$. Integrating the momentum balance from the surface to any depth and solving for the residual shear yields

$$\frac{\partial \bar{u}}{\partial z} = -\frac{1}{\overline{k_m}}\int_z^h \frac{\partial \bar{u}}{\partial t}dz - \frac{1}{\overline{k_m}}\int_z^h \frac{1}{\rho_0}\frac{\partial \bar{p}}{\partial x}dz - \frac{1}{\overline{k_m}}\left(\overline{k'_m\frac{\partial u'}{\partial z}}\right). \qquad (2.32)$$

The first term is due to the acceleration of the residual flow. The second term contains the tidally-averaged pressure gradient. This term balances the residual circulation for the case of constant eddy coefficients (Hansen and Rattray (1965), Equation 2.11). The third term is tidal asymmetry, the mechanism addressed in the studies of Jay and Musiak (1996) and Geyer et al. (1999).

The top panels of Figure 2.5 show the residual velocity for three of the model runs shown in Figure 2.4, two runs with cyclic conditions ($U_{tide} = 0.90$ m s^{-1} and $U_{tide} = 0.72$ m s^{-1}) and one with runaway conditions ($U_{tide} = 0.60$ m s^{-1}, results shown after one tidal cycle into the run). The residual circulation increases as tidal amplitude decreases. In the runaway case, the increase is particularly pronounced in the upper three meters of the water column where a discontinuity in shear marks the beginning of the nearly-inviscid surface layer.

The lower three panels show the magnitude of each term in Equation 2.32. The total residual shear (solid line) is the sum of the terms containing acceleration (dash-dotted line), the pressure gradient (dashed line), and tidal asymmetry (dotted line). In both cyclic cases, tidal asymmetry balances most of the residual shear from the surface to about four meters above the bottom. In the runaway case, the term containing the pressure gradient is largest near the bottom and in the upper three meters where the flow is accelerating. In the middle of the water column, residual shear is balanced primarily by tidal asymmetry, similar to the balance in the cyclic cases.

The magnitude of the residual circulation decreases with increasing tidal ampli-

50
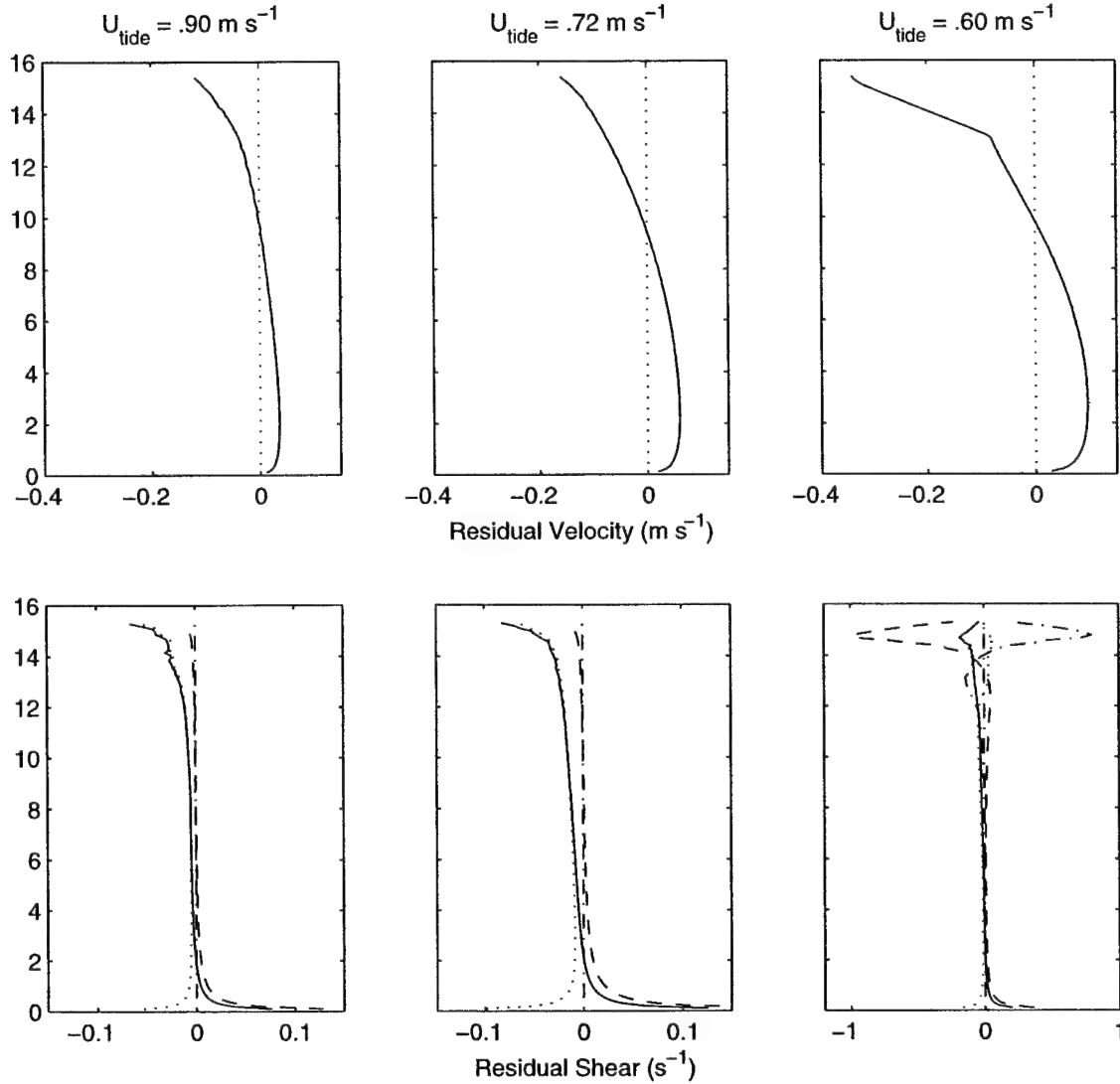
Figure 2.5: Residual velocity from three model runs (top panels), two cyclic ($U_{tide} = 0.90$ m s^{-1} and $U_{tide} = 0.72$ m s^{-1}) and one tidal cycle into a runaway run ($U_{tide} = 0.60$ m s^{-1}). The bottom panels show the four terms from Equation 2.32: the term containing residual shear (solid line), the pressure gradient (dashed line), tidal asymmetry (dotted line), and acceleration (dash-dotted line).

tude, as does the residual circulation with constant eddy coefficients (Equation 2.11). However, the magnitude of the residual circulation in the model is the result of the depth and inter-tidal variations of the eddy viscosity. During runaway conditions, the lower the amplitude of the tidal velocity, the lower the depth that vertical mixing extends in the water column, and the faster the shear increases. During cyclic conditions residual shear can be almost entirely described by tidal asymmetry,

$$\frac{\partial \bar{u}}{\partial z} \approx \frac{1}{\overline{k_m}} \overline{k'_m \frac{\partial u'}{\partial z}}. \tag{2.33}$$

The decrease of the residual shear with increasing tidal velocity is primarily due to an increase in the tidally-averaged eddy viscosity.

The residual stratification

The tidally-averaged salt balance can be written in the same manner as the momentum balance by splitting the vertical salt flux into a term containing the tidally-averaged diffusivity acting on the residual stratification $(\overline{k_h} \frac{\partial \bar{S}}{\partial z})$ and a term containing the tidal covariance of stratification and diffusivity $(\overline{k'_h \frac{\partial S'}{\partial z}})$,

$$\frac{\partial \bar{S}}{\partial t} = -\bar{u} \frac{d[\bar{S}]}{dx} - \frac{\partial}{\partial z} \left(\overline{k_h} \frac{\partial \bar{S}}{\partial z} \right) - \frac{\partial}{\partial z} \left(\overline{k'_h \frac{\partial S'}{\partial z}} \right). \tag{2.34}$$

Integrating from the surface to any depth and dividing by $\overline{k_h}$ at each level, the residual stratification can be expressed as the sum of three terms,

$$\frac{\partial \bar{S}}{\partial z} = -\frac{1}{\overline{k_h}} \int_z^h \frac{\partial \bar{S}}{\partial t} dz - \frac{1}{\overline{k_h}} \int_z^h \bar{u} \frac{d[\bar{S}]}{dx} dz - \frac{1}{\overline{k_h}} \left(\overline{k'_h \frac{\partial S'}{\partial z}} \right). \tag{2.35}$$

Figure 2.6 shows the residual stratification for the same three runs in Figure 2.5. The residual stratification (top panels) increases with decreasing tidal velocity, most

52
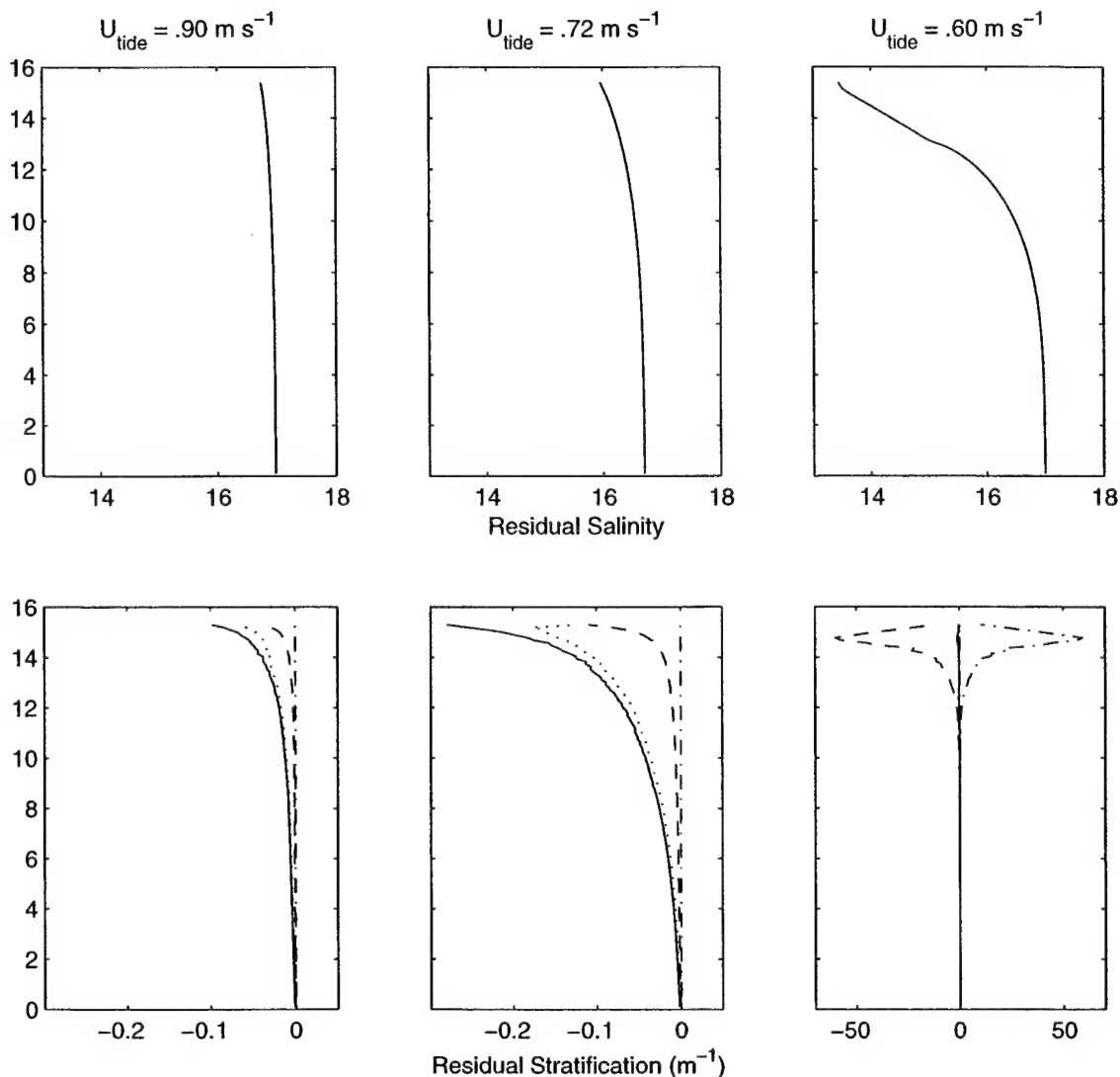
Figure 2.6: Residual salinity from three model runs (top panels), two cyclic ($U_{tide} = 1.2$ m s^{-1} and $U_{tide} = 0.85$ m s^{-1}) and one tidal cycle into a runaway run ($U_{tide} = 0.75$ m s^{-1}). The bottom panels show the terms in the expression for residual stratification (solid line): the terms containing the pressure gradient (dashed line), tidal asymmetry (dotted line), and change of salt with time (dash-dotted line).

markedly near the surface in the runaway case (shown averaged over the first tidal cycle). The lower panels show the terms that balance the residual stratification (solid line) as they appear in Equation 2.35. The tidal asymmetry (dotted line) balances the residual stratification for most of the water column during cyclic conditions. The advection of salt by the residual flow (dashed line) becomes important only near the surface where mixing is weaker. During runaway conditions, the increase of salt with time (dash-dotted line) balances most of the advection of salt in the upper three meters. The balance in the lower part of the water column is similar to that during cyclic conditions.

The magnitude of the residual stratification decreases with increasing tidal amplitude, as does the residual stratification with constant eddy coefficients (vertical derivative of Equation 2.13). However, the magnitude of the residual stratification in the model is the result of the depth variations and inter-tidal variations of the eddy diffusivity. During runaway conditions, the lower the amplitude of the tidal velocity, the lower the depth that vertical mixing extends in the water column, and the faster the stratification increases. During cyclic conditions residual stratification can be almost entirely described by tidal asymmetry,

$$
\frac{\partial \bar{S}}{\partial z} \approx \frac{1}{\overline{k_h}} \overline{k'_h \frac{\partial S'}{\partial z}}.
\tag{2.36}
$$

The decrease of the residual stratification with increasing tidal velocity comes from both an increase in the tidally-averaged eddy diffusivity and a decrease in the tidal covariance of the eddy viscosity and stratification.

54

2.4.5 Oscillatory salt transport

Oscillatory salt transport (circles on Figure 2.4) changes character on either side of the Ri_x transition. For runaway cases the salt transport is unsteady and the magnitude and sign fluctuates throughout the run. The magnitude of the oscillatory salt transport is orders of magnitude smaller than the estuarine salt transport during these runs. For cyclic cases the transport asymptotes to a constant value within the run. The magnitude of the oscillatory salt transport in cyclic cases increases slightly with increasing tidal amplitude. At higher magnitudes of tidal velocity it produces more of the total salt transport than the estuarine salt transport. The magnitudes of both, however, are small.

The variations of oscillatory salt transport are similar to those in the analytic expressions. In the model, however, the vertical flux of salt is accomplished by both tidal fluctuations of eddy diffusivity as well as the tidal-mean eddy diffusivity acting on the stratification. The structure of the vertical oscillatory salt transport with fluctuating eddy coefficients is also similar to the structure of salt transport with constant eddy coefficients. Figure 2.7 shows profiles of the oscillatory salt transport, the covariance between the tidal velocity and salinity, for the two cyclic runs and the runaway run. In all three cases, salt transport in the lower part of the water column is seaward (negative values). In the lower water column, vertical salt flux is upward during the flooding tide and downward during the ebbing tide, which delays the salinity relative to the velocity, creating a net salt transport out of the estuary, similar to the vertical salt transport with constant eddy coefficients (Figure 2.1). As in the case of constant eddy coefficients, the loss of salt from the lower part of the water column is compensated by a gain of salt in the upper part. In the cyclic condition with higher tidal velocity (solid line), the zero crossing of tidal salt transport occurs at two-thirds of the depth above the bottom. Salt moves into the upper third of the water column during floods and out during ebbs, leading to a
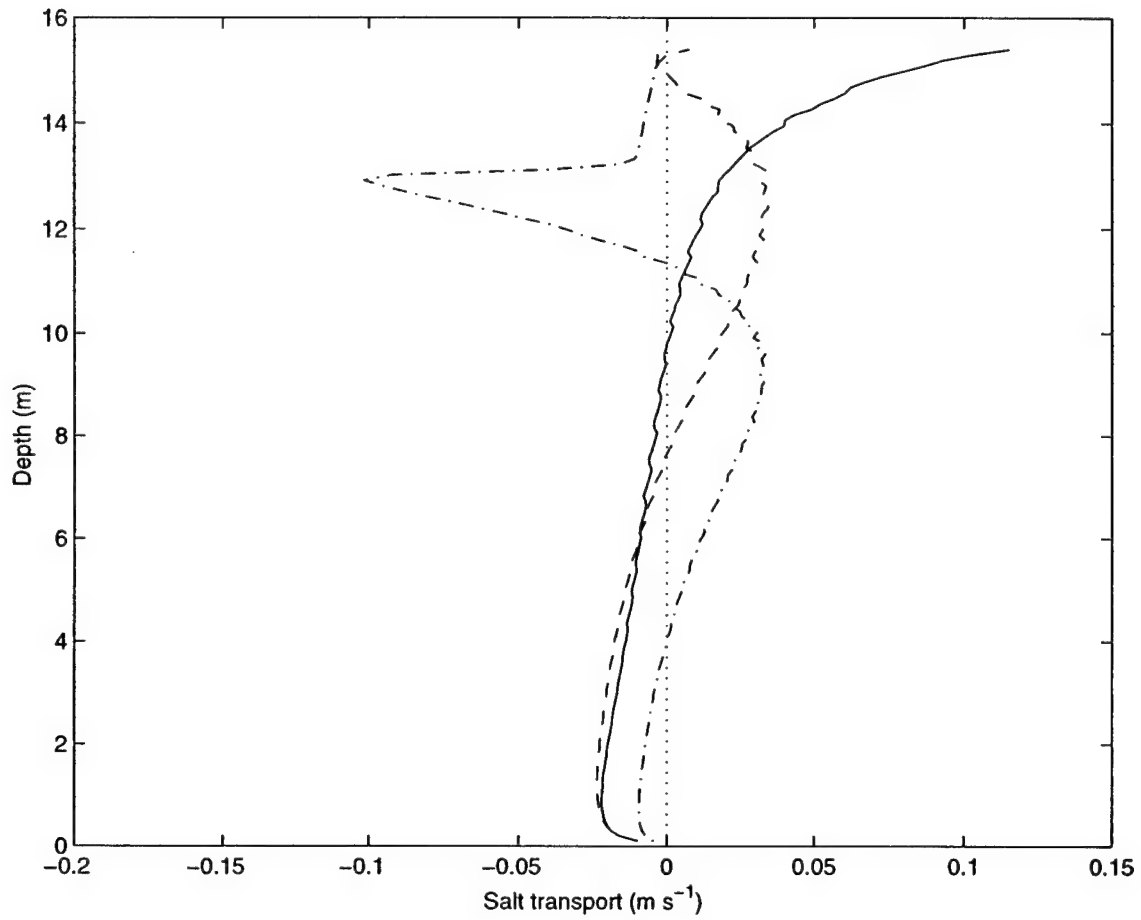
55

Figure 2.7: Three vertical profiles of oscillatory salt transport from two cyclic runs, $U_{tide} = 0.90$ m s^{-1} (solid line), and $U_{tide} = 0.72$ m s^{-1} (dashed line), and one tidal cycle in to a runaway run), $U_{tide} = 0.60$ m s^{-1} (dash-dotted line).

landward, or down-gradient, transport of salt.

Oscillatory salt transport is more complicated in both the cyclic case of lower tidal velocity (dashed line) and in the runaway case (dash-dotted line). In the cyclic case for 0.72 m s^{-1} (dashed line), a very small region of counter-gradient salt transport appears near the surface. The change from down-gradient transport in the middle of the water column to counter-gradient transport near the surface is due to the timing of mixing events within the tidal cycle. Near the bottom, mixing takes place throughout the tidal cycle. Further up in the water column, most of the mixing is comprised of two large events during maximum flood and maximum ebb shears. The stratification near the surface at the end of ebb increases with decreasing tidal energy, increasing the time that it takes for the flood shear to remove stratification to the point where mixing can occur. The pulse of mixing that occurs during flood tides is delayed and, as a result of the small timing change, salt transport changes sign. Oscillatory salt transport is no longer the result of phase shifts in the semidiurnal velocity and salinity, as it is in the analytical solutions; with variable eddy coefficients, it is the result of the phase shift of mixing.

In the runaway case (Figure 2.7, dash-dotted line), the salt transport in the regions below the halocline has the same behavior as the cyclic cases: counter-gradient transport occurs near the bottom, down-gradient transport higher in the water column. Above the lobe of down-gradient flux, a region of counter-gradient transport appears at the bottom of the highly-stratified layer by the same mechanism as the cyclic case discussed above. Above the halocline, there are long periods without any vertical mixing. The velocity and salinity have trends that cannot be removed by averaging over a tidal cycle. The magnitude of salt transport is highly variable and its direction fluctuates as the run progresses. The magnitude of the oscillatory salt transport, however, is much smaller than the estuarine salt transport, and makes a negligible contribution to the total salt transport.

2.5 Comparison with observations

2.5.1 Comparison of velocity and salinity

The model results are compared to observations of velocity and salinity from the Hudson Estuary (see the next chapter for details of the observations). The model parameters are selected to approximate the conditions at a location in the estuary where velocity and salinity measurements were made continuously at several depths. The model depth is held constant at 15.5 meters. The tidal barotropic pressure gradient is specified using observations of the semidiurnal tidal pressure gradient calculated from moored pressure sensors (Figure 2.8, first panel, and expressed as an inviscid, free stream tidal velocity, equal to the amplitude of the tidal pressure gradient divided by both density and the tidal frequency. Thirty-five tidal cycles are chosen from the observations, beginning with spring tides, decreasing to a minimum during neaps seven days later, and increasing back to spring tides. This period of the observations is chosen because it encompasses the full range of conditions in the estuary, a transition from springs to neaps and back to springs.

The salinity gradient in the model was initially set to 0.0003 m^{-1}. During neap tides surface salinity in the model approaches fresh and near bottom salinity approaches oceanic. In order to simulate the decrease of the salinity gradient towards the river and the ocean, the salinity gradient at each level was varied as a function of the salinity at each level following the salinity distribution observed during a hydrographic survey of the Hudson (Day 240, Figure 3.6b). When salinity at a level dropped below 10 or rose above 28, the salinity gradient was changed to 0.00015 m^{-1}. Below 1 or above 31, the salinity gradient was set to zero.

Stratification in the model simulation (Figure 2.8, second panel, salinity plotted every meter) develops rapidly at about day 7, during neap tides, and gradually decreases, beginning near day 12, as the amplitude of the tidal velocity increase into

58
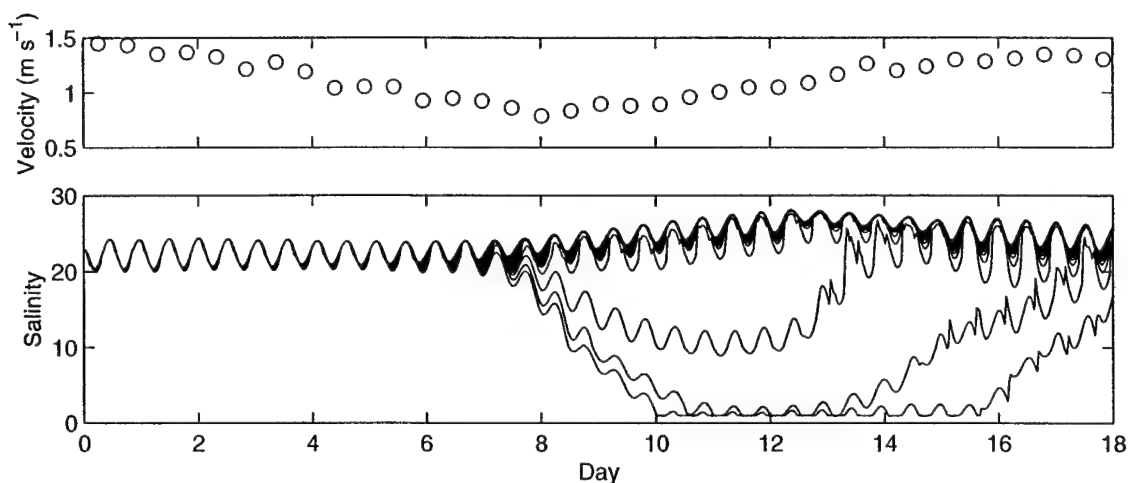
Figure 2.8: Comparison of observations and model. The top panel shows the magnitude of the semi-diurnal pressure gradient every tidal cycle (expressed as a free-stream velocity) from observations in the Hudson Estuary. A fifteen-day section of the record has been chosen (beginning on September 8, 1995) that encompasses the transition from spring tides to neap tides and back to springs. The lower panel shows salinity every meter from the numerical model simulation.

springs. Most of the stratification during the highly-stratified portion of the run is confined to a three-meter thick surface layer. The salinity difference over the rest of the water column only reaches about 3 at the end of ebb tides (part of the tidal cycle where the salinity is freshest). The salinity difference over the entire water column during spring tides is even smaller: salinity differences are less than 1 at the end of spring ebbs.

The observations display more velocity and salinity structure than the model fields over much of the water column. The salinity difference between the highest and lowest moored temperature/conductivity sensors, located at 4 and 11 meters above bottom, (Figure 2.9, upper panel, solid line) is generally about 1 rather than becoming fresh as they do in the model. There is no evidence for salinity differences of 20 over the upper four meters.

In summary, the model produces a spring-neap cycle of stratification with a tran-

59
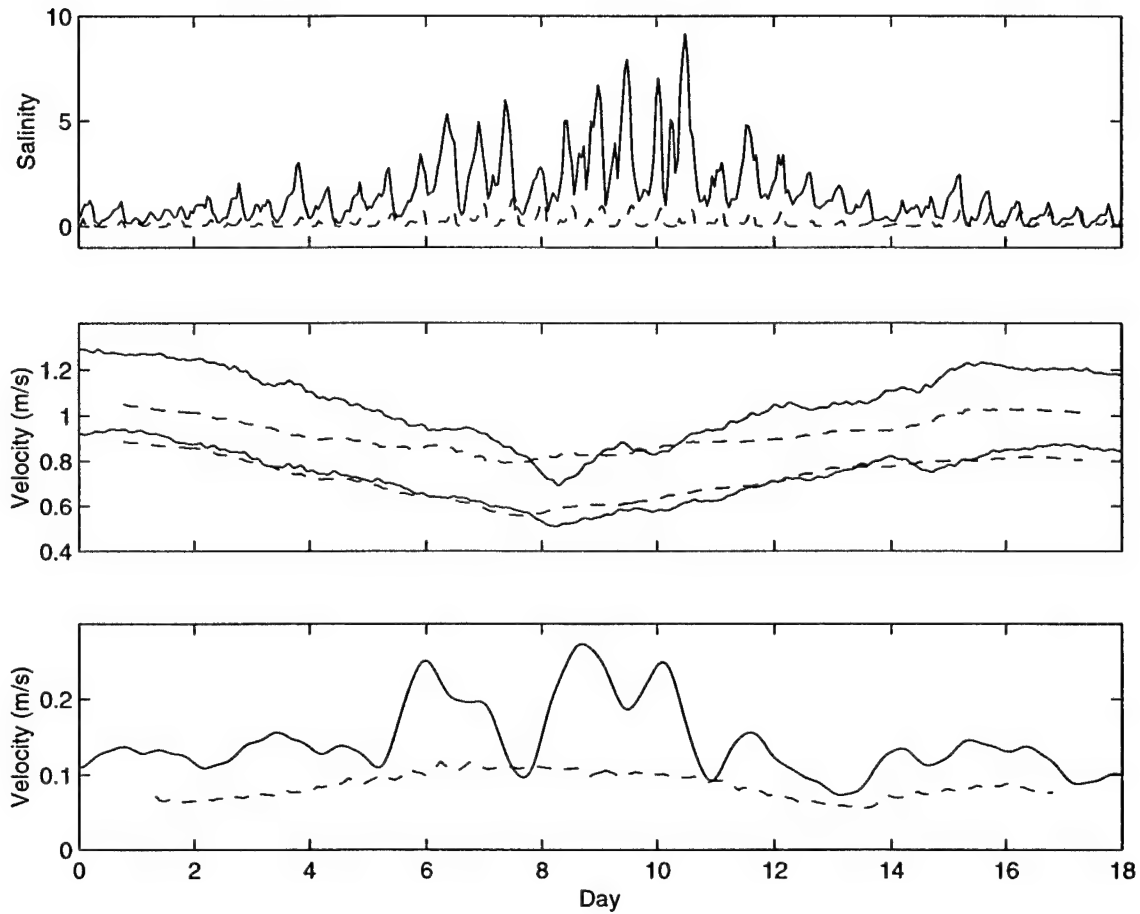
Figure 2.9: The top panel shows the salinity difference between 4 and 11 meters above bottom from two moored conductivity/temperature sensors (solid line) and from the identical depths in the model (dashed line). The middle panel shows the amplitude of the tidal velocity at 4.5 and 11.5 meters above bottom from the moored ADCP (solid lines, upper line is 11.5 meters, lower line is 4.5 meters) and from identical depths in the model (dashed lines). The lower panel shows the residual velocity difference between the same two depths (upper velocity subtracted from the lower velocity, positive into estuary) for the observed velocity at the ADCP (solid line) and the same depths in the model (dashed line).
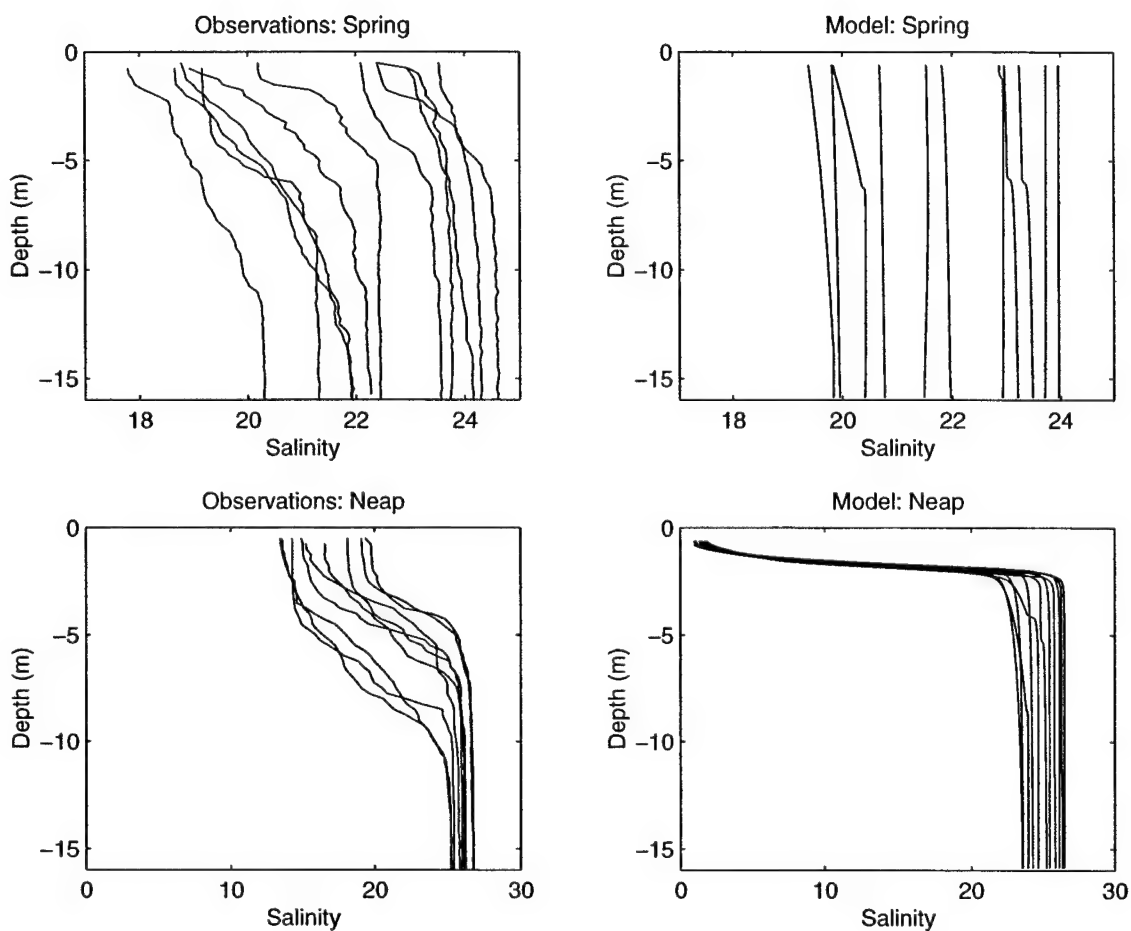
Figure 2.10: Salinity over one tidal cycle from CTD casts at the central mooring in the Hudson Estuary (left column) and the one-dimensional model run (right column). Profiles in the upper row are during spring tides (casts taken on August 14, 1995) and profiles in the lower row are during neap tides (casts taken on August 4).

sition to stratified conditions near the transition in the observations. However, the model produces less vertical structure of salinity and velocity throughout much of the water column. During neap tides the model produces a thin, highly-stratified, strongly-sheared layer over a thick, well-mixed boundary layer. The observed halocline and shears are spread over a larger range of depths.

2.5.2 Discussion of the reasons for model/data differences

The differences between the model and the observations could come from three sources: 1) the model may not be forced with the same conditions that produced the observed fields; 2) the turbulence closure may not accurately describe the vertical mixing; or 3) the processes at this location may be inherently dependent on the missing advective terms in the momentum and salt balances. The first issue can, in part, be addressed here. The second and third are discussed only briefly.

The first issue, the realism of the forcing conditions, was investigated in additional model runs. The model was forced with the depth-averaged measured flow in an attempt to include the effects of the diurnal and weather band motions. The model failed to produce realistic tidal shears. The responses of the runs varied, but a robust feature in common was the transition to stratified conditions near the same tidal velocity as the observations.

A possible reason that the model near-surface salinities run away is that the model does not contain sources of mixing from winds, waves, and boats. Applying a stress to the model surface does create a surface mixed layer. However, with the maximum observed wind velocity applied as a stress directed towards the river in order to maximize the destratifying shear, the model still produces too much stratification. Even with an unrealistically strong source of mixing and destratifying shear at the surface, the model still requires more mixing across the halocline to come closer to

62

the observed stratification. Heavy, continual vessel traffic on the estuary may help mix the upper meters of the water column and spread the halocline [1]. This is not likely to explain the model-data differences, however.

The model tends to underpredict the spring magnitudes of tidal and residual shear and stratification and overpredict the neap magnitudes. One possible reason for this may be discrepancies between the vertical mixing in nature and the turbulence closure in the model. The difference between the modeled and observed stratification in this study are consistent with the results of previous studies that suggest that the MY level 2.5 mixing scheme tends to undermix during periods of strong stratification (Simpson et al. 1996; Stacey et al. 1999) and overmix during periods of weak stratification (Stacey et al. 1999).

Advection of salt and momentum along and across the channel could also prevent the observed stratification from running away to the extent the model stratification does. The point at which runaway stratification develops in the one-dimensional model depends on the square of the depth (Ri_x, Equation 2.49). The onset of highly-stratified conditions in an entire estuary depends on the evolution of momentum and salt as water is mixed and exchanged over a wide range of depths. Mixing extends higher in the water column in the shallower regions of the estuary. Secondary flows could exchange water in shallower regions with more stratified water at the same depth in the center of the estuary and spread the halocline.

---

[1] The decrease in potential energy due to the residual shear acting on the along-channel can be scaled and compared to an estimate of the rate of energy available from vessel traffic for mixing. The decrease of potential energy averaged over the water column is 6×10^{-7} W kg^{-1}, using an along-channel salinity gradient of 0.0003 m^{-1} and assuming a linear velocity profile with a shear of 0.2 s^{-1} over the water column. The rate of energy from vessel mixing available for buoyancy flux is estimated at 10^{-7} W kg^{-1}, assuming 4 tugs per day traveling at 1 knot and delivering 500 hp to a cross sectional area of 13,000 m^2 with a 10% efficiency. The calculation suggests that vessel traffic is not instrumental in determining the stratification in the estuary but is capable of altering the structure of the upper few meters.

2.6 Summary

The results in the chapter illustrate the variation of salt transport due to an along-channel salinity gradient and a tidal flow. The trends in estuarine and oscillatory salt transport are similar whether the vertical mixing is parameterized with constant or variable eddy coefficients. The estuarine salt transport is the dominant mechanism of salt transport with increasing along-channel salinity gradient, decreasing tidal velocities, and deeper water columns. The oscillatory salt transport is more important for the opposite conditions and is less sensitive to variations of the parameters.

Despite the similar variation, much of the salt transport in the model is the result of the temporal and spatial variability of the eddy coefficients. For runs in which $Ri_x > 0.33$, a reduction of mixing near the surface produces a thin, nearly-inviscid layer, creating a steadily increasing estuarine salt transport and a much smaller, highly variable oscillatory salt transport. For runs in which $Ri_x < 0.33$, the estuarine salt transport is principally due to tidal asymmetry, the result of tidal covariances of velocity and salinity with the eddy coefficients. Variations in the eddy coefficients are also responsible in part for the tidal variations of the vertical fluxes of salt that determine the oscillatory salt transport. The model results indicate that although the trends in salt transport are similar to the salt transport with constant eddy coefficients, the magnitude and variation of salt transport depends inherently on the temporal and spatial variations of vertical mixing.

A comparison of the model results with velocity and salinity observations from the Hudson Estuary shows several discrepancies that prevent the model from providing a realistic, quantitative prediction of salt transport. Most significantly, the model produces considerably more stratification during the neaps than is observed in the estuary. Although missing sources of mixing and secondary flows would bring the model stratification closer to that observed, the tendency of the Mellor-Yamada 2.5

closure to overpredict strong stratification (Simpson et al. 1996; Stacey et al. 1999) and underpredict weak stratification (Stacey et al. 1999) may explain much of the discrepancy.

Chapter 3

Salt transport in the Hudson Estuary

3.1 Introduction

According to the estuarine classification scheme of Hansen and Rattray (1966), landward salt transport in partially-stratified estuaries, such as the Hudson Estuary, is primarily due to estuarine salt transport with tidal dispersion playing a more minor role. Observational evidence supports this claim. Based on shipboard velocity and salinity profiles over two four-day periods, Pritchard (1956) hypothesized that the salt balance of the James Estuary was primarily between estuarine salt transport and the transport of salt due to the net outflow. He postulated that this should be true of other partially-stratified estuaries. Hunkins (1981) also observed that estuarine salt transport was the dominant contribution to landward salt flux from a 25-hour series of measurements at a section in the Hudson Estuary. Neither study addressed the spring-neap variability of salt transport or assessed the contributions of each mechanism to the longer-term salt balances.

Spring-neap fluctuations in the mechanisms of salt transport should be most evident in partially-stratified estuaries, where stratification has been observed to alternate between well-mixed and highly-stratified conditions over the spring-neap cycle (Haas 1977; Jay and Smith 1990). Nunes and Lennon (1987) observed an increase in salt transport in Spencer Gulf due to an increase in stratification and circulation during neap tides. They noted that the strength of the residual circulation during neap tides was much greater than the strength necessary to maintain the annual salt balance. Nunes Vaz et al. (1989) proposed that pulses of estuarine salt transport during neap tides are a dominant factor in determining the longer-term salt balance in estuaries.

The spring-neap tidal cycle should also modulate the magnitude of tidal dispersion. Mechanisms of tidal dispersion are believed to increase with increasing amplitude of the tidal velocity (Geyer and Signell 1992; Fischer et al. 1979; Smith

1980), and provide most of the salt transport during well-mixed conditions (Hansen and Rattray 1966; Fischer 1976). Smith (1980) derived a complete description of estuarine and oscillatory salt transport for a well-mixed estuary with a uniform cross section. Although his solutions potentially describe salt transport mechanisms for well-mixed conditions, observational verification has proved difficult (West and Mangat 1986).

Several issues of temporal and spatial sampling arise when interpreting salt transport mechanisms from observations. An accurate estimate of salt transport requires measuring the residual circulation and stratification, quantities that are usually much smaller than the tidally-varying fields, and determining the phase shift between tidal fields to within minutes. Another complication is the large number of variables that could potentially change the magnitude of salt transport during any given study. Without a way of gauging the sensitivity to tidal strength, magnitude of the longitudinal density gradient, river flow, and the local bathymetry, a measurement of salt transport often ends up as one number meaningful only for those specific conditions (van de Kreeke 1990; Jay et al. 1997).

The sensitivity of salt transport mechanisms to the specific bathymetry of an observational location is potentially the most troublesome unknown. Many theoretical and numerical studies of salt transport mechanisms have considered estuaries of a uniform cross-section (Fischer 1972; Smith 1980; Scott 1994), but several studies suggest measurements of tidal dispersion may be complicated by the three-dimensional nature of circulation and stratification. Dronkers and van de Kreeke (1986) suggested that variation in cross sectional shape creates an oscillatory flux, that they call the "non-local" salt transport, whose magnitude is a function of a variation of topography within a tidal excursion rather than processes responsible for the overall salt transport in an estuary. Geyer and Nepf (1996) illustrated one such process in which the tidal flow through a constriction deflected the halocline,

69

producing a large value of tidal dispersion that diminished away from the constriction. Given the sensitivity to bathymetry, the first place to measure and interpret salt transport is at a uniform cross-section where salt transport mechanisms should be closest to those addressed in quasi two-dimensional studies.

Because of the difficulties of measuring salt transport, many studies have estimated the transport indirectly. In these studies, salt transport is found by measuring the freshwater flow and the distribution of salt along the channel, assuming a steady salt balance, and calculating the necessary landward salt transport (Fischer et al. 1979; Posmentier and Raymont 1979; van de Kreeke 1990). However, the distribution of salt is the integrated history of salt transport and does not necessarily reflect the magnitude of salt transport at the time of measurement. If the salt balance is unsteady, this indirect estimate of the salt transport is erroneous (Fischer et al. 1979; Uncles and Radford 1980). The salt balance can only be assessed with measurements of both the salt transport and the salt content of an estuary. Although some studies have found variations in salt transport and corresponding changes in the length of the salinity intrusion (Lewis and Lewis 1983; Jay and Smith 1990; Uncles et al. 1990; Uncles and Stephens 1996), there have been no studies in which the salt content and salt transport have been independently measured with adequate precision to constrain the time-dependent salt balance.

In this chapter, I examine the mechanisms and variability of salt transport in the Lower Hudson Estuary from a 70-day moored time series. The long time series resolves oscillatory motions that would create large errors in short-term salt transport estimates and provides several realizations of the spring-neap cycle and the resulting variability of salt transport. The measurements were collected during a period of relatively constant freshwater flow, so, unlike most studies, variability of salt transport during most of the deployment is primarily due to one external factor, the spring-neap tidal cycle. In addition, the measurements were made in the straightest

70

section of a single-channel estuary where the mechanisms of salt transport should be most easily interpreted.

A central part of the study concerns the spatial structure of salt transport and the signature of the mechanisms that produce it. The results from Chapter 2 and a three-dimensional model are used to postulate the structure of salt transport at the cross section and estimate the cross sectional average necessary for the salt balance. Finally, the estimates of total integrated salt transport at the section are compared to a sequence of measurements of the salt content of the estuary to assess the salt balance.

The next section includes a description of the observational program in the Hudson Estuary and the environmental conditions during the experiment. Section 3.3 describes the methods used to calculate the salt transport and the salt content of the estuary. The results of the salt content calculations are shown in Section 3.4. Estimates of each mechanism of salt transport at the experiment site are shown in Section 3.5. A discussion of lateral structure and spring-neap variability follow in Section 3.6. Sections 3.7 and 3.8 discuss the salt balance of the estuary and a scaling for the adjustment time. The conclusions of the chapter are summarized in Section 3.9.

3.2 Observations

The measurements used in the study are part of a larger experiment funded by the National Science Foundation and jointly carried out by scientists and staff at the Woods Hole Oceanographic Institution and the State University of New York, Stony Brook. The study had several objectives, including quantifying the turbulent transport of momentum, the momentum balance, and the salt balance. A summary of the project can be found in Fredericks et al. (1998) and results of the analysis

in Trowbridge et al. (1999), Geyer et al. (1999), and Peters and Bokhorst (1999). This study focuses on one aspect of the project goals: quantifying the variability of longitudinal salt transport and its effect on the salt balance of a partially-stratified estuary.

3.2.1 Site description

The Hudson Estuary (Figure 3.1) is a river valley system whose lower reaches have been inundated by the ocean in the last 12,000 years (Coch and Bokuniewicz 1986). Tidal influence extends 250 kilometers from the Battery at the tip of Manhattan Island to the Green Island Dam at Troy. Approximately 75% of the freshwater enters the river above the dam. Five main tributaries in the lower watershed contribute most of the additional flow, almost all of which join the Hudson upriver of the salinity intrusion. The landward extent of salt, which defines the extent of the estuarine portion of the system, lies well below the dam. It can range between Poughkeepsie (Figure 3.2), 120 kilometers above the Battery, and Yonkers, 30 kilometers above the Battery, depending on the freshwater flow (Abood 1974; Wells and Young 1992), and is typically 80 km north of the Battery during low discharge (Abood 1974).

At the Battery, the Hudson Estuary joins New York Harbor, which eventually connects with the ocean 35 km south of the Battery (Figure 3.2). The Hudson is connected directly to the East River by the Harlem River, a small channel which separates Manhattan Island from the mainland.

The main measurement effort took place in the Lower Hudson Estuary off Manhattan Island (Figure 3.3). This site was chosen because the regular bathymetry provided one of the simplest estuarine settings in which to measure the salt and momentum balances. The measurement program took place in late summer to take advantage of several environmental conditions: winds are weak during this season,
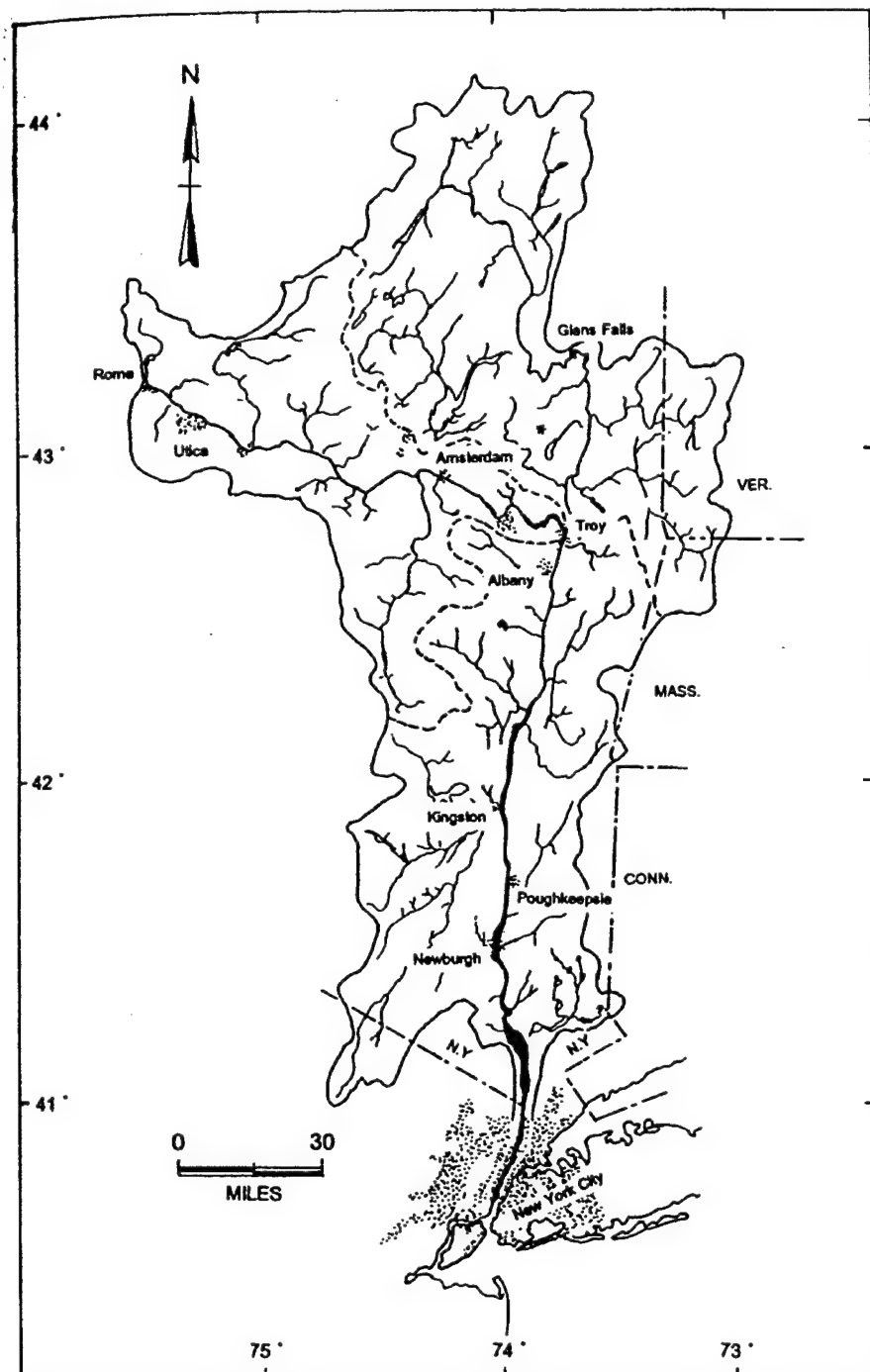
Figure 3.1: Hudson River basin showing tributaries (reprinted by permission of the State University of New York Press from <u>Estuarine Research in the 1980s</u> by C. Lavett Smith, 1992, State University of New York, All Rights Reserved).

73
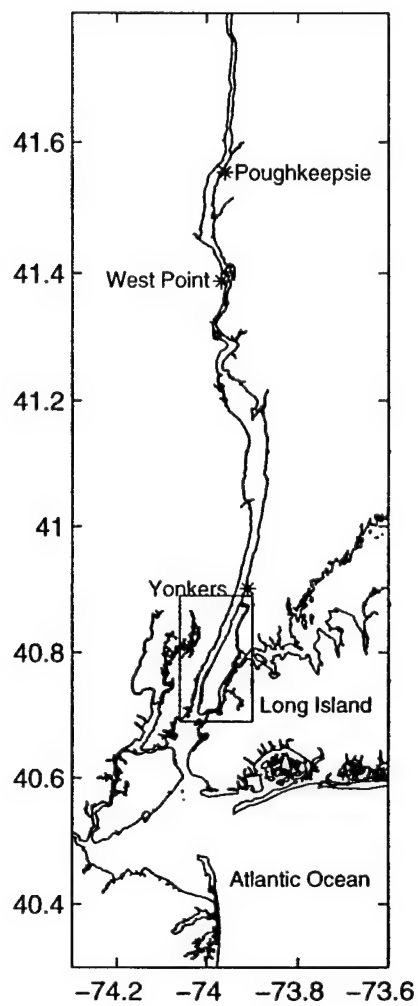
Figure 3.2: The Hudson Estuary. The box indicates the main site of the HUDMIX experiment.
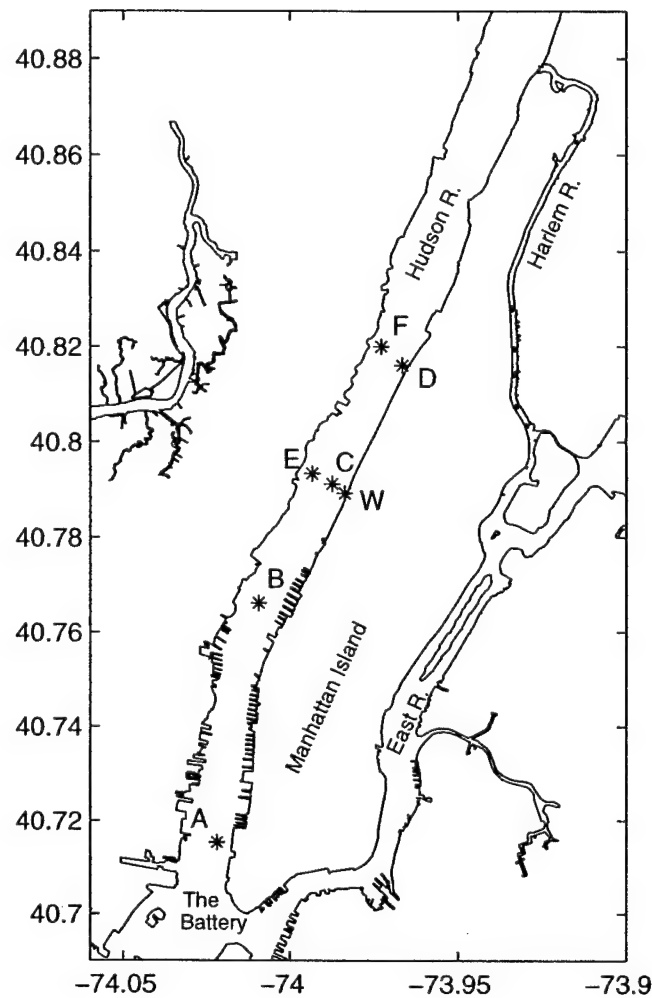
Figure 3.3: Mooring sites of HUDMIX. Sites A, B, D, E, and F are bottom tripods. Site C is the central mooring. Site W is the location of the meteorological package.

freshwater flow is relatively constant, and previous studies reported periods of stratification necessary to test the proposed questions.

3.2.2 Measurement program

The measurement program consisted of a seventy-day deployment of moored instruments from August 15 to October 26, 1995, and two short-term shipboard studies at the beginning and end of this period. A central mooring was situated in the middle

of the straightest section of the estuary, 10.5 kilometers upriver from the Battery, where the width is approximately one kilometer (Figure 4, location C). The site lay approximately one tidal excursion ($\approx$ 10 kilometers) from the Battery. It was chosen so that water parcels sampled at the mooring remained within the well-defined channel of the estuary throughout a tidal cycle. The mooring supported six temperature/conductivity sensors (Figure 3.4) that were used to estimate salinity for salt transport calculations. The uppermost conductivity sensor, an S4 electromagnetic instrument 3 meters below the surface, was fouled after eighteen days and was not used after this time. Occasional periods of inverted stratification from the temperature and conductivity records of the five Seacats on the mooring were attributed to sediment accumulating in and flushing out of the conductivity sensor tubes. Corrections were based on the assumption that the water column was never unstably stratified, but that it approached well-mixed conditions in the boundary layer at the end of flood tides, consistent with profiles from shipboard CTD casts. The size of the corrections are an order of magnitude smaller than the tidal signal.

An upward-looking 1.2 MHz Acoustic Doppler Current Profiler (ADCP) was deployed approximately 150 meters away from the main mooring (Figure 4, between locations C and E). This provided velocity measurements at one meter intervals throughout most of the water column (Figure 3.4). The velocities were used to estimate salt transport at the center of the section. The velocity profiles had a zigzag structure that diminished with height and appeared to be an artifact of signal processing internal to the instrument. Discrepancies between bins were included in the error estimates.

Five bottom tripods and two surface buoys were deployed along and across the channel to provide measurements of the spatial structure of pressure, conductivity, temperature, and velocity (Figure 4, locations A, B, D, E, F). Estimates of salt transport were made at the locations of the D, E, and F tripods to provide some
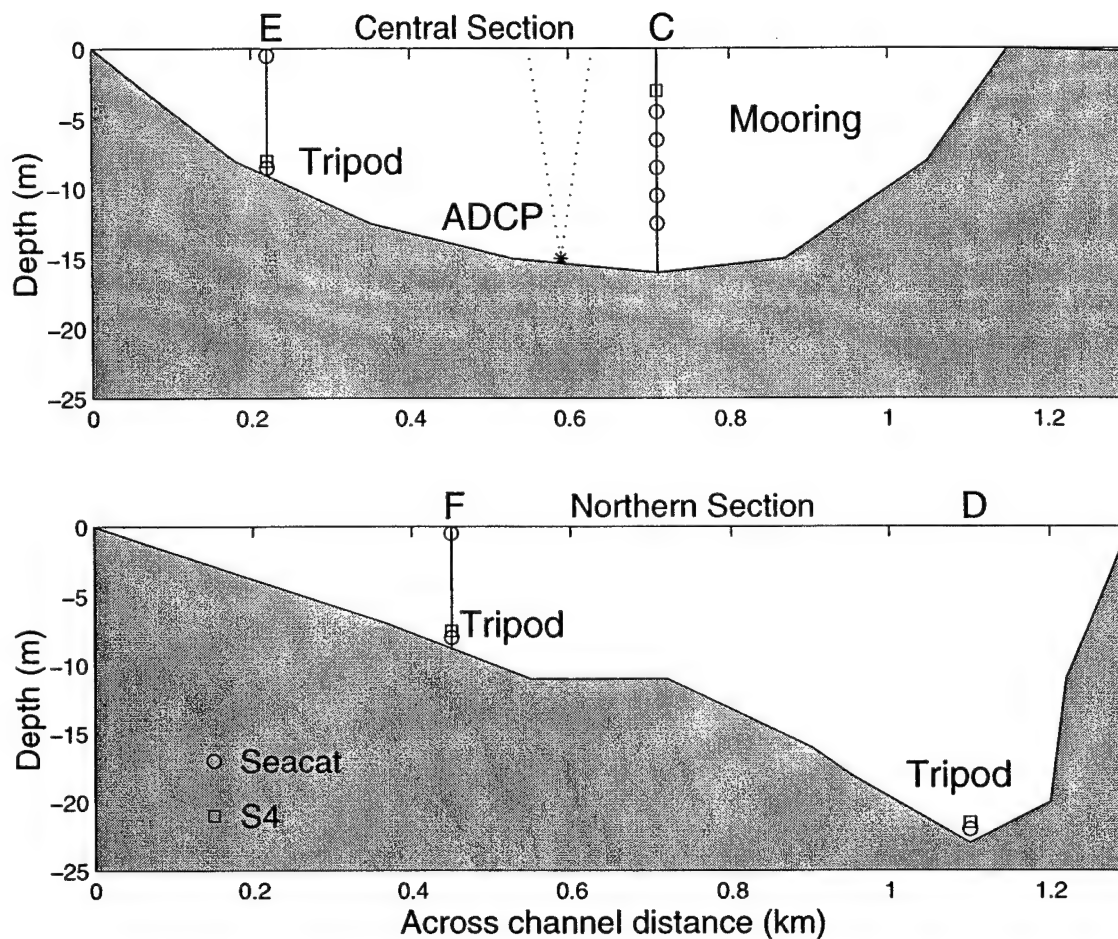
Figure 3.4: a. Cross section at the central mooring site looking upriver (New York to the right, New Jersey to the left). A mooring with six conductivity/temperature sensors was deployed in the center of channel at site C. An upward-looking ADCP was deployed 150 meters away. At site E, on the New Jersey side, a bottom tripod and surface mooring were deployed. b. Cross section three kilometers north of the central site contained two bottom tripods. The D site was in the center of the channel; the F site was on the shallower side.

information about the lateral variability. These three tripods were equipped with both S4 current meters and either Seacat or Seagauge temperature/conductivity sensors. The conductivity sensors were fouled within several weeks of the deployment and these records were not used beyond these points.

Meteorological observations were made from a Weatherpak system, including an anemometer, barometer, and thermometer, which was located on a piling near the Manhattan shore directly across from the central mooring (Figure , location W).

At the beginning and end of the seventy-day moored time series, two short-term studies were conducted, each approximately two weeks in length and capturing both neap and spring tidal conditions. During the short-term studies, the spatial structure of the velocity and salinity fields around the moorings were sampled by a shipboard CTD (Ocean Sensors OS200) and a shipboard ADCP (1.2 MHz RDI). The lateral (across-channel) transects are used in this study to estimate the spatial structure of velocity and salinity around the moored measurements.

The large-scale density structure of the estuary was sampled in four longitudinal (along-channel) transects from the Battery to the full extent of the salinity intrusion (to less than 1 depth-averaged salinity). These transects were made at the beginning and end of both short-term studies providing two surveys of the entire density structure of the estuary during neaps and two surveys during springs. Figure 3.5 shows three of these surveys. Each survey provided an estimate of the salt content of the estuary.

3.2.3 Environmental conditions

Freshwater flow

Freshwater flow at the Green Island dam and five main tributaries in the lower watershed are gauged by the USGS. Peak freshwater flow in the Hudson River
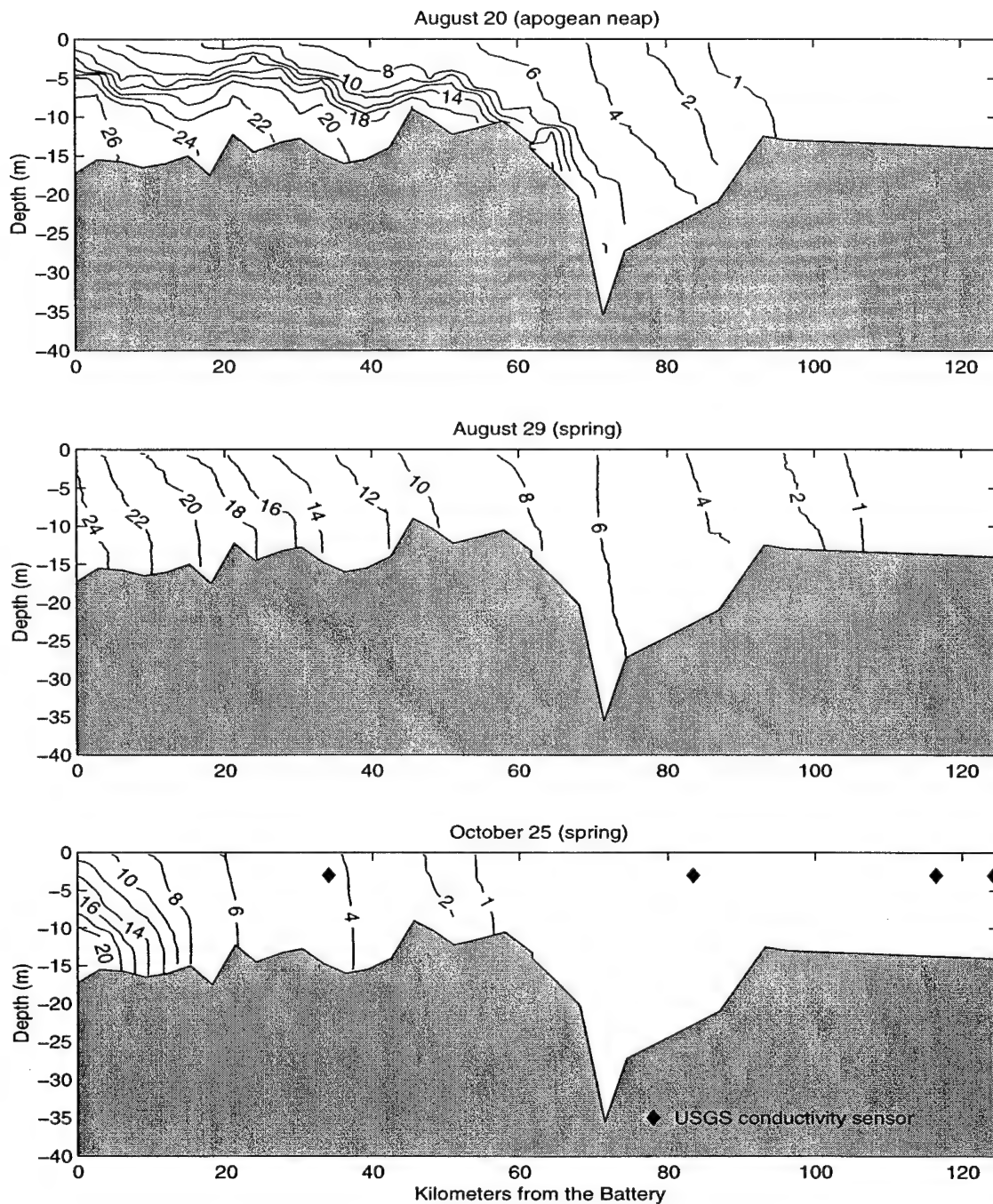
Figure 3.5: Longitudinal surveys of salinity in the Hudson Estuary. Surveys begin at the Battery and the distances given are in kilometers along the river. The central mooring, Yonkers, West Point, and Poughkeepsie are at river kilometer 10, 34, 70, and 120, respectively. a. August 20 (Day 231), apogean neap tides. b. August 29 (Day 240), spring tides. c. October 25 (Day 297), spring tides after large rainfall event. USGS conductivity sensors (diamonds) provide estimates of salinity throughout the experiment period.

79
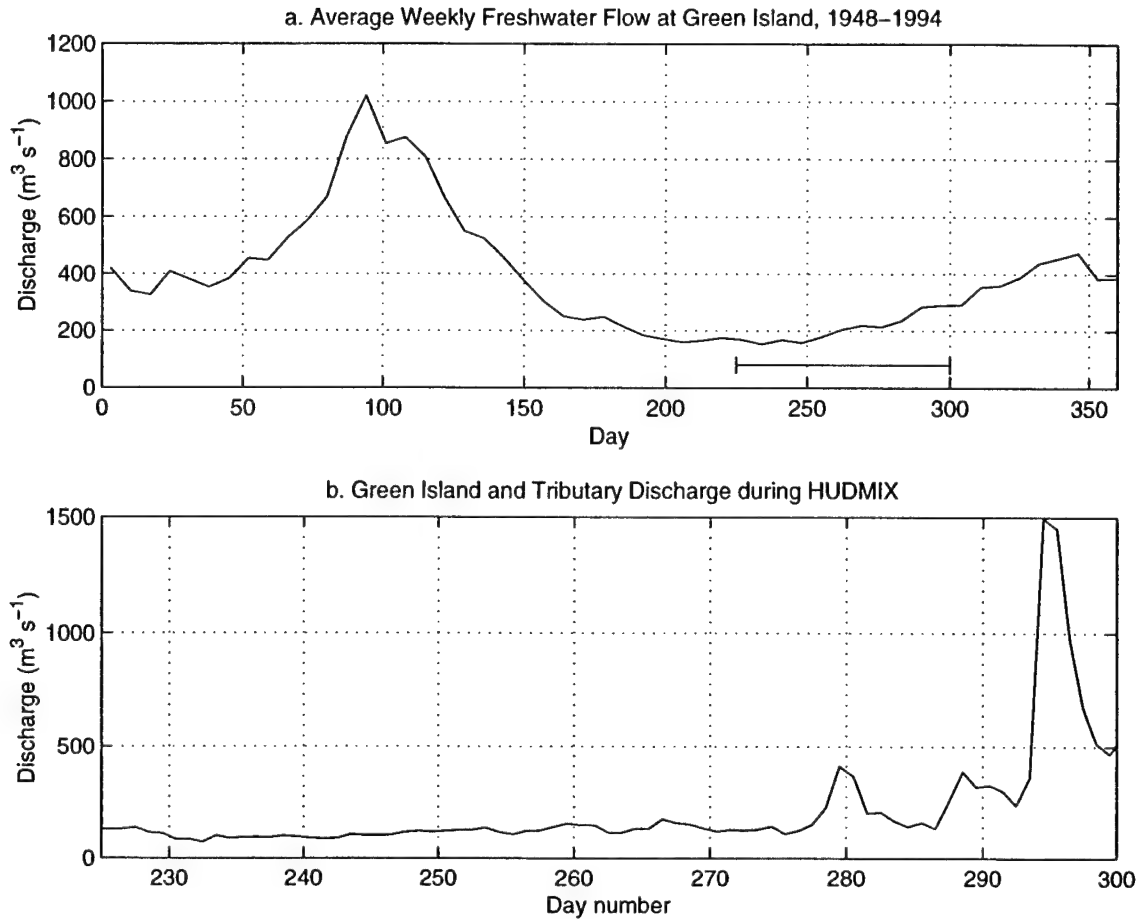
Figure 3.6: a. Freshwater flow at the Green Island dam averaged by week for all years between 1948 and 1994. b. Freshwater flow from the Green Island dam and five major tributaries during the HUDMIX experiment.

occurs from March through May (day numbers 60–150) when the snow pack melts (Figure 3.6a). Flows taper off to a minimum during the late summer. Autumn storms end the dry season in late September.

The experiment was conducted during the summer of 1995 during a period of severe drought (Figure 3.6b). A minimum flow rate of 100 m^3s^{-1} was maintained at the Green Island dam to prevent the salinity intrusion from compromising drinking water quality at Poughkeepsie. In late August, the salt content of water at Poughkeepsie briefly rose above allowable drinking water standards. About 25 m^3s^{-1} of

water was released from a reservoir in the Upper Hudson watershed starting September 3 (day number 245) in order to halt the advance of salt (DeVries, personal communication). Two small storms on October 6 and 14 (day numbers 278 and 286) brought rain to the watershed and ended the drought. A week later, during the last days of the experiment, a severe fall storm battered the region and freshwater flow rates increased fifteen-fold.

Meteorological forcing

Weather systems during late summer pass by on roughly three-day cycles as shown by the fluctuations in barometric pressure (Figure 3.7a). As the fall begins, the magnitude and period of the weather systems increase. Storms passed through the area on October 6, 14, and 21 (days 278, 286, and 293) corresponding to the subsequent increases in freshwater flow. Wind variability (Figure 3.7b) has roughly the same periodicity as the atmospheric pressure fluctuations, but the buildings of Manhattan shielded the estuary from the strong October storms that came from the Atlantic. The wind stress was, at most, 10% of the bottom stress, the latter which is mainly due to tidal velocity. In addition, the direction and magnitude of wind stress did not appear to correlate with the surface mixed layer depth (see extrapolation section of Appendix B). For these reasons this study does not consider the effects of the wind on salt transport.

Tidal forcing

The tidal pressure gradient is the strongest pressure gradient driving flow in the estuary. The semidiurnal tides have the largest magnitude, as can be seen in the sea level record (Figure 3.8a), with about 90% of the variance. The amplitude of the semidiurnal tidal sea level (Figure 3.8b) has a fortnightly spring-neap cycle due to the beat frequency of the M2 (principal lunar) and S2 (principal solar) frequencies, and
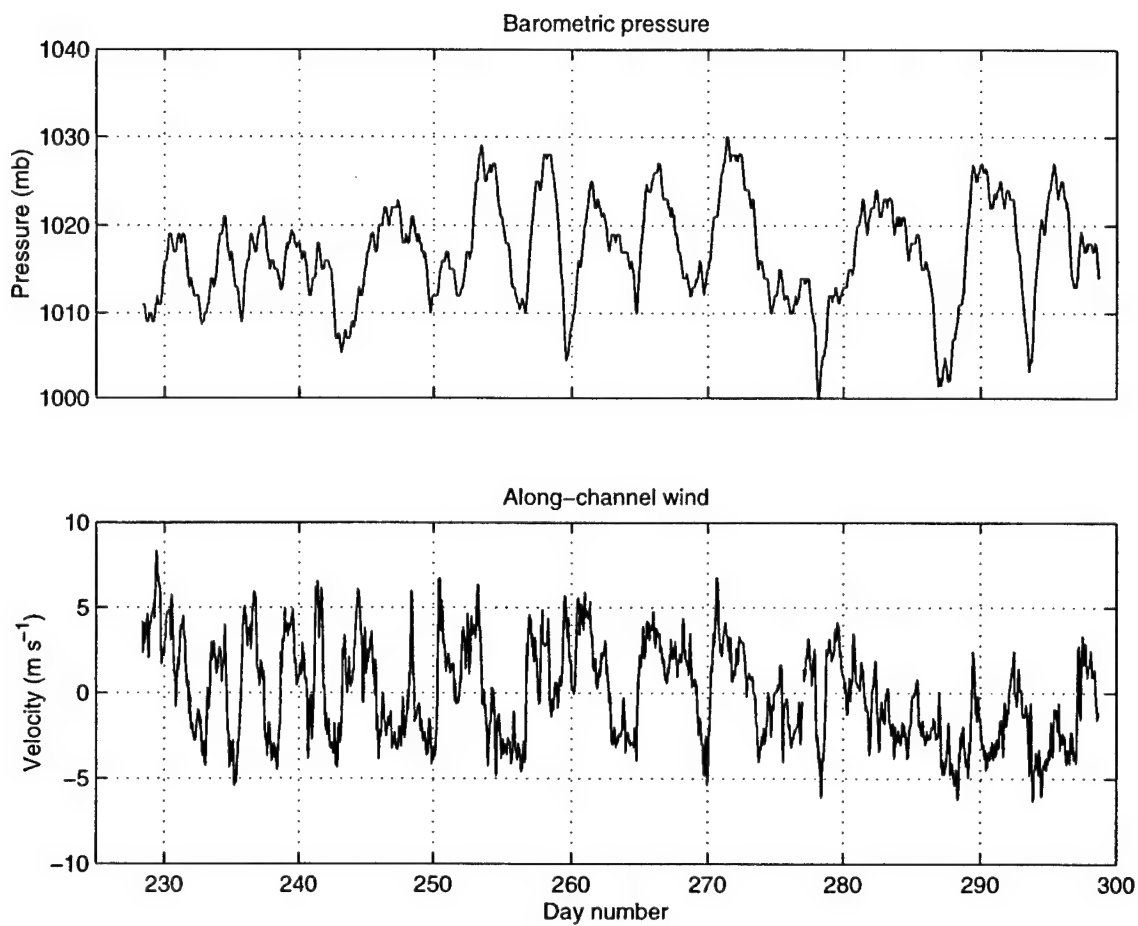
Figure 3.7: a. Barometric pressure at site W during the HUDMIX experiment. b. Along-channel wind at site W. Direction of maximum variance of the wind is along the main channel of the estuary.
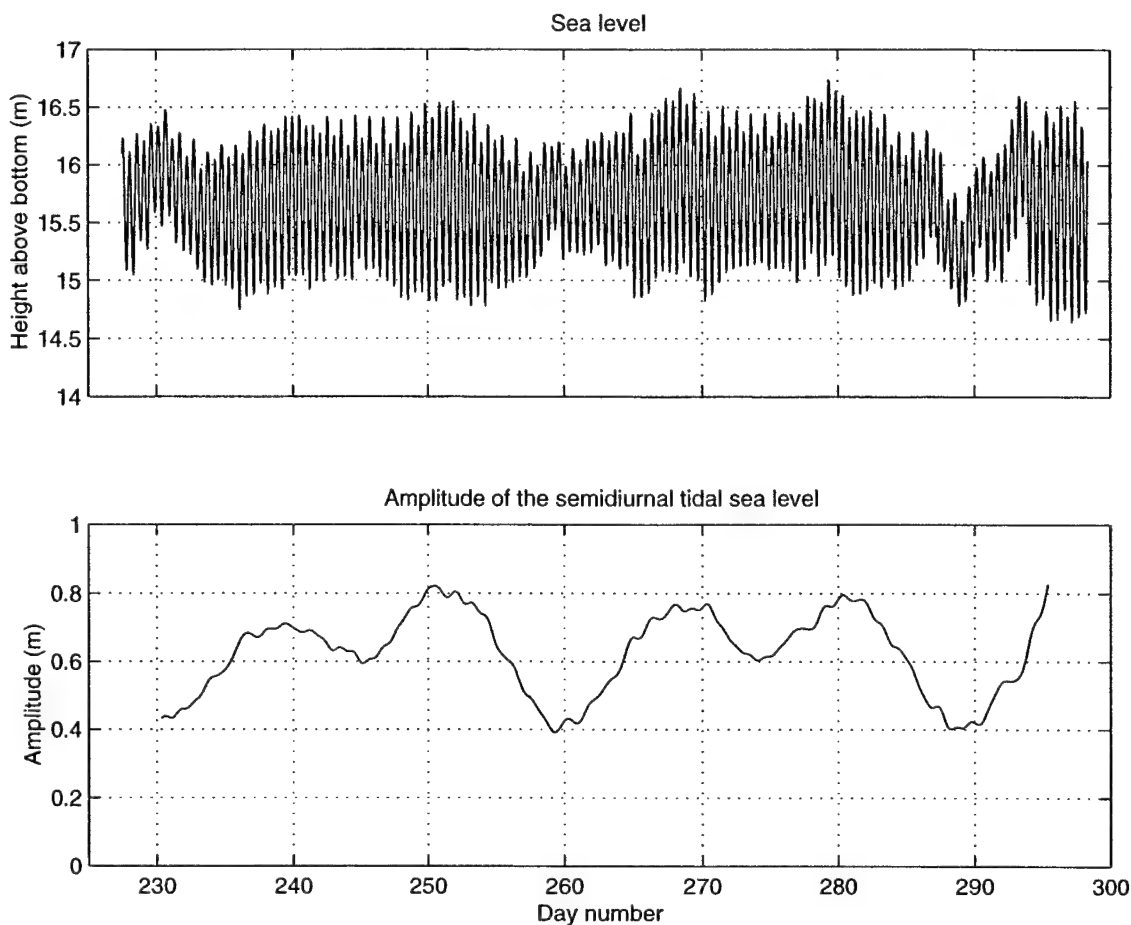
Figure 3.8: a. Sea level calculated from seagauge pressure measurements at the A tripod. b. Amplitude of the semidiurnal tidal sea level.

a monthly variability due to the beat of the M2 and N2 (lunar elliptic) frequencies. When the moon is near apogee, the furthest point in its elliptic orbit around the earth, the tidal energy is weakest. These weak neap tides will be referred to as the apogean neaps. The stronger neaps that occur when the moon is near perigee will be referred to as the perigean neaps. The remaining 10% of the sea level variance is contained in the diurnal tides, the 2-3 day weather band oscillations, and the higher frequency tidal harmonics.

Variability of velocity and salinity

Before calculating salt transport it is informative to look at the variations of velocity and salinity observed in the estuary during the deployment. The velocity measurements from the ADCP bin centered at 4.5 meters above the bottom (about 11 meters below the surface) illustrate the variability of the tidal forcing (Figure 3.9a). Velocities are of greatest magnitude during the spring tides. The currents are weakest during the apogean neaps which occur three times, at the beginning, middle, and near the end of the seventy day record (marked by 'A' in the figure). Tidal velocities diminish slightly from spring magnitudes during the two perigean neaps.

A low-pass filter (Limeburner 1985) was used to remove the semidiurnal and diurnal tidal flow from the lower frequency residual circulation. The residual velocity from the ADCP measurements (Figure 3.9b) has the characteristic features of estuarine circulation. Flow is into the estuary (positive) at depth (dashed line, from measurements 4.5 meters above the bottom) and out of the estuary (negative) near the surface (solid line, 11.5 meters above the bottom). Shear between these two levels increases, during apogean neaps, to a maximum of 30 cm s^{-1} over the 7 meters separating the measurements (Figure 3.9c). The velocity difference diminishes during spring tides to about 10 cm s^{-1}. The velocities at both levels and the shear between them are modulated by two to three day weather band fluctuations.

Salinity estimates from a moored temperature and conductivity sensor approximately 4.5 meters from the surface (about 11 meters above the bottom) show tidal variability of 5 to 10 (Figure 3.10a). The residual salinity at 4.5 meters below the surface (Figure 3.10b) remains relatively constant for the first fifty days of the experiment and then freshens in response to the increased freshwater flow. Salinity 11.5 meters below the surface increases during the three apogean neaps and then freshens towards the end of the record, especially during the largest storm. There
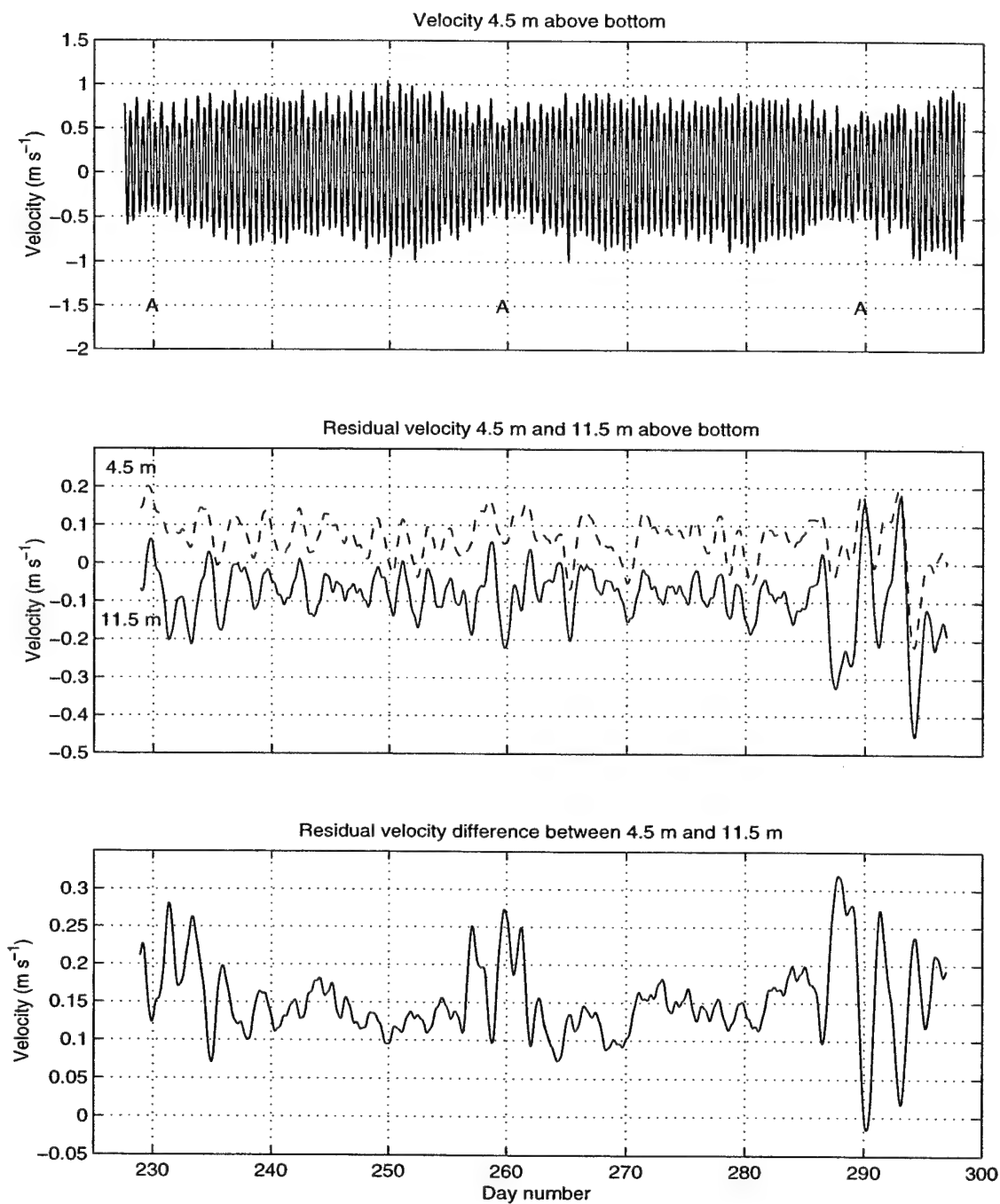
Figure 3.9: a. Velocity 4.5 meters above the bottom from the moored ADCP near site C. Flow into the estuary is positive. b. Residual velocity at 11.5 (solid line) and 4.5 meters (dashed line) above the bottom. c. Difference between 4.5 and 11.5 meter residual velocities.
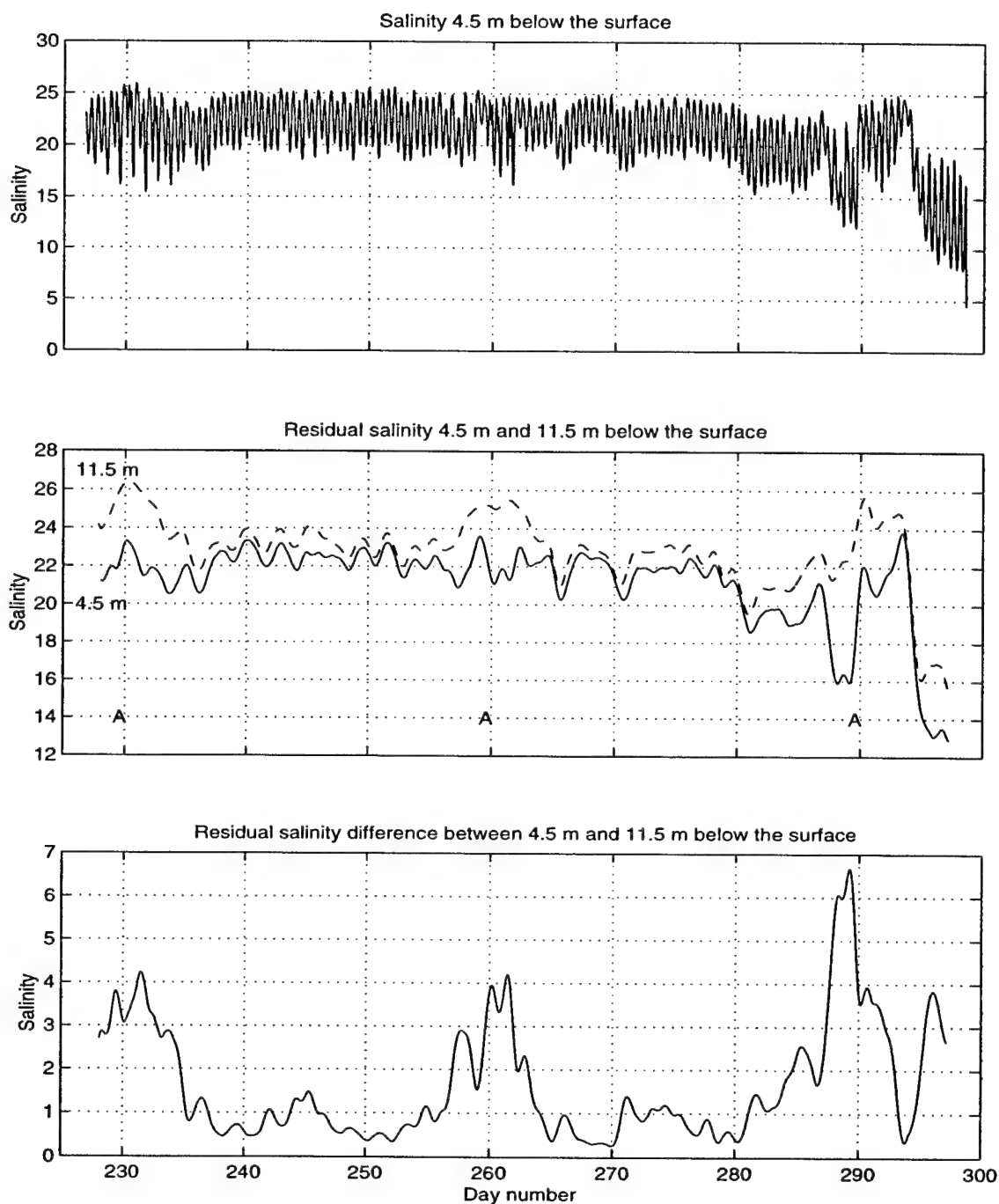
Figure 3.10: a. Salinity estimates from the sensor 11 meters above the bottom on the central mooring. b. Residual salinity estimates from two mooring sensors located 11 meters (solid line) and 4 meters above the bottom (dashed line). c. Residual salinity difference between the sensor 4 meters above the bottom and the sensor 11 meters above the bottom.

86

are also many fluctuations with periods of two to three days in which both the upper and lower parts of the water column grow fresher or saltier simultaneously. These correspond to, and are approximately in quadrature with, the residual variations of velocity, indicating advection of salinity.

The residual salinity difference between 4.5 and 10.5 meters clearly shows a spring-neap signal (Figure 3.10c). During the apogean neaps, the salinity difference across these 6 meters increases by a factor of eight from spring magnitudes. The stratification increases slightly during the perigean neaps, but only by about a factor of two. After the last apogean neap in the observational record, the stratification reaches low spring values and then increases in response to the sudden increase in freshwater flow. Despite the high spring tidal energy available for mixing, the stratification after the storm equals that of the previous apogean neaps.

Shipboard CTD and ADCP surveys at the central section provide estimates of the transverse structure of the velocity and salinity (Figures 3.11 and 3.12). During neap tides on August 18 (Figure 3.11), the ebb velocity has a subsurface maximum located in the pycnocline. By the end of ebb, stratification is present throughout most of the water column. At the end of flood, the pycnocline is high in the water column, overlying a thick well-mixed layer. During spring tides on August 28 (Figure 3.12), the maximum velocities are at the surface during both flood and ebb. The stratification is much weaker than stratification during neap tides, but it has similar tidal variation. Most of the stratification is confined to the upper five meters at the end of flood and then spreads throughout the water column as the ebb progresses.

The measurements from the E tripod (1 meter above bottom on the shallow, western side of the estuary) provide further information about the spatial structure of velocity, salinity, and salt transport. The amplitude of the tidal velocity at the E tripod, about 9 meters below the surface, is about 20 cm s^{-1} less than the amplitude at the same level in the center of the channel (Figure 3.13a). Tidal velocity at the

87
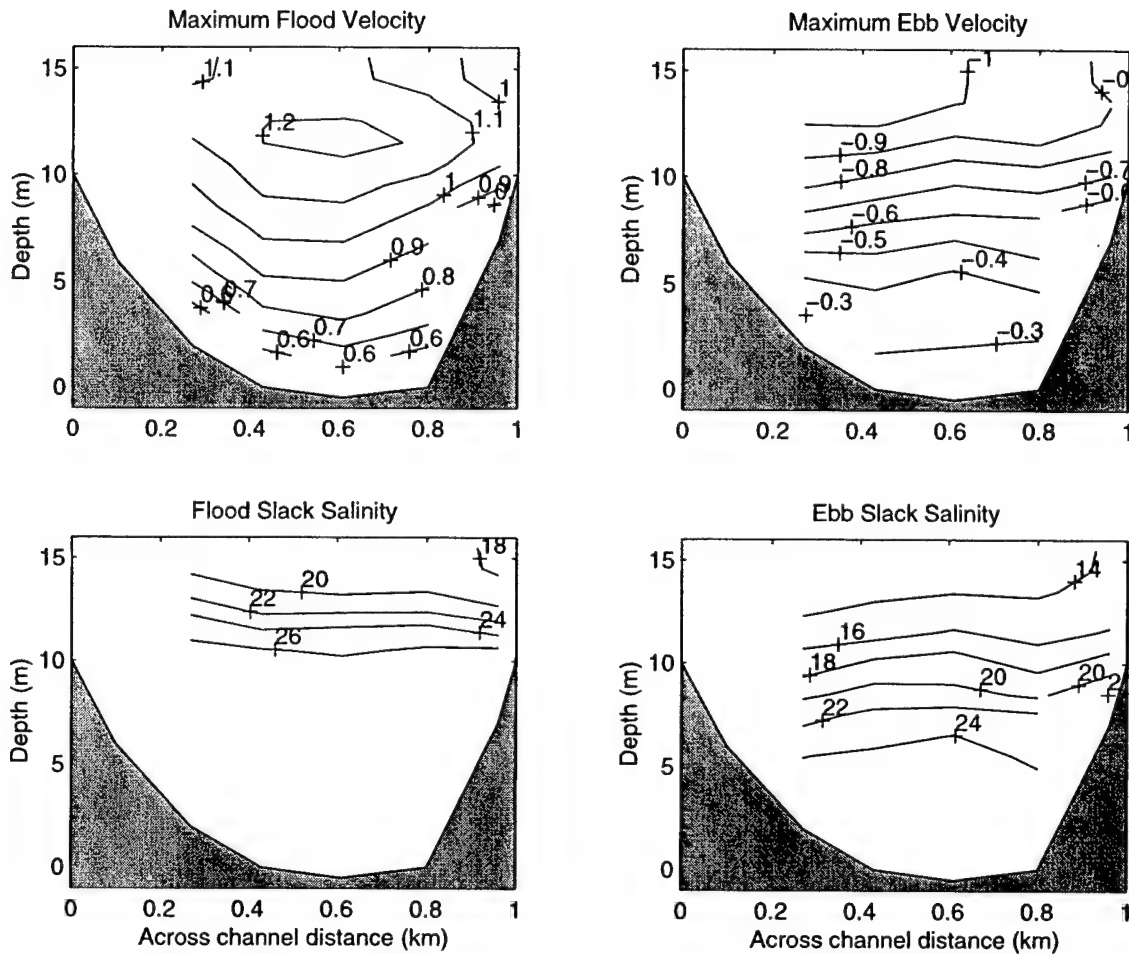
Figure 3.11: Salinity and velocity fields at the central cross section during one tidal cycle on August 18 (Day 230) during neap tides. Shipboard ADCP and CTD transects were interpolated to provide synoptic pictures of (a) maximum flood velocity, (b) maximum ebb velocity, (c) salinity at flood slack, and (d) salinity at ebb slack.
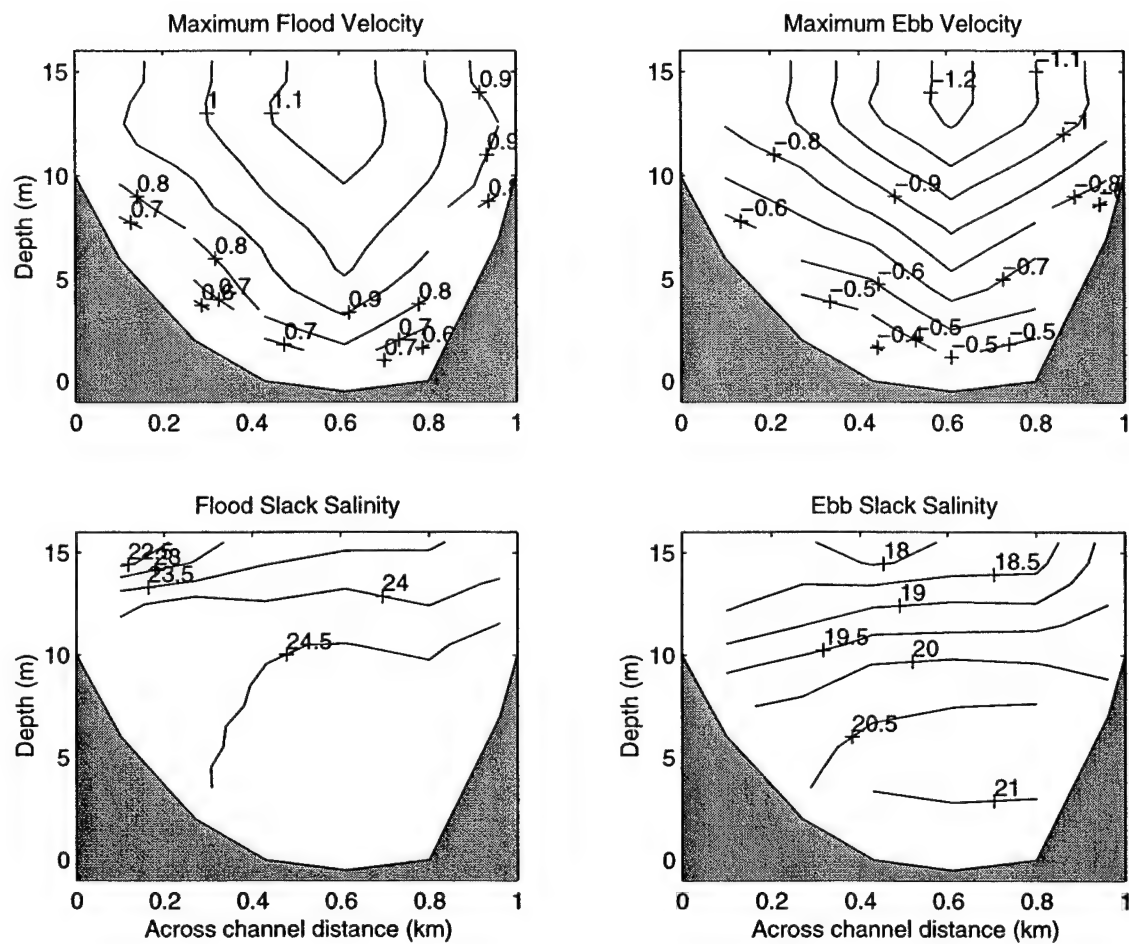
Figure 3.12: Same as Figure 12 but for a spring tidal cycle on August 28 (Day 239).

edge of the bank leads the tidal velocity at the center of the channel, indicating stronger frictional effects, which is to be expected, as the velocities at the edge of the bank are closer to the bottom boundary. The phase difference between the tidal velocities on the bank and at the mooring increases during neap tides and decreases during springs (Figure 3.13b).

Residual velocity at the E tripod (Figure 3.13c) is seaward for most of the deployment, except for a period of landward velocity during the second and third apogean neap tide. In contrast, the residual velocity at the center of the channel at both this level and 1 meter off the bottom is landward. The velocity difference across the channel is about 20 cm s^{-1}, which is similar to the vertical residual velocity difference at the central mooring.

For the first eight days, when the conductivity sensor on the E tripod Sea Cat was operational, the residual salinity estimates from the Sea Cat are about 2 fresher than the salinities at the same level at the central mooring. The transverse salinity differences during neap tides are much smaller than the vertical salinity differences, which is also apparent in the shipboard measurements.

Velocity and salinity at the D and F tripods, three kilometers upriver of the central section (Figures 3.3 and 3.4), are similar to the patterns of velocity and salinity at the main mooring and the E tripod. Residual flow at the D tripod, located in the deepest part of the channel, is landward, as is the residual flow near the bottom at the central mooring. At the F tripod, located on the shallower, western bank, the residual flow is near zero and occasionally landward.

3.3   Calculations of salt balance terms

A control volume is defined so that one end is far upstream in the river, $x = x_R$, where there is no salt, and the other is at the measurement cross section, $x = x_M$,
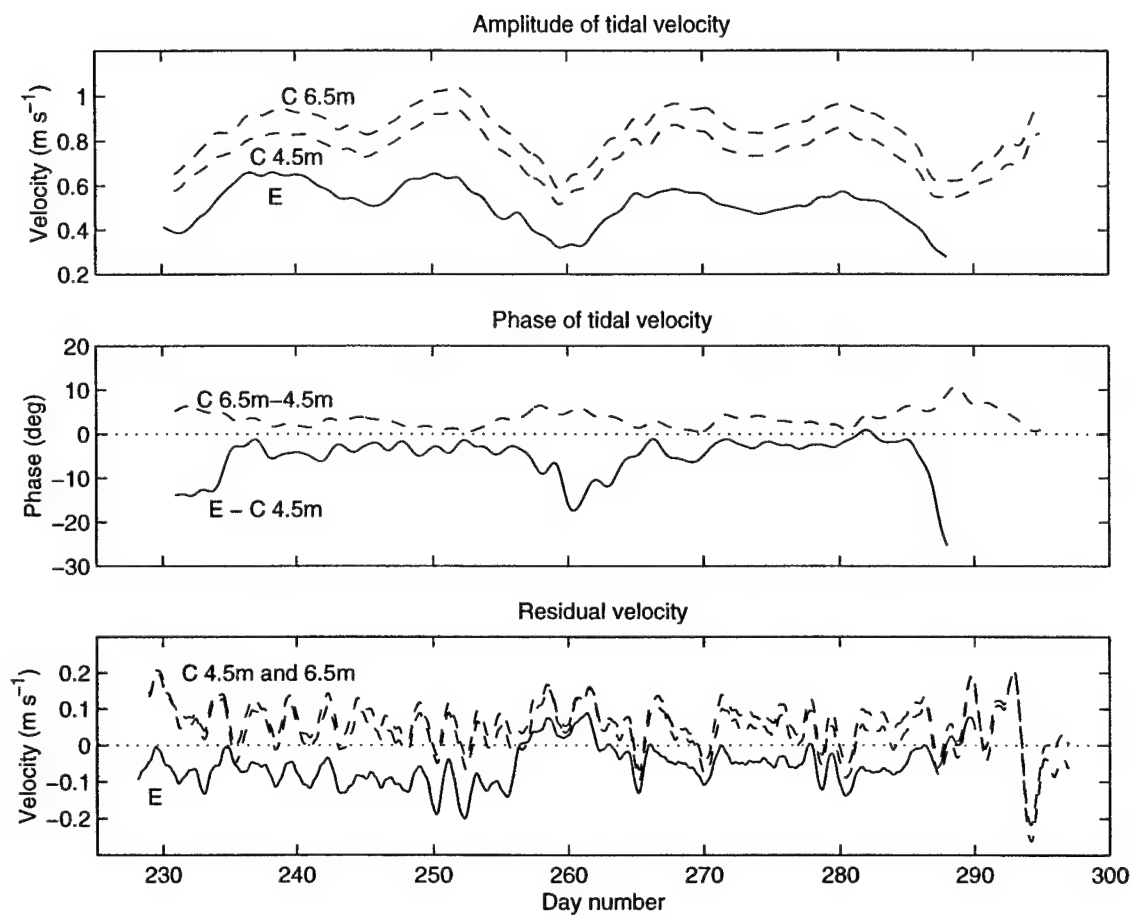
Figure 3.13: a. Amplitude of the semidiurnal tidal velocities at the central ADCP, 11 and 9 meters below the surface (4.5 and 6.5 meters above the bottom) (dashed lines), and at the S4 current meter on the E tripod, 9 meters below the surface (1 meter above the bottom) (solid line). b. Phase difference between the 9 meter and 11 meter tidal velocities at the ADCP (dashed line) and the phase difference between the E tripod and 11 meter ADCP velocity (solid line). c. Residual velocities at the ADCP and E tripod.

91

in the lower estuary. The rate of change of the salt content in this volume is equal to the total salt transport across the measurement cross section.

$$\frac{\partial}{\partial t} \int_{x_M}^{x_R} \overline{A(x)[S]} dx = \overline{A[uS]}|_{x_M} \tag{3.1}$$

Square brackets indicate an instantaneous average over the cross section, $A(x,t)$, and overbars indicate an average over semidiurnal and diurnal tidal cycles (using filter pl33, Limeburner (1985)). Filtered fields will be referred to as tidally-averaged or residual fields.

This balance simply states that any change in the amount of salt in the estuary landward of the measurement cross section must be due to a net salt transport through the cross section. The left hand side of the balance, the time rate of change of the salt content of the estuary, is estimated from hydrography and moored conductivity sensors. The salt transport at the central site in the lower estuary is estimated from measurements at the central mooring and ADCP, bottom tripods, shipboard observations, and spatial structure inferred from a model.

Calculating salt content of the estuary

The salt content of the Hudson Estuary was estimated in four surveys on August 20 (day 231), August 25 (day 240), October 16 (day 288), and October 25 (day 297), from the Battery to the point at which the salinity was 1 (96 km, 110 km, 90 km, and 61 km from the Battery, respectively). CTD casts were taken every three kilometers in the deepest part of the channel. Figure 3.5 shows three surveys, the first during neap tides (day 231), the second nine days later during spring tides (day 240), and the third (Day 288) after a large storm at the end of the drought. Three of the surveys were completed within four hours to minimize the aliasing of the tidal signal (days 240, 288, and 297). In addition, three of the surveys were

taken in the propagation direction of the tidal wave (days 231, 240, and 297). Salt content was estimated by multiplying the cross-sectional area of the estuary at the location of the cast with the depth-averaged value of salinity from the cast for all the casts between the location of the mooring and the 1 location. Corrections and error estimates of the salt content are made by accounting for lower salinity in the shallower parts of each cross section and the phase of the salinity intrusion due to tides (see Appendix B for details). The overestimate of the salt content during neap tide surveys, due to sampling only in the deepest part of the channel, is estimated at less than 20% of the salt content. Uncertainties during spring surveys are estimated at 5% of the salt content.

Additional estimates of the salt content of the estuary are made from an array of four conductivity sensors three meters below the surface, deployed by the USGS to monitor the position of the salt front. The gauges were operational during the entire experiment and provide conductivity at Hastings-on-Hudson (34.0 kilometers from the Battery), West Point (83.4 km), south of Poughkeepsie (116.4 km), and north of Poughkeepsie (124.3 km).

An estimate of the salt content from these sensors was made during the four spring tides when the water column was observed to be well-mixed in the lower estuary and measurements of conductivity at these sensors should more closely reflect the cross-sectional average salinity. The structure of the salinity field in between the conductivity sensors was assumed to follow that observed in the two August hydrographic surveys, since conditions were similar. The value of the salinity at the central mooring and the cross-sectional area as a function of distance along the estuary were also used in the estimate. Errors are based on the uncertainty in the conductivity and temperature measurements and the variability of the salt content produced by meteorological fluctuations. The uncertainty from these estimates is 10% of the salt content (see Appendix B).

Calculating salt transport

The salt transport averaged over the measurement cross section, $\overline{A[uS]}|_{x_M}$ is divided into components corresponding to components of the flow (Geyer and Nepf 1996). The velocity is divided into three components, the tidally-averaged cross-sectionally averaged flow velocity, u_0, the tidally-averaged, spatially-varying flow, u_{est}, and the tidal flow, u_{tide},

$$u = u_0 + u_{est} + u_{tide}, \tag{3.2}$$

where

$$u_0 = \frac{\overline{A[u]}}{\bar{A}} \quad , \quad u_{est} = \frac{\overline{A(u - [u])}}{\bar{A}} \quad , \quad u_{tide} = u - u_0 - u_{est}. \tag{3.3}$$

Dividing the salinity in the same manner,

$$S = S_0 + S_{est} + S_{tide}. \tag{3.4}$$

The salt transport at the cross section is then

$$\overline{A[uS]} = \overline{A[(u_0 + u_{est} + u_{tide})(S_0 + S_{est} + S_{tide})]}. \tag{3.5}$$

In this study salt transport is expressed as a product of velocity and salinity by dividing by the tidally-averaged area of the cross section. The velocity and salinity are multiplied through to yield nine salt components of salt transport

$$\frac{\overline{A[uS]}}{\bar{A}} = u_0 S_0 + [u_{est} S_{est}] + \frac{\overline{A[u_{tide} S_{tide}]}}{\bar{A}} + 6 \text{ cross terms.} \tag{3.6}$$

94

The first term is the salt transport through the cross section due to the residual cross-sectionally averaged flow. The second term is the estuarine salt transport. The third term is tidal dispersion. The remaining terms are cross correlations of the area and the components of velocity and salinity.

Calculating salt transport due to the residual, cross-sectional average flow

After averaging over diurnal and semidiurnal tidal cycles, the residual, cross-sectional average flow, u_0, consists of two to three day weather band variability and the net outflow due to the river. The contribution of the weather band fluctuations of net flow to the salt transport is small (as will be shown in Section 3.5.4).

The net flow due to the river is out of the estuary at all times and produces a salt transport equal to the product of the flow rate and the salinity at the cross section. The salt transport due to the net outflow is estimated by using estimates of the net river flow and the cross channel average salinity. Freshwater flow was estimated from USGS gauges at the Green Island dam and the five major tributaries. An estimate of the cross sectional average residual salinity was made by first filtering the mooring salinity to remove the diurnal and semidiurnal tidal signal and then assuming flat isohalines across the cross section. Transverse shipboard measurements suggest that this estimate of the cross channel salinity has less than 10% error. The errors in the net flow and the cross section salinity produce a combined uncertainty of about 15% (Appendix B).

Calculating salt transport at the central site

The estuarine and oscillatory salt transport are estimated at the central mooring by extrapolating velocity and salinity to the surface and bottom, placing them on a stretched grid (explained below), and calculating the salt transport at each level

95

and averaging over depth.

The velocity and salinity profiles at the central site were extrapolated to the surface and bottom based on other observations. Shipboard measurements show average surface mixed layer thicknesses of one meter and average bottom mixed layer thicknesses of two meters. A parabola was used to match the stratification and shear of the uppermost salinity and velocity measurements to one-meter layers of constant velocity and salinity. Near the bottom a parabola was used to match the stratification and salinity of the lowest two salinity estimates to a two-meter thick mixed layer. Velocities were extended using a log layer up to two meters above the bottom and a parabola matched the log layer to the velocity and shear of the lowest ADCP bin. More details on the extrapolations are contained in Appendix B.

Periods of strong stratification during the second and third apogean neaps in the upper 4.5 meters were not sampled due to the fouling of the uppermost instrument on the mooring. An estimate of this structure was made during the second and third apogean neap tides from the salinity differences observed between the two uppermost instruments during the first apogean neap tides. This extrapolation matched well with shipboard CTD casts during the third apogean neap tides and provides a realistic way of accounting for this structure during these periods of similar conditions.

The velocity and salinity profiles are projected onto a regular vertical grid that expands and contracts with the variable depth. A Lagrangian grid facilitates the salt transport calculation by separating oscillatory salt transport from Stokes drift (Geyer and Nepf 1996). The water depth is estimated from pressure measurements from a sensor mounted on a tripod at the base of the C mooring. The gridded velocity and salinity can now be divided into components corresponding to those previously defined, but now defined relative to depth,

$$u = u_{0h} + u_{esth} + u_{tide} \qquad (3.7)$$

where

$$u_{0h} = \frac{\overline{h < u >}}{\bar{h}} \quad , \quad u_{esth} = \frac{\overline{h(u- < u >)}}{\bar{h}} \quad , \quad u_{tide} = u - \frac{\overline{hu}}{\bar{h}}, \qquad (3.8)$$

where the angle brackets denote averaging over the instantaneous depth.

Salinity is divided into similar components,

$$S = S_{0h} + S_{esth} + S_{tide}. \qquad (3.9)$$

The salt transport at the mooring can be written,

$$\frac{\overline{h < uS >}}{\bar{h}} = u_{0h}S_{0h} + < u_{esth}S_{esth} > + \frac{\overline{h < u_{tide}S_{tide} >}}{\bar{h}} + 6 \text{ cross terms} \qquad (3.10)$$

The first term, $u_{0h}S_{0h}$, was not used because an estimate was made of the cross sectional average of the salt transport, $u_0 S_0$, as described earlier.

The second term, $\overline{< u_{esth}S_{esth} >}$, is the estuarine salt transport calculated at the central site relative to the depth-averaged residual values. Removing the depth-averaged fields removes the transverse structure of velocity and salinity leading to an underestimate of the estuarine salt transport in the center of the channel. However, much of the salinity structure is in the vertical (see Figures 3.11 and 3.12), especially during neap tides when the estuarine salt transport is greatest. The spatial structure of the estuarine salt transport will be considered further in a later section. The third term is the oscillatory salt transport at the central site. It is not affected by the depth-averaging of the residual fields. The spatial structure of this component will

97

be considered in a later section. The six cross terms were calculated and found to be much smaller than the estuarine and oscillatory salt transport.

Uncertainties in salt transport in the center of the channel are estimated from measurement errors in the velocity and salinity and variability of mixed layer depths in the surface and bottom extrapolations (see Appendix B). Greatest uncertainty arises during the apogean neap tides when the salinity structure in the upper water column is least resolved. The uncertainty in the estuarine salt transport is about 50% during apogean neaps. Uncertainty of the depth-averaged oscillatory salt transport is about 40% during springs and perigean neaps and between 80% and 100% during apogean neaps.

Calculating salt transport at the bottom tripods

Measurements at the D, E, and F bottom tripods were used to provide information about the cross-channel structure of salt transport. Oscillatory salt transport at the tripods was estimated by multiplying the tidally-varying velocity and tidally-varying salinity and tidally averaging the product. Oscillatory salt transport could only be estimated for the first weeks of the deployment when the salinity estimates are reliable.

Estuarine salt transport was estimated from the residual velocity and salinity. Although the salinity was not measured throughout the deployment, the direction of estuarine salt transport could be estimated by the direction of the residual velocity. In general, the salinity at the E tripod was fresher than the cross sectional average. A residual inflow was then a seaward transport of salt and an outflow larger than the freshwater velocity, a landward salt transport. At the northern section, the D tripod was in the deepest part of the channel and had a higher salinity than the cross section average. A landward residual flow at the D tripod was thus a landward transport of salt. The F tripod, located on the shallow bank at the northern cross section, was

fresher than the average salinity at the cross section. A seaward residual flow larger than the net outflow at the F tripod thus indicated a landward salt transport.

3.4 The salt content of the estuary

The estimates from the hydrography and conductivity sensors show that no significant change in salt content occurred between Day 231 and the rainfall on Day 278 (Figure 3.14). Increased freshwater flow from three storms in October rapidly removed salt from the estuary. The first survey after the Day 278 rainstorm shows that total salt in the estuary decreased by about a third from the drought value. The last survey in the experiment (Figure 3.5), after two more storms, found the head of salt less than 60 km from the Battery, and the total salt content only about one quarter of the drought value. The length of the salinity intrusion after the storm is half its length during the drought. One third of the change in length is due to seaward advection of the salinity intrusion, which is indicated by a decrease of the mean salinity at the mouth. Two thirds of the change is due to the compression of the salinity distribution, which corresponds to a strengthening of the along-channel density gradient.

3.5 Salt transport

3.5.1 Salt transport due to net outflow

The salt transport due to the net outflow, $u_0 S_0$ (Equation 3.6), is constant for most of the deployment (Figure 3.15a) when the freshwater flow remained low. After the first rainstorm the salt transport increases to three times the drought value and after the last storm increases to fifteen times the drought value.

In addition to river discharge, there are three other possible sources or sinks
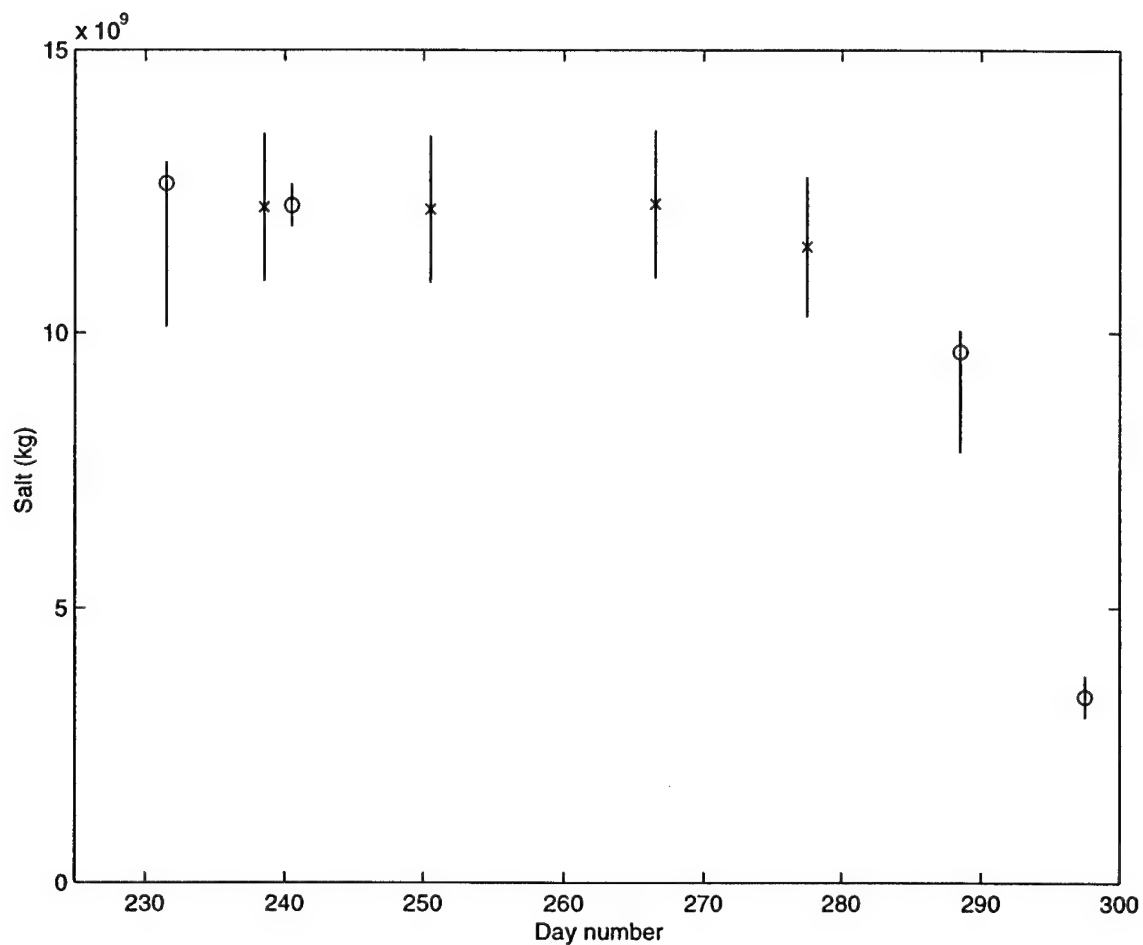
Figure 3.14: Salt content of the Hudson Estuary estimated from the four HUDMIX surveys (circles) and from the USGS conductivity sensors (crosses). Vertical bars indicate uncertainty in the salt content estimates and, in the case of the two neap HUDMIX surveys (days 231 and 288), an estimate of bias due to sampling in the deepest part of the cross section.

100
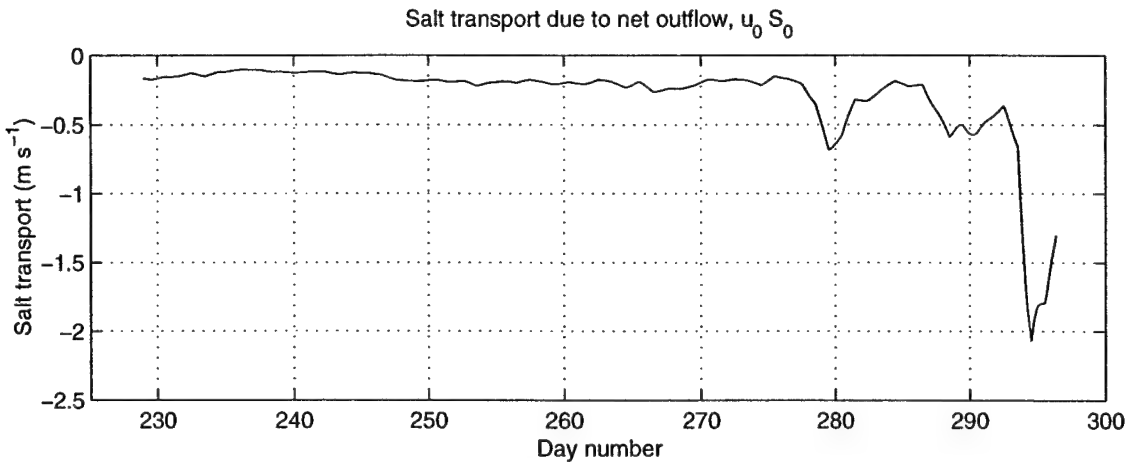
Figure 3.15: Salt transport at the cross section estimated from the net freshwater flow and depth-averaged salinity at the mooring. Negative values indicate salt transport out of the estuary.

of water: withdrawals of water for public use, outflow from wastewater treatment plants, and evaporation. The difference between the withdrawals and return outflows from public water use should be small, less than 5% of the drought river flow, based on the amount of drinking water needed for the population. Evaporation is estimated at less than 2% of the drought river flow using a typical wind speed, a typical relative humidity, the surface area of the river, and the advection time of the net outflow.

3.5.2 Estuarine salt transport

Figure 3.16 shows the estuarine velocity (u_{est}), estuarine salinity (S_{est}), and estuarine salt transport ($u_{est}S_{est}$) at three depths that span the range of the measurements in the water column. The magnitude of the estuarine velocity and salinity is weakest at the 8 meters depth and increases both above and below. The magnitude of the estuarine velocity and salinity increases at all depths during apogean neaps, leading to a monthly increase in estuarine salt transport at all depths. An estimate of the depth-averaged, estuarine salt transport is found using the surface and bottom extrapolations (Figure 3.17, solid line).

101
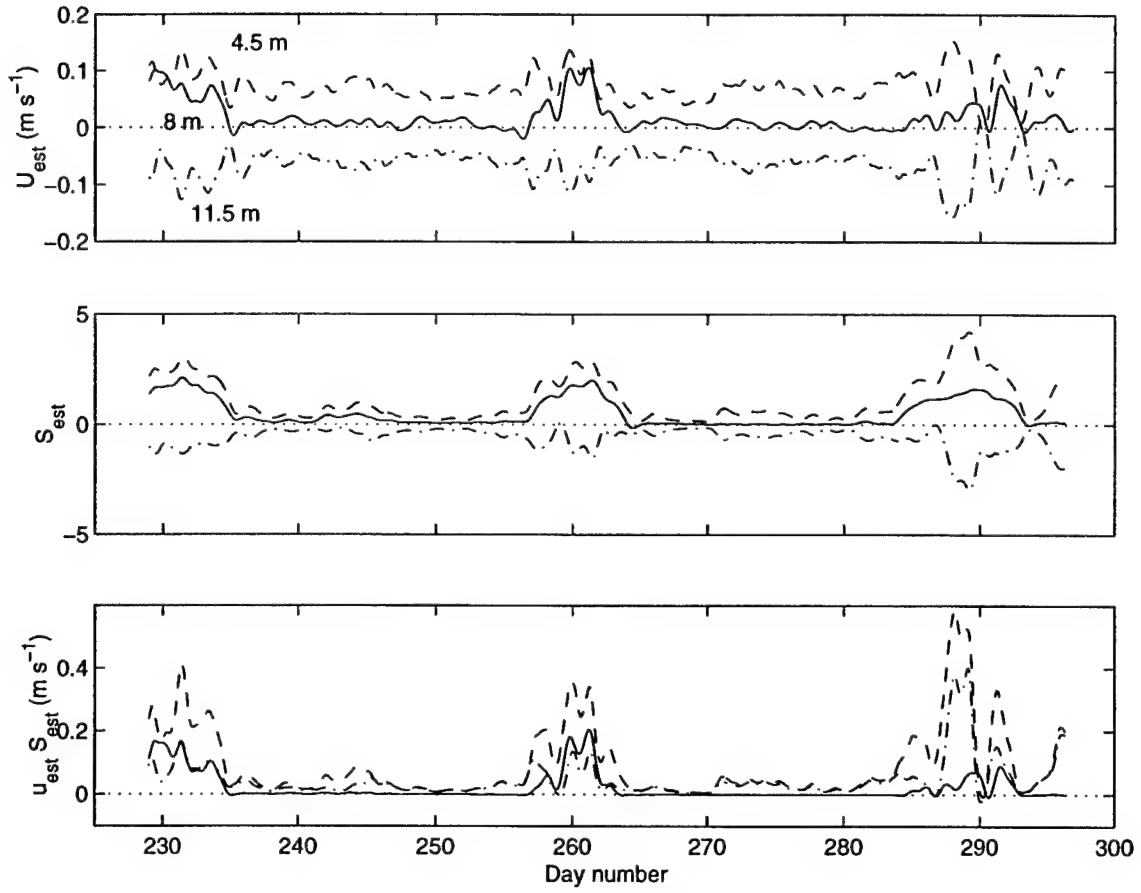
Figure 3.16: a. Estuarine circulation (u_{est}), b. estuarine salinity (S_{est}), and c. estuarine salt transport at three depths that span the range of observations in the water column. 11.5 meters (dash-dotted line), 8 meters (solid line), and 4.5 meters (dashed line) above bottom.
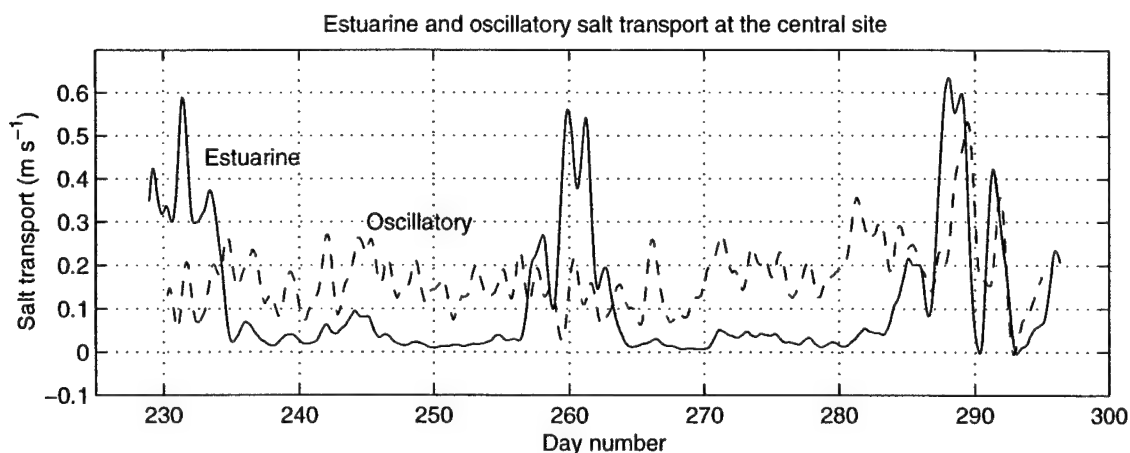
Figure 3.17: Depth-averaged estuarine (solid line) and oscillatory (dashed line) salt transport at the central site estimated from the salinity at the mooring and velocity at the moored ADCP. Positive indicates salt transport towards the river, negative towards the ocean.

At the E tripod, the direction of estuarine salt transport fluctuates. Salinity at the E tripod location on the shallower side of the estuary is less than the depth-averaged salinity at the mooring so the direction of salt transport depends on the direction of the residual flow. As shown in Figure 3.13, the residual flow at the E tripod is seaward for most of the deployment but can be landward at times, with no clear spring-neap or weather band signal.

Observations of residual flow at the D and F tripods (not shown), located in the center of the channel and on the bank three kilometers north of the central site, show a similar structure to the measurements at the central site and the E tripod. Residual velocity is landward at the D tripod near the bottom and center of the channel, indicating a landward transport of salt. The residual flow can be of either direction at the shallower F tripod, with no discernible spring-neap or weather band signal.

103

3.5.3 Oscillatory salt transport

The oscillatory salt transport is the result of the magnitude of the tidal velocity and salinity and the phase shift between them. Figure 3.18 shows the amplitude of the semidiurnal velocity, the semidiurnal salinity, and the phase difference between them, and the resulting oscillatory salt transport at 11.5, 8, and 4.5 meters above bottom. The amplitude and phase of the tidal velocity and salinity are found by fitting diurnal, semidiurnal, and quarter diurnal sinusoids to the record in thirty-three hour windows. The errors from the fit are less than 0.01 m s^{-1} for velocity, 0.1 for salinity, and phase errors are less than 1 degree. The amplitudes of the tidal velocity and salinity have a clear spring-neap modulation. Both reduce markedly during apogean neap tides. The phase shift between the velocity and salinity has compensating spring-neap variability. During neap tides, the amplitudes decrease and the salinity and velocity are further from quadrature. During spring tides, the amplitudes are larger and the phase between the velocity and salinity is closer to quadrature. As a result, the oscillatory salt transport has no distinct spring-neap variation.

The amplitude of oscillatory salt transport increases with depth above bottom. At 4.5 meters above bottom the values are near zero. The phase between the velocity and salinity is nearly in quadrature. Salinity and velocity are further out of quadrature at 8 and 11.5 meters and the oscillatory salt transport is into the estuary. An estimate of the depth-averaged oscillatory salt transport at the central site, using the extrapolations of the profiles, is shown by the dashed line in Figure 3.15a.

Oscillatory salt transport at the E tripod, located at the side of the channel, was not significantly different from zero during the first eight days of the deployment. Oscillatory salt transport in the center of the channel, at the same level as the E tripod, is clearly landward, suggesting that oscillatory salt transport diminishes
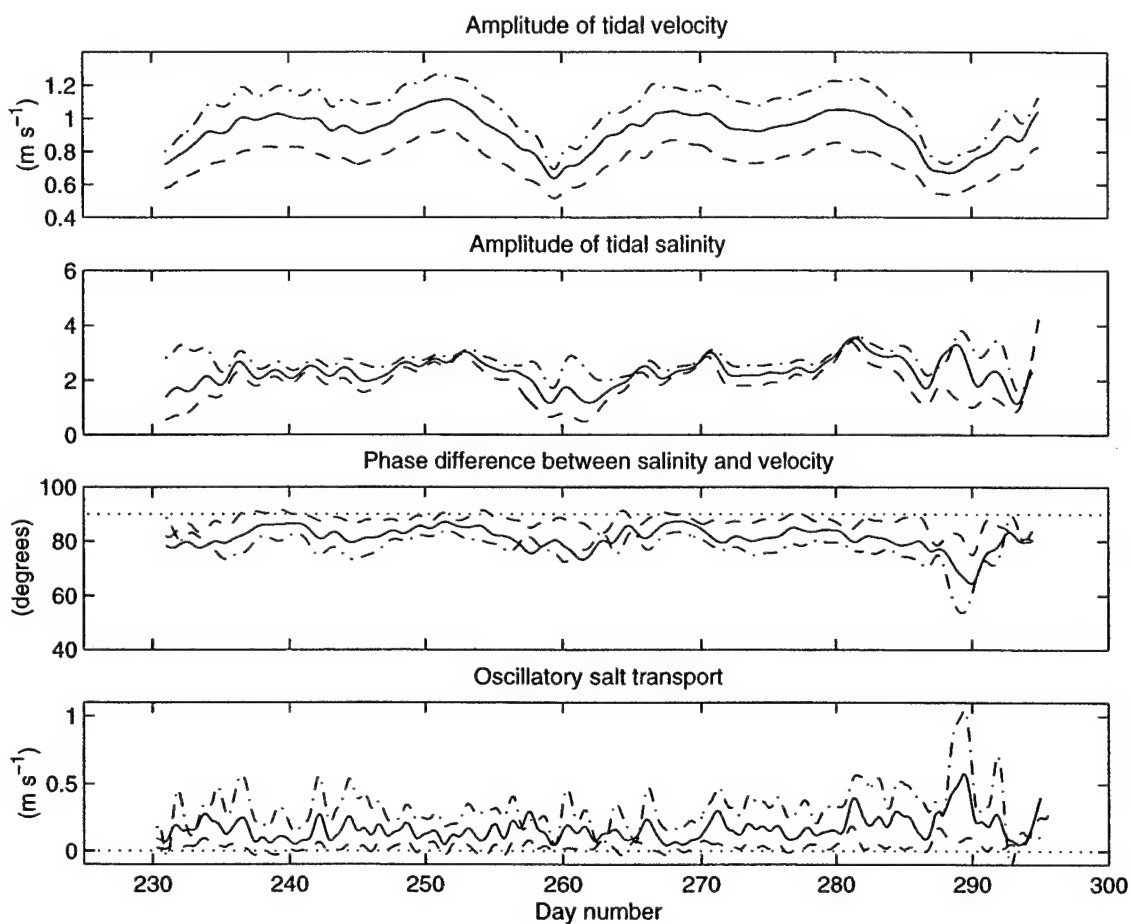
Figure 3.18: a. Amplitude of tidal velocity, b. Amplitude of tidal salinity, c. Phase difference between salinity and velocity, and d. Oscillatory salt transport at three depths that span the range of observations in the water column. 11.5 meters, (dash-dotted line), 8 meters (solid line), and 4.5 meters (dashed line) above bottom.

towards the sides of the channel during apogean neaps. Transverse structure will be discussed more completely in later sections.

3.5.4 Weather band salt transport

The residual, depth-averaged velocities are dominated by two to four day fluctuations of about 7 cm s^{-1} magnitude with no significant mean (Figure 3.9b shows simultaneous fluctuations at two depths). The residual depth-averaged salinity has two-to-three day fluctuations of about .2 around a mean of about 22 (Figure 3.10b shows simultaneous fluctuations at two depths). The instantaneous salt transport due to depth-averaged weather band fluctuations of velocity and salinity is about 0.01 m s^{-1}, which is not significantly different from zero. Weather band oscillations are still present in the shear and stratification (Figures 3.9c and 3.10c) and produce variability in, but little net contribution to, the estuarine and oscillatory salt transport (Figure 3.17).

3.5.5 Other sources of salt

The freshwater and wastewater flows contribute to the net flow but do not bring salt into the estuary. The increase of salinity due to evaporation is negligible. The only possibly significant source or sink of salt comes from the Harlem River, a tidal passage between the Hudson River and the East River. The contribution of the Harlem to the salt balance of the Hudson can be estimated using the flow rate of the Harlem and the salinity difference between the position of the Harlem River and the measurement cross section. Estimates of flow through the Harlem River show a inflow to the Hudson through most of the drought, changing to an outflow during the periods of elevated flow (A. Blumberg, personal communication). Residual flow through the Harlem is about 20% of the drought flow in the Hudson (A. Blumberg,

personal communication). The salinity difference between the measurement cross section and the inflow of the Harlem is about 3 , about 15% of the salinity at the measurement cross section. The effect of the Harlem on the salt balance is therefore only about 3% of the contribution of the net outflow at the measurement cross section. The effect of the Harlem River can be neglected in the salt balance of the Hudson.

3.6 Mechanisms of salt transport

Averaged over the two monthly tidal cycles during drought conditions, the landward salt transport at the mooring is comprised of roughly 65% oscillatory salt transport and 35% estuarine salt transport. At all times except apogean neaps the oscillatory salt transport is larger than estuarine salt transport. The magnitude of oscillatory salt transport is surprising based on previous studies of salt transport in the James and Hudson estuaries which have concluded that the salt balance is primarily between estuarine salt transport and the salt transport due to the net outflow (Pritchard 1956; Hunkins 1981). From a 25-hour survey in the Hudson during summer low flow conditions, Hunkins (1981) found the landward salt transport was entirely due to estuarine salt transport with a magnitude equivalent to a cross section average of 0.2 m s^{-1}. His estimate lies between the apogean neap and spring magnitudes of estuarine salt transport in this study. Hunkins's (1981) estimate of oscillatory salt transport was an order of magnitude less than his estimate of estuarine salt transport and directed towards the ocean. In this study, oscillatory salt transport at the mooring is clearly landward and orders of magnitude larger than Hunkins's (1981) estimate.

In addition, comparison of the measurements in this study with Smith's (1980) analytical model for salt transport in a vertically well-mixed estuary provides more

evidence that oscillatory salt transport at the mooring is much larger than expected. Using Hudson parameters for the channel bathymetry, along-channel salinity gradient, and tidal strength, Smith's (1980) model predicts that the landward transport of salt during weakly-stratified conditions should still be dominated by residual circulation, although a circulation with transverse shear instead of vertical shear, of about 0.06 m s^{-1}. Smith's analysis also predicts that tidal dispersion, due primarily to transverse oscillatory shear dispersion, should be more than an order of magnitude smaller. This is not consistent with observations of oscillatory salt transport at the mooring.

The oscillatory salt transport at the mooring is also two orders of magnitude larger than the salt transport during vertically well-mixed conditions from the one-dimensional model in Chapter 2 (Figure 2.4). The discrepancy in magnitudes suggests that oscillatory salt transport at the mooring is not likely to be the result of vertical exchange of salt within the tidal cycle.

3.6.1   Lateral structure of oscillatory salt transport

The large magnitude of oscillatory salt transport at the mooring may not reflect the cross-sectionally averaged, oscillatory flux. In Chapter 2 the vertical structure of oscillatory salt transport was shown to have a region of counter-gradient transport in the lower portion of the water column, a structure also noted by Larsen (1977) and Ou et al. (1999). A similar process can occur in the transverse dimension from a lateral exchange of salt between the slower moving water at the sides of the channel and the faster moving water in the center. As with the vertical example, the regions of slower moving water produce counter-gradient salt transport and the regions of faster moving water produce regions of down-gradient salt transport.

The spatial structure of oscillatory salt transport from lateral and vertical ex-

108

change of salt is shown in two idealized pictures (Figure 3.19), one in which all of the variation is in the lateral and the other in the vertical. The structures are the solutions of the spatially-dependent oscillatory salt transport, developed in Chapter 2, Section 2.3.2. Parameters are chosen to approximate the Hudson Estuary by using an idealized rectangular channel 10 meters deep and 1 kilometer wide with a longitudinal salinity gradient of 0.0003 m^{-1}. Figure 3.19a shows salt flux with a tidal velocity of 60 cm s^{-1} amplitude, a sinusoidal tidal velocity difference of 30 cm s^{-1} across the channel, and a constant transverse mixing of 0.9 m^2s^{-1}. This magnitude of transverse mixing produces the maximum oscillatory shear dispersion in this simple model (as discussed in section 2.3.2). In the slower moving water at the sides of the estuary, the salt transport is counter-gradient (towards the ocean), while in the middle of the channel, it is down-gradient (towards land). The cross sectional average salt transport is landward and 17% of the magnitude at the center of the channel. Figure 3.19b shows salt transport for the same channel but with a vertical velocity difference of 30 cm s^{-1}, and a constant vertical mixing of 1.4 cm^2s^{-1} that produces the maximum vertical shear dispersion. Salt transport near the bottom is counter-gradient while the near the surface it is down-gradient. The salt transport averaged over the cross section is down-gradient and, as in the lateral case, about 17% of the surface magnitude.

The measured oscillatory salt transport at the center of the channel has features of a combination of the two model distributions. Observed oscillatory salt transport (Figure 3.18) is near zero towards the bottom of the water column and increases towards the surface. It has vertical structure similar to the model with vertical mixing, but the depth-averaged value is larger and down-gradient, similar to the model with transverse mixing. A three-dimensional numerical model of the Hudson Estuary provides a more sophisticated tool to understanding the salt transport with the combined effects of vertical mixing and lateral circulation (details of the model
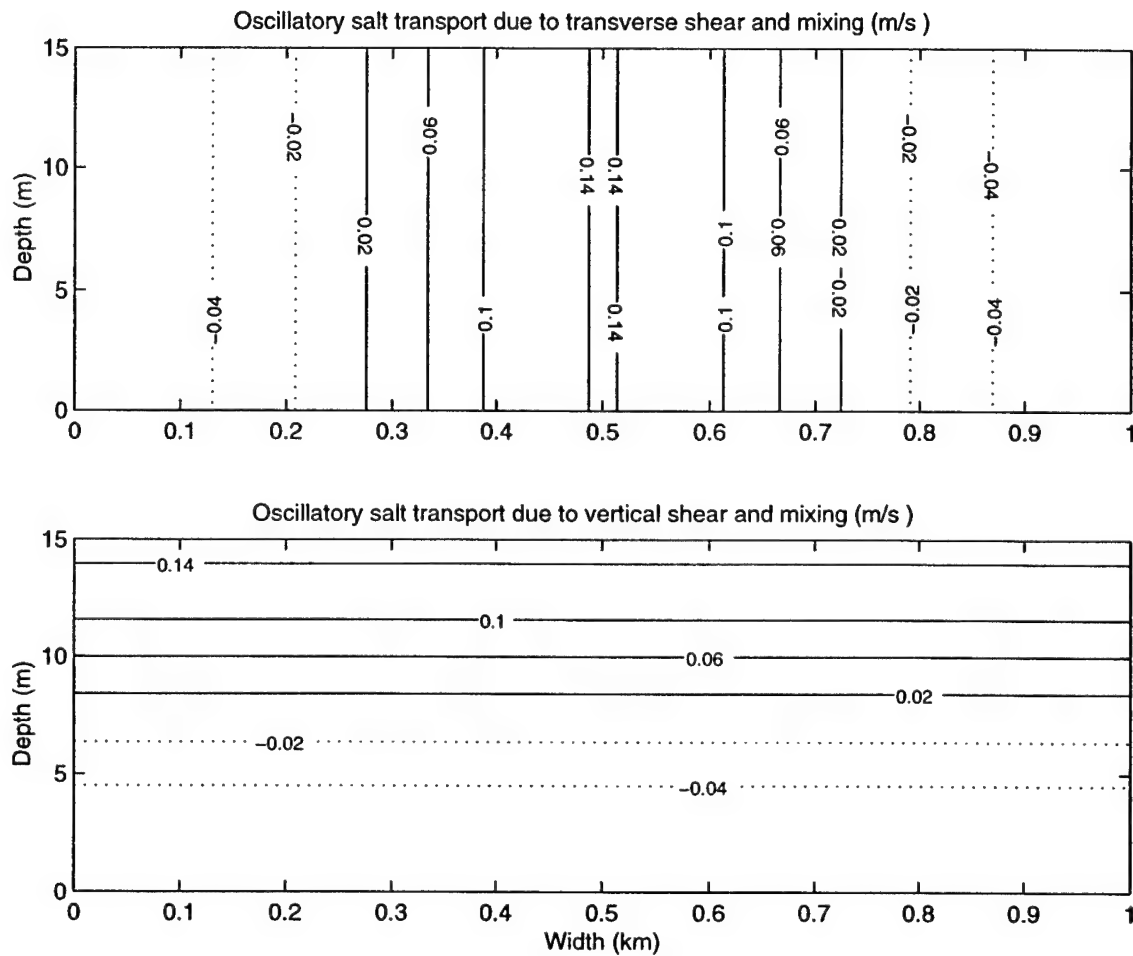
Figure 3.19: Spatial structure of oscillatory salt flux for a two-dimensional estuarine cross section. Both have a net tidal flow of 60 cm s^{-1} and an along-channel salinity gradient of 0.0003 m^{-1}. a. Spatial dependence of salt flux due to transverse shear and mixing. A sinusoidal transverse salinity difference of 60 cm s^{-1}, in phase with the net tidal flow, and a transverse diffusivity of 0.9 m^{2}s^{-1} which produces the maximum dispersion. b. Spatial dependence of vertical oscillatory shear dispersion has a sinusoidal vertical salinity difference of 60 cs s^{-1}, in phase with the net tidal flow, and a vertical diffusivity of 1.4 m^{2}s^{-1} which produces the maximum dispersion.

are in Geyer et al. (1998)). Two model runs, corresponding to spring conditions and apogean neap conditions, were compared with the observations at the moored ADCP and the E tripod. The spring amplitudes and phases of the tidal velocity and salinity in the model are close to those observed. The neap tide conditions do not compare as well for reasons that are unclear. The model is not able to produce the transverse structure seen during highly-stratified periods in the estuary.

The agreement between the model and observed tidal velocity and salinity during spring tides holds promise for representing the oscillatory salt transport in the estuary during those conditions. The oscillatory salt transport in the model (Figure 3.20a) shows structure similar to a combination of the simple schematics. Salt transport in the model is landward near the surface and the center and seaward near the sides and towards the bottom. The magnitude and depth variation of oscillatory salt transport in the center of the model cross section are consistent with the observed profiles at the central site. Salt transport in both observed and model profiles is landward near the surface and becomes seaward near the bottom. Integrating the oscillatory salt transport in the model over the cross section produces a net oscillatory flux that is one quarter of the depth-averaged value at the center. The model results suggest that measurements of oscillatory salt transport during spring tides in the center of the channel are an overestimate of the cross-sectional average due to regions of negative salt transport at the sides.

The model results also illustrate another mechanism of oscillatory salt transport. In addition to shear dispersion, oscillatory salt transport can also be produced by along-channel convergences and divergences of salt during the tidal cycle. For example, Geyer and Nepf (1996) show how elevation of the pycnocline in a constriction during flooding tide results in a large covariance of tidal salinity and velocity and "tidal pumping" of salt, corresponding to the non-local salt transport of Dronkers and van de Kreeke (1986). The increase in oscillatory salt transport in Geyer and
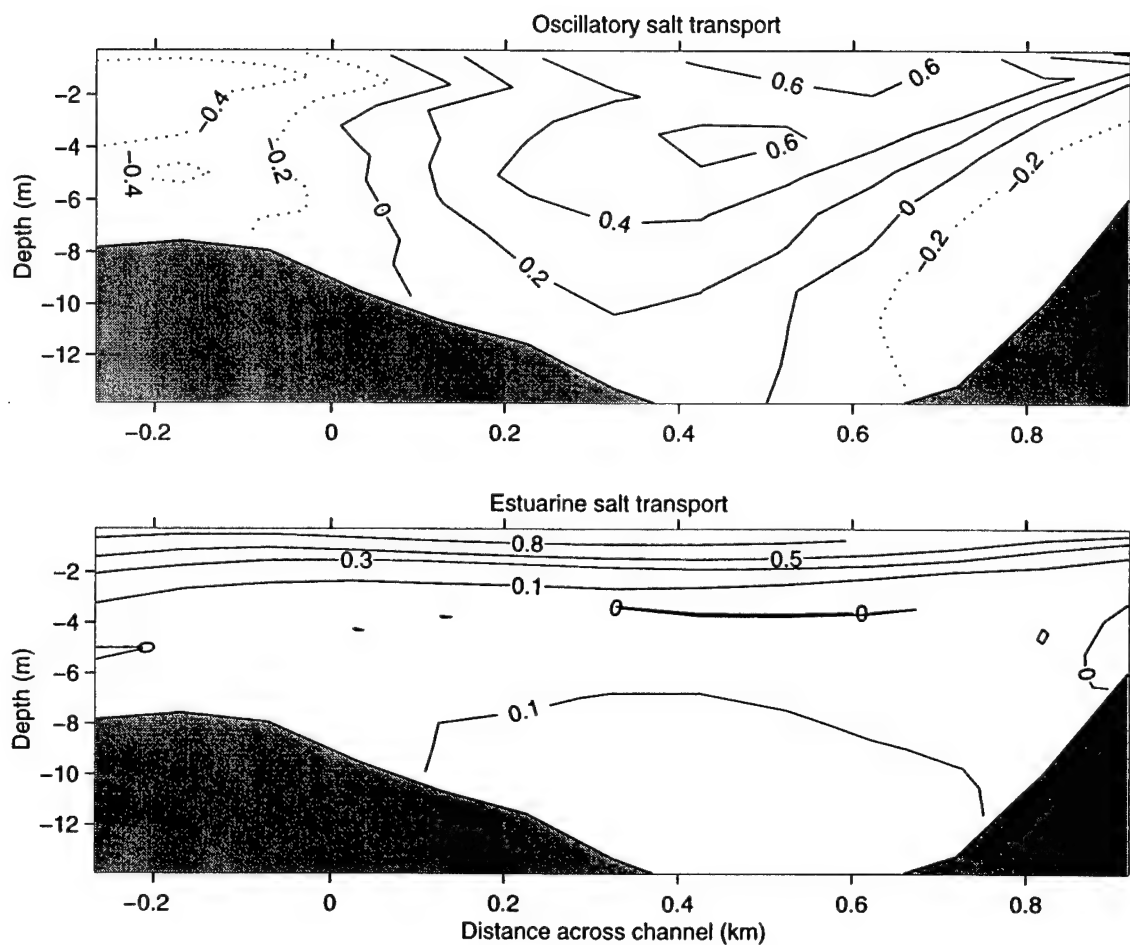
Figure 3.20: Salt transport (m s^{-1}) at the central cross section from a three-dimensional model of the Hudson Estuary (Geyer et al, 1998) run with spring tidal conditions. a. Oscillatory salt transport. b. Estuarine salt transport.

Nepf (1996) is a response to the along-channel variation of bathymetry.

In the model, non-local salt transport comprises only one quarter of the tidal dispersion at the cross section. This suggests that for spring tides at this location in the Hudson Estuary, the effects of changing bathymetry over the tidal excursion contribute little to the oscillatory salt transport at the section and that the mechanisms of salt transport are primarily the result of the lateral and vertical processes described by shear dispersion.

Measurements at the E tripod provide only a little information about transverse structure at the cross section. Oscillatory salt flux can only be estimated during the first apogean neap tide. During that time, the flux is near zero at the E tripod. The location of the E tripod is also near the location of the zero contour of oscillatory salt flux in the model run. The model run, however, is based on spring tide conditions, and the agreement may be coincidence. The E tripod flux does suggest that oscillatory salt transport decreases at the bottom on the sides of the cross section, as well as in the center, during apogean neaps.

Based on the lateral structure of the numerical model fields, the magnitude of the cross channel average of oscillatory salt transport is estimated as one quarter of the depth-averaged value observed in the center of the channel.

3.6.2   Lateral structure of estuarine salt transport

Observations and model indicate that estuarine salt transport, unlike oscillatory salt transport, has little lateral structure. Shipboard transects show that salinity and velocity have much more vertical structure than lateral, especially during neap tides when estuarine salt transport has the greatest magnitudes (Figure 3.11). The relatively weak lateral structure suggests that the estuarine salt transport is likely to be similar in sign to that at the mooring, which is landward at all depths (Figure 3.16).

The three-dimensional Hudson Estuary model provides a qualitative, if not quantitative, dynamically-consistent picture of the estuarine salt transport (Figure 3.20). In the model, estuarine salt transport is predominantly landward, increasing both near the surface and at depth, as it does in the observations. Measurements at the E tripod provide little additional information: the residual velocity fluctuates in sign which may indicate fluctuations of estuarine salt transport near the bottom at the sides. Small areas of counter-gradient estuarine salt transport are also located near the sides of the channel in the three-dimensional model.

3.6.3 Cross-sectionally averaged salt transport

The estimates and inferences of lateral structures, from observations, analytic models, and a three-dimensional numerical model, indicate that estuarine salt transport should be landward over almost the entire cross section, while oscillatory salt transport may have regions of counter-gradient flux near the banks. An estimate of the effect of lateral structure on the flux of salt was made by weighting the estuarine and oscillatory flux at the central site. An estimate of the cross section average of estuarine salt transport was made by assuming the value at each depth at the mooring is constant across the section, consistent with the numerical model fields through much of the water column. The value of depth-averaged oscillatory salt transport was multiplied by one-quarter, the weighting from the numerical model, to find a cross-sectional average. Based on these estimates of lateral structure, the estuarine salt transport produces 70% of the total landward transport at the cross section and the tidal dispersion 30%. These values are more consistent with previous estimates of salt transport from shorter-term shipboard studies over cross sections in the James (Pritchard 1956) and Hudson Estuaries (Hunkins 1981).

114

3.6.4 Spring-neap variability of salt transport

The variability of the sum of the estuarine and oscillatory salt transport (Figure 3.21a) is dominated by the monthly variability of the estuarine salt transport.

The estuarine salt transport at the central site has a clear monthly variation produced by the spring-neap cycle of residual stratification and circulation in the estuary (Figure 3.16). However, as noted in Section 3.5.3, the oscillatory salt transport does not have a discernible spring-neap signal in spite of the large variations in the tidal velocity and salinity (Figure 3.18). The phase shift between the velocity and salinity compensates for the variation in the tidal amplitudes. This result is unexpected because most formulations of dispersion predict greater dispersion for larger tidal amplitudes (Geyer and Signell 1992; Smith 1980; Young et al. 1982).

Because the vertical turbulent exchange does not increase during neap tides, the change in phase shift between spring and neap tides must be due to a change in the lateral or longitudinal fluxes. One explanation for the variation in phase is a greater rate of transverse exchange of salt during neap tides. An increase in the phase shift at the mooring during neap tides could also be due to an along-channel convergence or divergence of salt within the tidal cycle. This mechanism is "non-local" salt transport produced by bathymetric variations along the channel (Dronkers and van de Kreeke 1986). Salt transport should be more sensitive to along-channel variations in bathymetry during neap tides because small movements of the pycnocline during the tidal cycle can produce large oscillatory salt transport. For example, Geyer and Nepf (1996) showed that a one meter displacement of the pycnocline in a constriction led to an oscillatory salt transport at the center of the channel of order 10 m s^{-1}. The observations in this chapter are from a more uniform section of the Hudson Estuary than those in Geyer and Nepf (1996) and a much smaller signal is expected. The increase in phase during apogean neaps is strongest
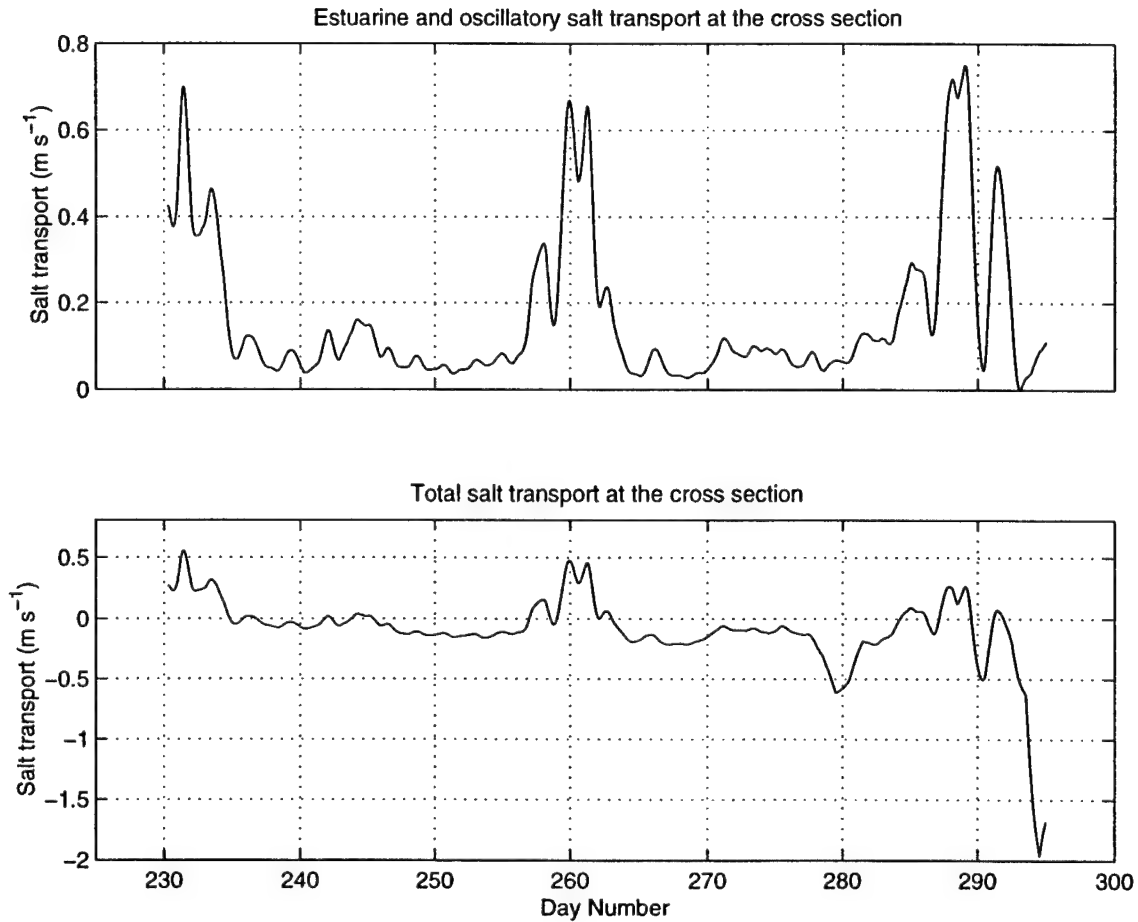
Figure 3.21: Estimated cross sectional average sum of estuarine and oscillatory salt transport (top panel). The sum of the estuarine salt transport, oscillatory salt transport, and salt transport due to the net outflow at the cross section (bottom panel).

at 8 meters (Figure 3.18), a depth that is close to the pycnocline, suggesting that small fluctuations of the pycnocline might be responsible for the shift.

3.7 The salt balance

An estimate of the total salt transport at the measurement cross section (Figure 3.21b) is made by adding the estimated oscillatory and estuarine salt transport at the section (Figure 3.21a) to the salt transport due to the outflow (Figure 3.15).

116

The total salt transport fluctuates around zero over the monthly spring-neap cycle. During apogean neaps (around Days 230 and 260), a pulse of salt enters the estuary. Between the apogean neaps salt leaves the estuary. Salt leaves the estuary more rapidly during the first rainfall event (Day 278), enters the estuary for the next apogean neap tide (Day 288), and rapidly exits the estuary during the large storm (Day 293).

The time integral of the estimated total salt transport (Figure 3.22, solid line) through the measurement cross section is consistent with the measurements of the salt content of the estuary. The pulses of salt transport during the monthly apogean neap tides lead to approximately 10% increases in salt content of the estuary. The salt transport also shows a rapid decrease during the storm at the end of the record. The consistency with the last salt content estimate cannot be checked because the moorings were recovered before the last survey.

The dashed curve in Figure 3.22 is an estimate of the total salt transport based on the transport at the central mooring, without taking into account transverse variations. This overestimates the amount of salt entering the estuary. The estimate incorporating transverse information is more consistent with the measured salt content.

3.8   The adjustment of the estuarine salt balance

The salt transport at the cross section has considerable variability over the spring-neap cycle, yet the salt content of the estuary changes very little. The weak response suggests that the salt content adjusts to changes in the salt transport over a time scale longer than the monthly spring-neap cycle. Park and Kuo (1996) found a similar situation in the Rappahannock Estuary, another partially-stratified estuary, for a similar period of drought conditions and a series of spring-neap cycles. Using a
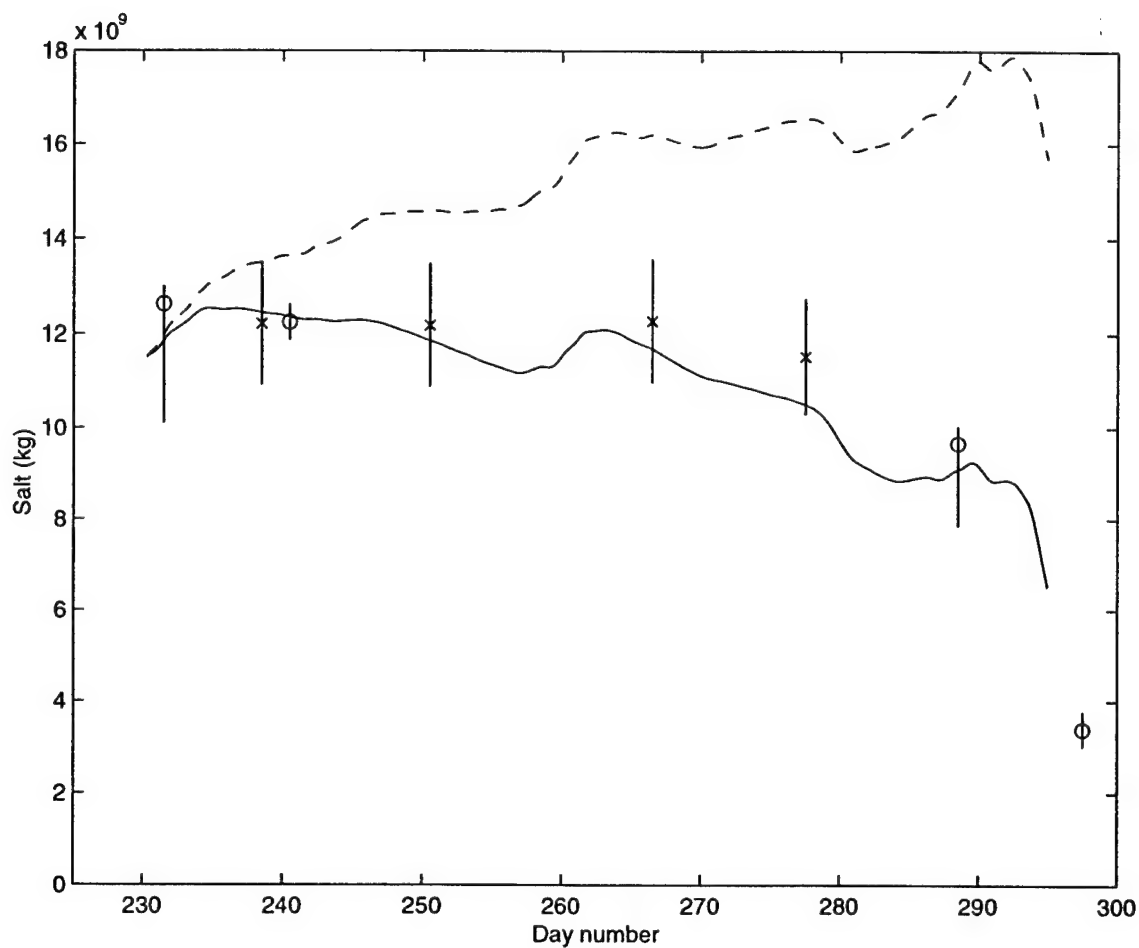
Figure 3.22: Estimates of salt content of the Hudson Estuary (circles and crosses, with vertical bars indicating uncertainty and bias) and integrated net transport of salt from the freshwater flow and estimates of cross section average estuarine and oscillatory salt transport (solid line). Also shown is another estimate of integrated salt transport that assumes oscillatory salt transport at each depth at the mooring is constant across the section (dashed line). A constant has been added to the integrals of salt transport so that they start in the center of the first salt content estimate.

two-dimensional model tuned to match observations in the Rappahannock, Park and Kuo (1996) demonstrated that the time scale of the adjustment of the salt balance to spring or neap amplitudes of tidal velocity was much longer than the spring-neap cycle, suggesting that the spring-neap modulation of the tidal velocity has a minor effect on the salt content. The time scale of response to spring-neap variations will be explored in the next chapter.

The salt content decreases due to three storms in October. The third storm is the largest, and produces a rapid decrease in salinity at the mooring. Abood (1974) noted that the freshwater flow and length of the salinity intrusion in the Hudson were strongly correlated. He suggested that the time lag of the response of the salinity intrusion to the peak flow was about five to ten days, depending on the magnitude of the flow, with more rapid adjustment times during extreme flows. The observations in this study do suggest that the length of the salinity intrusion responds more rapidly to the largest storm. The decrease in the length of the salinity intrusion between the two salt content surveys is 35 kilometers, in good agreement with an advective displacement of 38 kilometers from the average flow of 0.06 ms^{-1} during that time. The process of adjustment of the salinity intrusion to a pulse of freshwater flow will be investigated in the next chapter.

The elevated freshwater flow removes salt from the estuary but as it does so it increases the salinity gradient at the mouth (Figure 3.5c), increasing the residual circulation (Figure 3.9c), stratification (Figure 3.10c), and landward salt transport (Figure 3.15b). Although the measurements stopped before the next neap tides, the reduction of tidal energy should further increase the estuarine salt transport, and bring more salt into the estuary. When the elevated freshwater flow subsides, the salinity intrusion should move landward in pulses with greater landward excursions during apogean neaps when estuarine salt transport increases.

119

3.9 Summary

Measurements of salt content and salt transport in the Hudson Estuary have provided insights into the mechanisms and variability of salt transport and the nature of the salt balance in a partially-stratified estuary.

The mechanisms that bring salt into the estuary display very different temporal variability. Estuarine salt transport increases by an order of magnitude once a month during the apogean neaps, when tidal energy is minimum and strong residual stratification and shear can develop. Oscillatory salt transport has no discernible spring-neap variability because changes in phase between tidal velocity and salinity compensate for the variation in tidal amplitudes. The phase variations are presumed to be due to differences in the tidal transport of salt during well-mixed and stratified conditions.

The results of the study also suggest that salt transport has significant transverse structure. The spatial structure of oscillatory salt transport from analytical and numerical models suggests that oscillatory salt transport measurements in the center of the channel overestimate the cross-channel average. Accounting for areas of counter-gradient oscillatory salt transport near the banks reduces the contribution of oscillatory salt transport. Models suggest that estuarine salt transport has less transverse structure than oscillatory salt transport and that the magnitude in the center of the channel is more representative of the cross-channel average. Accounting for the transverse structure brings the relative contribution of each mechanism in closer agreement with previous studies of salt transport in partially-stratified estuaries. The revised estimate is also consistent with the overall salt balance.

The salt balance of the estuary is assessed by combining the estimates of estuarine and oscillatory salt transport at the section with the salt transport out of the estuary due to the net outflow. The estimate suggests that pulses of salt of about 10% of

the total salt content come into the estuary during the monthly apogean neap tides. Fluctuations of this size are consistent with measurements of the total salt content in the estuary. Towards the end of the experiment, three-quarters of the salt content is removed by rapid adjustment to a series of storms.

Chapter 4

The length of the estuarine salinity intrusion

4.1 Introduction

Many partially-stratified estuaries are long, drowned river valleys whose lower reaches have been inundated by the ocean (e.g., the James and Hudson Rivers). In these estuaries, the distance that salt penetrates into the river is determined by the dynamics, rather than the topography as is the case in fjords. The length of the salinity intrusion in a partially-stratified estuary defines the extent of habitat and the limit of drinking water supply (Monismith et al. 1996; Wells and Young 1992). It is also intrinsically coupled to the circulation and stratification (Chatwin 1976). The length of the salinity intrusion and the evolution of the salt balance are determined by the magnitude and variation of salt transport along the channel of the estuary.

Early studies assumed that the salt transport and the salt balance are in equilibrium with the freshwater flow and the tides (Knudsen 1900; Hansen and Rattray 1965; Hansen and Rattray 1966), producing an equilibrium distribution of salt along the estuary (Festa and Hansen 1976; Chatwin 1976). Festa and Hansen (1976) used a two-dimensional numerical model to illustrate the variability of the length of the salinity intrusion over a range of depths, vertical mixing coefficients, and freshwater flows. Chatwin (1976) used an analytic expression for the salt balance to find a scale for the length of the salinity intrusion as a function of depth, freshwater flow, vertical mixing, and salinity at the mouth of the estuary. Although both Festa and Hansen (1976) and Chatwin (1976) showed that the equilibrium length of the salinity intrusion in an estuary can vary considerably for realistic variations in freshwater flow and vertical mixing, neither addressed the process of adjustment to such variations.

Several studies have addressed the temporal response of the salinity intrusion using numerical models. Godfrey (1980) found qualitative agreement between changes in the length of the salinity intrusion in the James River and a model of the salt

balance forced by observed mouth salinity, amplitude of tidal velocity, and freshwater flow. Park and Kuo (1996) used a two-dimensional model of the Rappahannock Estuary to illustrate the response of the salt balance to the spring-neap cycle. They demonstrated that the salinity intrusion would require at least four months to come into equilibrium with the amplitude of either the spring or neap tidal velocities, a much longer time than the spring-neap cycle. These studies suggest that the salt balance of an estuary may often be out of equilibrium with the forcing.

Two studies have considered the adjustment of the estuarine salt balance for more general bathymetries and variations in forcing (Kranenburg 1986; MacCready 1999). Kranenburg (1986) derived an adjustment time scale of the salt balance of an estuary to changes in freshwater flow from a perturbation about an equilibrium salt balance. His results suggested that an equilibrium salt balance adjusts more quickly at high flow rates than at low flow rates. MacCready (1999) used a two-layer model to examine the adjustment of the salt balance to step changes of freshwater flow and tidal velocity. He also derived analytical time scales that described the adjustment of model simulations for deep, highly-stratified estuaries and shallow, well-mixed estuaries. He noted that simulations with intermediate depths, corresponding to partially-stratified estuaries, were poorly described by the analytic time scales. In addition, these estuaries were the slowest to adjust to changes in conditions, suggesting the salt balance may often be out of equilibrium.

In this study a simple model of the salt balance of a partially-stratified estuary illustrates the adjustment of the salt balance to variations in freshwater flow and tidal mixing. Chatwin's (1976) derivation of the equilibrium length of the salinity intrusion is revisited briefly in Section 4.2. The time-dependent model of the salt balance is developed in Section 4.3. The adjustment to pulses of freshwater flow and the spring-neap cycles of vertical mixing are presented in Sections 4.4 and 4.5. The effects of including tidal dispersion are discussed in Section 4.6. The chapter is

summarized in Section 4.7.

4.2 An equilibrium salinity intrusion length

A brief description of Chatwin's (1972) equilibrium length is given below. The parameter dependence of the length scale is compared to observations to motivate the use of a time-dependent version of his model.

Chatwin (1976) assumes that the steady-state salt balance in a partially-stratified estuary is between the landward estuarine salt transport and the seaward advection of the salinity (S) by the net outflow (u_f). Using the Hansen and Rattray (1965) expression for the estuarine salt transport (Equation 2.32), the salt balance at every location along the channel (x) is

$$1.3\text{x}10^{-5}\,\frac{g^2\beta^2 h^8 Pr}{k^3}\left(\frac{d[\bar{S}]}{dx}\right)^3 = u_f[\bar{S}], \tag{4.1}$$

where the square brackets indicate a cross-sectional average, overbars indicate a tidal average, h is the depth, β is the coefficient of saline contraction, k is the eddy viscosity, and Pr is the Prandtl number. The assumptions of the Hansen and Rattray (1965) expression are valid as long as $10^{-3}\frac{h^4}{k^2}\beta g\frac{\partial^2[\bar{S}]}{\partial x^2} \ll 1$ (see Chatwin (1976) for a complete discussion).

The expression can be solved for $[\bar{S}]$ as a function of position along the estuary, with a boundary condition of $[\bar{S}] = S_0$ at the mouth,

$$[\bar{S}] = S_0\left(1 - \frac{x}{L}\right)^{\frac{3}{2}}, \tag{4.2}$$

where the length of the equilibrium salinity intrusion, L, is

126

$$L = 0.35 \frac{1}{k} \left(\frac{g^2 \beta^2 S_0^2 h^8 Pr}{|u_f|} \right)^{\frac{1}{3}}.$$
(4.3)

Comparison of the length scale with observations

The length of the salinity intrusion in several estuaries has been observed to have a similar variation with freshwater flow as Equation 4.3. Abood (1974) found the length of the salinity intrusion in the Hudson Estuary has a roughly $u_f^{-\frac{1}{3}}$ dependence on the weekly-averaged flow rate, for a range of lengths between 60-120 km and a range of freshwater flows between 1-5 cm s^{-1}. Fischer analyzed data from two flume studies (from Rigter (1974); also quoted by Prandle (1985)) and found the dependence of the salinity intrusion on the freshwater flow was $u_f^{-0.25}$ (Savenije 1993), a slightly weaker dependence than $u_f^{-\frac{1}{3}}$. The salinity intrusions of the Delaware Estuary (Garvine et al. 1992) and San Francisco Bay (Stephen Monismith, personal communication) show an even weaker dependence on the flow rate, which may be due to variations in bathymetry not accounted for in the formulation of Equation 4.3.

Observations of the response of the salinity intrusion to the spring-neap cycle and changes in mouth salinity indicate similar trends as the equilibrium length (assuming k in Equation 4.3 varies proportionally with U_{tide}). Jay and Smith (1990) found that the length of the salinity intrusion in the Columbia Estuary increased during neap tides when tidal mixing was reduced. Godfrey (1980) suggested a reduction in the length of the salinity intrusion in the James Estuary was primarily due to decrease of salinity at the mouth.

4.3   The time-dependent model

In an estuary the freshwater flow may vary by an order of magnitude within a day, and the tidal velocity may change by almost a factor of two over the spring-neap

cycle. Variations of this magnitude suggest that the length of the salinity intrusion would vary by a factor of two. Thus the assumption of a steady-state salt balance is an unrealistic limitation. In this section a time-dependent version of Chatwin's (1976) salinity intrusion model is derived in order to address the response to time variability.

Combining the salt balance at a location with continuity yields

$$\frac{\partial S}{\partial t} + \frac{\partial(uS)}{\partial x} + \frac{\partial(vS)}{\partial y} + \frac{\partial(wS)}{\partial z} = 0. \tag{4.4}$$

Averaging over a semidiurnal tidal cycle (overbar) and over a rectangular cross section (square brackets) that is invariant with time, the salt balance at the cross section is

$$\frac{\partial[\bar{S}]}{\partial t} + \frac{\partial}{\partial x}[\overline{uS}] = 0. \tag{4.5}$$

The salt transport can be divided into three terms, using tildes to indicate spatial deviations from the cross section average and primes to indicate tidal fluctuations,

$$\frac{\partial[\bar{S}]}{\partial t} + \frac{\partial}{\partial x}\left([\bar{u}][\bar{S}] + [\bar{\tilde{u}}\bar{\tilde{S}}] + [\overline{u'S'}]\right) = 0. \tag{4.6}$$

The first term, $[\bar{u}][\bar{S}]$, is the salt transport due to the net flow through the cross section. The second term, $[\bar{\tilde{u}}\bar{\tilde{S}}]$, is the estuarine salt transport. The third term, $[\overline{u'S'}]$, is the tidal dispersion.

Several studies suggest that estuarine salt transport is the primary mechanism of landward salt transport in partially-stratified estuaries (Pritchard, 1956; Hansen and Rattray, 1966; Chapter 3). For the time being tidal dispersion is neglected (to be considered later in Section 4.4.1). Estuarine salt transport, $[\bar{\tilde{u}}\bar{\tilde{S}}]$, is linked to the

128

external parameters through the Hansen and Rattray (1965) expression (Equation 2.32), as has been done in previous studies of partially-stratified estuaries (Chatwin 1976; Godfrey 1980; MacCready 1999). After making these substitutions and replacing $[\bar{u}]$ with u_f, the salt balance is

$$\frac{\partial[\bar{S}]}{\partial t} + \frac{\partial}{\partial x}\left(-1.3\mathrm{x}10^{-5}\frac{g^2\beta^2 h^8 Pr}{k^3}\left(\frac{\partial[\bar{S}]}{\partial x}\right)^3 + u_f[\bar{S}]\right) = 0 \tag{4.7}$$

The salt balance is a non-linear, advection-diffusion equation. Freshwater flow advects salt out of the estuary and the estuarine salt transport is written in the form of a non-linear diffusion of salt into the estuary.

There are two assumptions that have been made in the salt balance. It is implicitly assumed that the depth-averaged salinity ($[\bar{S}]$) adjusts on times longer than a tidal cycle, whereas the depth deviations ($\bar{\tilde{S}}$) adjust on the order of a tidal cycle. This assumption is consistent with the derivation of the Hansen and Rattray (1965) expression for estuarine salt transport ($[\bar{\tilde{u}}\bar{\tilde{S}}]$) in which the time dependent terms in the tidally-averaged momentum and salt balances are neglected.

In addition, the Hansen and Rattray (1965) expression for estuarine salt transport is derived with the assumption of a constant along-channel salinity gradient, $\frac{d^2[\bar{S}]}{dx^2} = 0$ (Section 2.3.1). Now $\frac{\partial^2[\bar{S}]}{\partial x^2} \neq 0$ and the advection terms in the momentum balance and vertical advection of salt in the salt balance are non-zero, but can be neglected if $10^{-3}\frac{h^4}{k^2}\beta g\frac{\partial^2[\bar{S}]}{\partial x^2} \ll 1$ (Chatwin 1976). The approximation of a constant along-channel salinity gradient becomes poorer the weaker the mixing, the deeper the estuary, and the shorter the length of the salinity intrusion.

A numerical model of the salt balance

Since there is no readily apparent analytical approach to the problem, a simple numerical model of the salt balance is used to provide insights into the response of

the salinity intrusion to changes in freshwater flow and tidal mixing. The model consists of a one-dimensional grid along a 100 kilometer channel with a constant depth of 12 meters. The grid spacing is 250 meters and the length of the channel is always greater than the length of the salinity intrusion. The salinity is held at 0.01 at the landward end of the domain and at 25 at the mouth.

The tidal velocity and freshwater flow are specified at each time step and are the same at every position along the channel. The strength of the vertical mixing is a function of the tidal velocity and depth, using $k_m = k_h = k = \gamma U_{tide} h$, where $\gamma = 0.00007$ to match the Hansen and Rattray (1965) expression to the amplitude of the tidal velocity, similar to the value used by Godfrey (1980). The value of the γ is intended to incorporate the effects of stratification on the salt transport. A more sophisticated closure is beyond the scope of this study.

The salinity is integrated in time according to Equation 4.7. The integration is accomplished by Strang splitting in which the salinity is diffused for half a step, followed by an advective step (using upwind differencing), and then the second half of the diffusion step. Initial conditions and forcing are discussed in each section.

4.4   Response to variable freshwater flow

Salt is removed from the estuary by the net outflow. Salt is brought back into the estuary by the estuarine salt transport. While the outflow depends only on the magnitude of the freshwater flow, the estuarine salt transport changes in response to the variation of the salinity gradient. The difference produces an asymmetric response of the salinity balance to variations of freshwater flow.

Figure 4.1 shows two examples of the adjustment of the salinity intrusion to a pulse of freshwater flow. The freshwater flow starts at a base value of 0.002 ms^{-1} and is increased to 0.05 ms^{-1} after five days (top panel). In one run the flow remains

130

elevated for a five-day period (top panel, dash-dotted line), while in another run, the flow remains elevated for twenty days (solid line). The model run begins with an equilibrium salinity distribution for a depth (h) of 12 meters, the base flow rate (u_0), a tidal velocity (U_{tide}) of 0.95 m s^{-1}, and a mouth salinity (S_0) of 25. Vertical mixing is held constant through the run, $k = \gamma U_{tide} h = 0.0008$ m^{2}s^{-1}. The distance of the isohaline where salinity equals 1 ($[\bar{S}] = 1$) (solid and dash-dotted lines) begins at the base equilibrium position of 77 kilometers (upper dotted line) and remains at the base equilibrium length until the freshwater flow increases. The equilibrium position for the elevated flow rate is 26 kilometers (lower dotted line).

Initially, the length of the salinity intrusion decreases linearly at the rate of the additional outflow. For the five-day event the length of the salinity intrusion shortens but does not reach equilibrium; it does reach equilibrium for the twenty-day event. Once the base flow resumes (Day 10 for dash-dotted line, Day 25 for solid line) the estuarine salt transport brings salt back into the estuary at a slower rate than it was removed. Recovery to the base equilibrium is slower because the estuarine salt transport decreases as the salinity intrusion lengthens. Fifty days after the return to base flow, neither salinity intrusion has reached the base equilibrium length. The length of the salinity intrusion increases slowly after the five-day pulse of freshwater. The length of the salinity intrusion rebounds more quickly after the twenty-day pulse, decreasing as the length of the salinity intrusion decreases.

Adjustment time

The sudden and large change in freshwater flow produces the asymmetry in the response of the salinity intrusion. For the onset of high discharge, the change in salt is balanced mainly by advection due to the increased flow, and the adjustment time can be approximated by the difference between the initial equilibrium length, L_i, and the final equilibrium length, L_f, divided by the difference between the elevated and

131
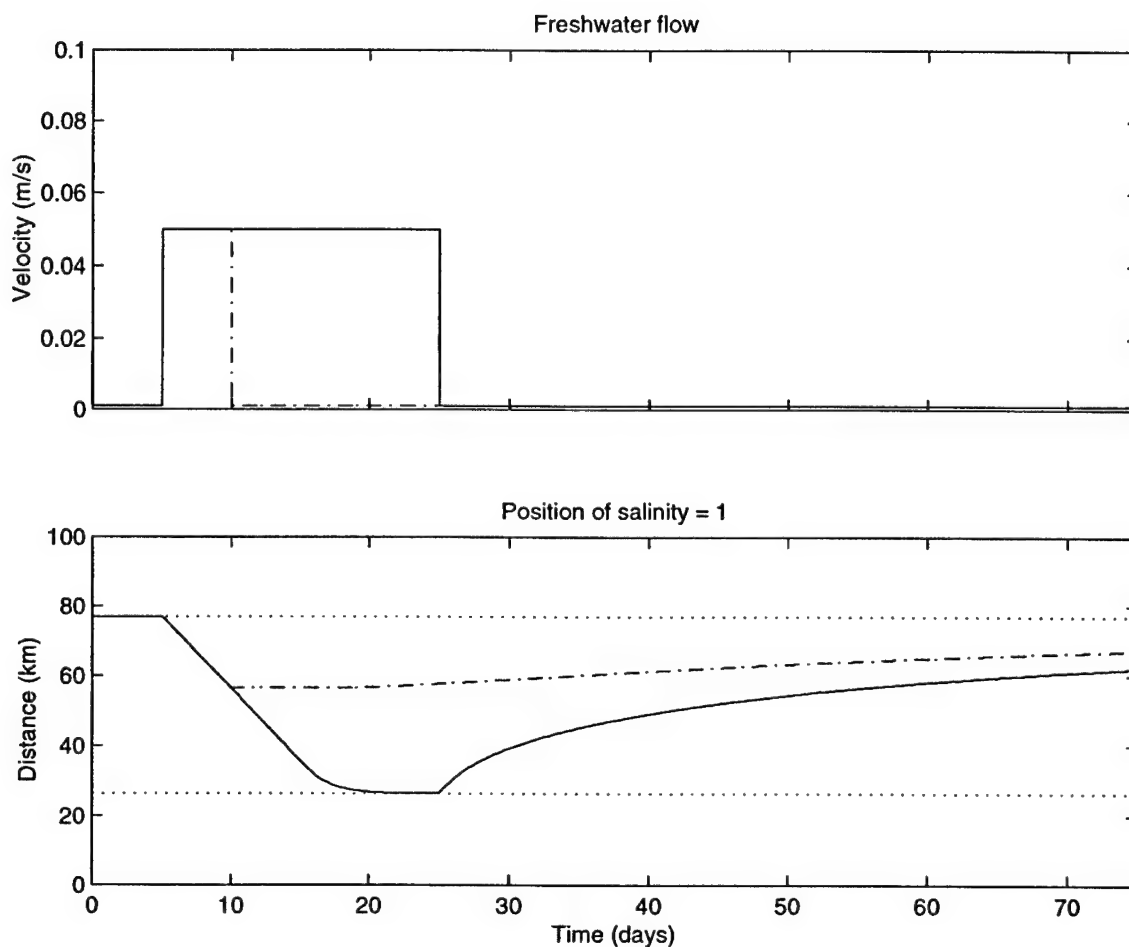
Figure 4.1: a. Freshwater flow for two events. Flow varies between a base value of 0.002 m s^{-1} and an elevated value of 0.05 m s^{-1} for pulses of five days (dash-dotted line) and twenty days (solid line). b. The position of the isohaline where salinity equals 1 in response to the five-day event (dash-dotted line) and the twenty-day event (solid line). The equilibrium positions for the base flow (77 kilometers) and elevated flow (26 kilometers) are shown by the upper and lower dotted lines.

the base freshwater flow, $|u_{fe}| - |u_{fb}|$. For a large increase of freshwater $|u_{fe}| \gg |u_{fb}|$, the time scale is

$$\tau_{adv} = \frac{L_i - L_f}{|u_{fe}|}. \tag{4.8}$$

For the example in Figure 4.1, the adjustment to high-flow conditions from low-flow conditions by advection would require a time, $\tau_{adv} = 10$ days. The five-day event is shorter than the adjustment time. As a result the length of the salinity intrusion does not reach the high-flow equilibrium length. The twenty-day event is longer than the adjustment time and the salinity intrusion does equilibrate.

When the discharge is abruptly decreased to the base value, the length of the salinity intrusion begins to increase and slowly approach the base-flow equilibrium length. The change in salt is balanced mainly by the estuarine salt transport. For the twenty-day pulse of flow, the estuarine salt transport is strongest immediately after the flow decreases, when the magnitude of the salinity gradient is maximum. As the salinity gradient decreases with time, the estuarine salt transport weakens, and the advance of the salinity intrusion into the river slows.

The response of the salinity intrusion to the five-day pulse of freshwater has a slightly different behavior. The length of the salinity intrusion increases very weakly immediately following the reduction in flow and increases at slightly higher rate further into the adjustment. The character of the adjustment is due to the shape of the salinity intrusion seaward of the 1 isohaline. During the five-day pulse the salinity intrusion is advected towards the ocean, increasing the salinity gradient near the mouth, and leaving the salinity gradient further upstream relatively unchanged. When the pulse of high discharge stops, the estuarine salt transport is largest near the mouth where the salinity gradient is larger. Eventually the estuarine salt transport brings salt into the upper portion of the salinity intrusion and the intrusion

133

length increases. Although the behavior of the salinity intrusion differs somewhat from that after the twenty-day pulse, both examples show a quick response to the pulse of flow and a longer recovery once the base flow resumes.

Observational examples

A dramatic observation of asymmetry in the response of the salinity intrusion occurred in Chesapeake Bay after Tropical Storm Agnes in 1972. Ten days of elevated flow from the storm moved the salinity intrusion fifty-five kilometers towards the ocean. Ninety days later the intrusion had finally returned to its pre-storm position (Davis, 1976).

Another example of adjustment to increased freshwater flow is provided by the observations from the Hudson Estuary in Chapter 3. Near the end of the experiment a large freshwater event occurred. The event was bracketed by two surveys of the salinity intrusion which showed that the length of the salinity intrusion moved seaward by about 35 kilometers in nine days. Over the nine days between the surveys, the average flow rate was 0.06 m s^{-1}. Displacement by the flow over the nine-day period is 38 kilometers. The close correspondence of the distances suggests that the decrease in length of the salinity intrusion was primarily through advection by the increased flow.

4.5 Response to the spring-neap cycle

In most estuaries the spring-neap cycle modulates the tidal velocity, producing a variation in the strength of vertical mixing. The effects of variable mixing enter the salt balance through the dependence of the estuarine salt transport on the eddy coefficient, k, in Equation 4.7. During neap tides, vertical mixing is weaker, the estuarine salt transport increases, and the salinity intrusion moves further into the

river. During spring tides, vertical mixing is stronger, the estuarine salt transport is reduced, and the salinity intrusion is moved seaward by the freshwater flow.

If the longitudinal transport of salt were instantaneous, so that the salt balance were always in equilibrium, the length of the salinity intrusion would contract and expand with the spring and neap tides. However, the salt balance requires time to adjust, producing a phase lag of the salinity intrusion with respect to the spring-neap cycle and reducing the magnitude of the response to less than the range of spring-neap equilibrium lengths. If the adjustment time is much longer than the spring-neap time scale, the length of the salinity intrusion changes very little over the spring-neap cycle. If the adjustment time is short relative to the spring-neap time scale, the length of the salinity intrusion has a corresponding variation.

Figure 4.2 shows three examples of the response of the salinity to a spring-neap cycle of vertical mixing. A fourteen-day spring-neap cycle of tidal velocity (top panel) modulates the vertical mixing, $k = \gamma U_{tide} h$. The results are shown once the solution becomes periodic. The lower panel shows the position of the 1 isohaline for three flows of increasing strength, $u_f = 0.002, 0.01, and 0.04$ m s^{-1}. The dashed line shows the position of the isohaline if the length of the salinity intrusion were in equilibrium with the vertical mixing.

For the lowest flow, the position of the isohaline varies very little over the spring-neap cycle. There is a slight variation of the length that is in quadrature with the spring-neap cycle. The length of the salinity intrusion decreases on the order of one kilometer after the spring tides, when the flow advects salt out of the estuary, and increases after neaps when the estuarine salt transport bring salt back in. The modeled isohaline moves only a small fraction of the instantaneous equilibrium length.

At the higher freshwater flows the length of the salinity intrusion is shorter, the
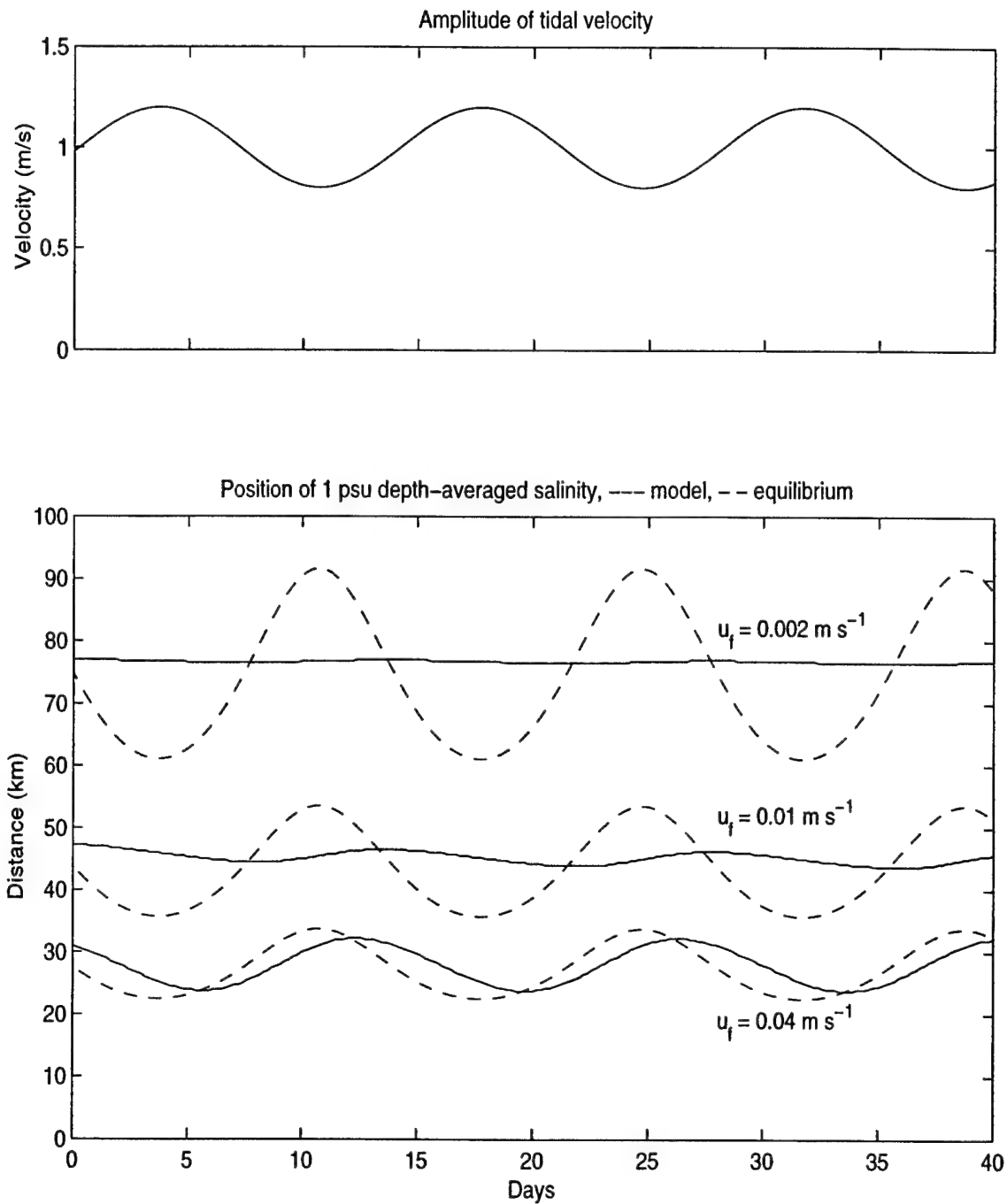
Figure 4.2: a. Amplitude of the tidal velocity during the spring-neap model runs. b. Solid lines indicate the position of the 1 isohaline for a freshwater flows of 0.002 m s^{-1}, 0.01 m s^{-1}, and 0.04 m s^{-1}. Dashed lines indicate the equilibrium position where salinity equals 1 for each value of the tidal velocity.

136

salinity gradient is stronger, the total amount of salt in the estuary is much less, and the length of the salinity intrusion responds more quickly to the spring-neap modulation of the tidal velocity. At the moderate flow the salinity intrusion varies over about a quarter of the range of the instantaneous equilibrium lengths. At the highest flow rate the length of the salinity intrusion varies over almost the entire range. As the flow rate increases, the variation of the length of the salinity intrusion moves from near quadrature to nearly in phase with the spring-neap tidal cycle.

Adjustment time

An adjustment time scale can be found from a perturbation of the salt balance about an equilibrium state. After scaling the along-channel derivatives with the equilibrium length (L_0), the linearized balance contains a response time scale that can be compared to the time scale of the spring-neap cycle. The time scale of the adjustment of the salt balance to small change about an equilibrium length is

$$\tau_{adj} = \frac{L_0}{3|u_f|}. \tag{4.9}$$

The adjustment times for the three flow rates, from lowest to highest flow, are 150 days, 17 days, and 3 days. The time scale for the lowest flow rate is much longer than the spring-neap time scale, $\omega_{sn}^{-1} = 2$ days, consistent with almost no movement of the salinity intrusion over the spring-neap cycle. The intermediate and higher flows have adjustment times closer to the time scale of the spring-neap cycle, consistent with the amplitude and phase of the length of the salinity intrusion approaching the equilibrium values.

137

Observational examples

A change in salt transport and the length of the salinity intrusion with the spring-neap cycle has been noted in the Columbia Estuary. Jay and Smith (1990) found the maximum intrusion occurred during neap tides. The length of the salinity intrusion was about 30 kilometers, the freshwater flow about 0.05 m s^{-1}, leading to a response time of about 2 days. The response time is comparable to the time scale of the spring-neap cycle and consistent with the rapid adjustment of the length of the salinity intrusion.

The observations in Chapter 3 demonstrate the other extreme of the behavior of the salinity intrusion in a partially-stratified estuary. During drought conditions in the Hudson Estuary the salinity intrusion was about 100 kilometers long with no measurable response to the spring-neap cycle. Using the length of the salinity intrusion and the freshwater flow of $u_f = 0.01$ m s^{-1}, the adjustment time scale is about 40 days. The time scale is much longer than the time scale of the spring-neap cycle, consistent with the relatively constant salt content of the estuary through the drought period.

4.6 Effects of tidal dispersion

Tidal dispersion also provides landward salt transport in an estuary. Customarily it is parameterized as a horizontal dispersion coefficient acting on the along-channel salinity gradient, $K_H \frac{d[\bar{S}]}{dx}$. The dispersion coefficient, K_H, may vary with any of the forcing parameters. Often it is considered proportional to some power of the magnitude of the tidal velocity (Geyer and Signell 1992; MacCready 1999). With this parameterization, an increase in tidal velocities produces an increase of tidal dispersion and simultaneous decrease of estuarine salt transport. Therefore, tidal dispersion is more effective at higher tidal amplitudes when the magnitude of estu-

arine salt transport is most diminished.

Tidal dispersion also depends on the first power of the salinity gradient whereas estuarine salt transport depends on the third power. The dependence suggests that the contribution of tidal dispersion to the total landward salt transport is greater when the salinity intrusion is longer. Tidal dispersion also becomes important when the length of the salinity intrusion is very short, on the order of a tidal excursion (Jay and Smith 1990). In these situations the salt transport is largely determined by the tidal processes at the mouth.

Given the assumed dependence of tidal dispersion on the salinity gradient and tidal mixing, the effects of tidal dispersion on the adjustment of the salt balance can be projected. For fresh water variations, tidal dispersion would assist in the adjustment to low flow when the salinity intrusion is long and the estuarine salt transport weak. The variation of tidal dispersion over the spring-neap cycle would oppose the variation of estuarine salt transport, reducing or possibly reversing the movement of the salinity intrusion.

4.7   Discussion and summary

This study addresses the time-dependence of the salt balance of an estuary, an aspect missing from the classic descriptions of the estuarine salt balance (Hansen and Rattray 1965; Chatwin 1976). A simple model of the salt balance is used to show the adjustment of the salinity in a partially-stratified estuary to variations of fresh water flow and tidal amplitude. The examples demonstrate an asymmetry in the adjustment of the salt balance to a pulse in freshwater flow. A more rapid response occurs during the adjustment to higher discharge when the salinity intrusion is advected seaward by the flow. Adjustment back to the lower base flow is controlled by the slower estuarine salt transport.

The response of the salinity intrusion to a spring-neap cycle of vertical mixing is illustrated for a series of fresh water flows. At low flows the length of the salinity intrusion remains essentially constant over the spring-neap cycle. At higher flows the length of the intrusion approaches the magnitude and phase of the instantaneous equilibrium length. The ability of the salinity intrusion to respond to variations of tidal mixing is characterized by comparing a response time of the salt balance to the time scale of spring-neap variations. When the adjustment time scale is orders of magnitude larger than the time scale of the spring-neap cycle, the length of the salinity intrusion has little variation. When the adjustment time scale is comparable to the spring-neap time scale, the length of the intrusion is nearly in balance with the spring-neap variation of vertical mixing.

The examples of the adjustment of the salinity intrusion to pulses of freshwater flow emphasize the processes that produce an asymmetric response. An advection time scale is derived that predicts the adjustment to an increase in freshwater flow. Previous studies have derived time scales of response based on perturbations of the salt balance (Kranenburg 1986; MacCready 1999). This approach is limited because rapid, order-of-magnitude variations of freshwater flow often occur in estuaries. Mac-Cready (1999) notes that numerical simulations appear to adjust somewhat faster than his predicted time scale for increased flow and somewhat slower for lower flow. His figures indicate that factor of two changes in freshwater flow may be sufficient to produce significant asymmetry in response.

The time scale of adjustment to the spring-neap cycle (Equation 4.9) is found from a perturbation of the salt balance. Kranenburg (1986) uses a similar approach to derive a time scale of adjustment to freshwater flow. The time scales in this study and that of Kranenburg (1986) are proportional to one another; the difference lies in the treatment of the along-channel gradients in the linearized salt balance. After scaling the along-channel salinity gradients with the equilibrium intrusion length, a

response time scale for the salt balance is found that characterizes the ability of the salinity intrusion to adjust to variations of tidal mixing within the spring-neap cycle. The examples in this study suggest that a time scale based on a perturbation is more suitable for understanding the response of the salinity intrusion to the spring-neap cycle rather than the response to variations of freshwater flow.

Chapter 5

Summary discussion

5.1 Thesis summary

The thesis has addressed the mechanisms and variability of salt transport in partially-stratified estuaries and implications for the behavior of the salt balance and the length of the salinity intrusion.

In Chapter 2 the mechanisms and variation of salt transport due to vertical variations of velocity and salinity were examined for a range of tidal velocities, along-channel salinity gradients, and depths. The trends of estuarine and oscillatory salt transport with variations in the forcing parameters are similar for both constant and variable eddy coefficients. These results suggest that the analytic solutions are useful guides for the tendency of salt transport with variations in the forcing conditions.

The one-dimensional numerical model was used to find the effects of variable eddy coefficients on salt transport. The stratification in the model goes through a transition from well-mixed to stratified conditions with the spring-neap cycle, as do observations in the Hudson Estuary. The similarity of the transition in the model and the observations and the connection to the Estuarine Richardson number (Appendix A) suggests that the critical value of Ri_x for the onset of persistent stratification is a useful predictor for any region with an along-channel density gradient and tidal mixing.

The variability of salt transport at a section in the Hudson Estuary was described in Chapter 3. The estuarine salt transport varies considerably over the monthly spring-neap tidal cycle, producing five-day pulses of salt transport during apogean neap tides when residual circulation and stratification have the greatest magnitudes. Pulses of increased estuarine salt transport during the periods of weakest mixing have also been noted in results from laboratory experiments (Linden and Simpson 1988) and measurements at Spencer Gulf (Nunes and Lennon 1987). This study,

144

however, is the first observation of a series of pulses of estuarine salt transport. These results suggest that periods of increased salt transport will occur during highly stratified times in other systems.

Oscillatory salt flux has no discernible spring-neap signal, despite the marked spring-neap variation in tidal velocity and salinity, contradicting previous parameterizations of tidal dispersion (Geyer and Signell 1992; Smith 1980) and measurements of oscillatory salt transport from the Tees Estuary (Lewis and Lewis 1983). These results suggest that oscillatory salt transport does not vary in a simple manner with the amplitude of the tidal velocity, even in regions of relatively simple bathymetry.

The transverse structure of salt transport was an important issue in the interpretation of the mechanisms of salt transport. After accounting for transverse structure, the estuarine salt transport provides most of the landward salt transport over the monthly spring-neap cycle. The dominant role of estuarine salt transport is in agreement with previous observations of salt transport in partially-stratified estuaries (Pritchard 1956; Hunkins 1981). It should be noted, however, that the observations in this study are obtained over a much longer time period than previous studies. In general, the marked spring-neap variability of salt transport observed in the Hudson Estuary suggests measurements over a few tidal cycles are not likely to represent the role of each mechanism in a longer term salt balance of an estuary.

A simple model of the salt balance in a partially-stratified estuary was used in Chapter 4 to examine the adjustment of the length of the salinity intrusion to variations of the freshwater flow and the spring-neap cycle. The examples in the chapter illustrate an asymmetry in the response of the salinity intrusion to step changes in freshwater flow. During periods of strong outflow the salinity intrusion shortens rapidly as it is advected by the outflow. Once lower flow resumes the salinity intrusion expands at a slower rate due to diffusion by the estuarine salt transport. This

145

study departs from the approaches of Kranenburg (1986) and MacCready (1999) by characterizing the response to order-of-magnitude changes in flow, variations typically found in many estuaries.

The adjustment of the salinity intrusion to the spring-neap tidal cycle is illustrated by modulating the strength of vertical mixing with a fortnightly period. A response time of the salt balance is found that characterizes the ability of the salinity intrusion to respond to variations in the vertical mixing. The response time depends on the ratio of the equilibrium length and the freshwater flow, proportional to the time scale Kranenburg (1982) used to characterize the response to small variations of freshwater flow. Estuaries with higher flow rates, such as the Columbia Estuary, have shorter salinity intrusion lengths and respond rapidly to the spring-neap cycle (Jay and Smith 1990). Estuaries with lower flow rates, such as the Rappahannock and Hudson Estuaries in summer, have salinity intrusions whose length appears to have no dependence on spring-neap tidal variations (Park and Kuo, 1996; Chapter 3). This study shows that these two extremes in the response of the salt balance to the spring-neap cycle can be connected and explained by a simple model of the salt transport.

The results of the thesis suggest that any system in which conditions encompass the critical Ri_x will have rapid changes in the mechanisms and magnitude of horizontal salt transport. This study indicates that the variations of salt transport, in response to the modulation of tidal amplitude and the fluctuating freshwater flow, produce a salt balance which is often unsteady. The inherent time dependence of the salt balance must be introduced into our classification and observation of estuaries if we are to progress in the prediction of their behavior.

5.2 Outstanding questions

The thesis has demonstrated several aspects of the variation of salt transport in estuaries. A large number of questions remain.

The observational analysis in Chapter 3 suggests that an accurate estimate of the salt transport in a partially-stratified estuary rests on quantifying the magnitude of the estuarine salt transport during neap tides. The one-dimensional modeling results in Chapter 2 have the largest discrepancies with the observations during neap tides. Surface salinity in the model simulation becomes almost fresh; CTD casts from the Hudson suggest surface salinities remain near 10. Observations from the Columbia and the subestuaries of Chesapeake Bay also indicate that the surface salinities do not decrease to fresh during neap tides (Haas 1977; Jay and Smith 1990). Determining what processes produce the observed neap stratification and to what extent these processes are incorporated in our models of these systems are important steps in predicting the expected magnitude of salt transport.

The contribution of tidal asymmetry to the estuarine salt transport in a partially-stratified estuary is also an unresolved question. Descriptions of estuarine salt transport do not take tidal variations of vertical mixing into account (Hansen and Rattray 1965), yet observations suggest it determines a portion of the residual shear (Jay and Musiak 1996; Geyer et al. 1999). In Chapter 2 of this study it was shown that varying the amplitude of the tidal velocity produced trends in estuarine salt transport due to tidal asymmetry that are similar to those of the analytic expressions with constant eddy coefficients. Although the contribution of tidal asymmetry to salt transport in an estuary cannot be quantified from these results they do suggest that it is a process whose contribution to salt transport deserves further investigation.

In general, the observations in Chapter 3 illustrate the success of using moored time series to estimate salt transport due to the ability to separate residual fields

147

from fluctuating ones and resolve small phase shifts in the tidal fields. Future estimates of salt transport could be improved with more attention to measurements near the surface of the water column and at the sides of the channel. Although some authors have argued otherwise (Lewis and Lewis 1983), this study does illustrate the need to measure the lateral variations of salt transport, even in an estuary with relatively uniform bathymetry.

Appendix A:
The connection between Ri_x and Ri_E

In this section, Chatwin's (1972) equilibrium length scale of the salinity intrusion (Equation 4.3) is used to link the salinity gradient to the freshwater flow, illustrating the connection between the horizontal Richardson number, Ri_x, and the estuarine Richardson number, Ri_E.

In Chapter 2 one-dimensional model results were divided into cases in which stratification is weak and periodic and cases in which stratification runs away. The transition between the types of runs can be predicted by the horizontal Richardson number (Stacey 1996; Monismith et al. 1996),

$$Ri_x = \frac{g\beta h^2}{C_D U_{tide}^2}\frac{d[\bar{S}]}{dx}.$$ (1)

Fischer (1972) introduced another Richardson number that describes whether an estuary is stratified or well-mixed (Figure 1),

$$Ri_E = \frac{\beta g S_0 Q_f}{W U_{tide}^3},$$ (2)

where Q_f is the freshwater discharge, and W is the width of the estuary.

In an estuary of relatively constant depth, the prediction of a transition in stratification at a location, Ri_x, should occur for the same parameters as a transition of the entire estuary, predicted by Ri_E. Chatwin's (1972) scale for the length of the salinity intrusion provides the link between the salinity gradient at a location, in Ri_x, and the strength of the freshwater flow, in Ri_E.

Scaling $\frac{d[\bar{S}]}{dx}$ with $\frac{S_0}{L}$ and using the dependence of L on the dimensional parameters (Equation 4.3), Ri_x becomes,

$$Ri_x \sim \frac{k}{U_{tide}^2} \left(\frac{g\beta S_0 |u_f|}{h^2} \right)^{\frac{1}{3}}. \tag{3}$$

Substituting in $k \sim U_{tide}h$ and cubing the expression,

$$Ri_x^3 \sim \frac{g\beta S_0 h |u_f|}{U_{tide}^3}. \tag{4}$$

Recognizing that $Q_f = U_f hW$, the relationship to Ri_E is evident,

$$Ri_x^3 \sim \frac{g\beta S_0 Q_f}{W U_{tide}^3} = Ri_E. \tag{5}$$

The above derivation shows the equivalent parameter dependence of Ri_E and Ri_x^3. The actual transition values of Ri_E and Ri_x^3 are also similar. Fischer's (1972) diagram of estuarine stratification (Figure 1) shows a transition between well-mixed conditions and stratified conditions between $Ri_E = 0.03 - 0.07$. The transition value of $Ri_x^3 = (0.33)^3 = 0.04$ is within the range.

An equality between Ri_x^3 and Ri_E requires the numerical coefficient, comprised of non-dimensional parameters, to be close to unity. The numerical coefficient is $\left(\frac{\alpha\gamma}{0.35 C_D} \right) \frac{1}{Pr}$, where α is a factor near one relating the salinity gradient to $\frac{S_0}{L}$ and γ is from $k = \gamma U_{tide}h$. The coefficient could be near unity if, at the transition between well-mixed and stratified conditions, $Pr \approx 1$ and $\gamma \approx 10^{-3}$.

The threshold estuarine Richardson number can also be compared with the values of fresh water flow, tidal amplitude, and mouth salinity from the Hudson Estuary study in Chapter 3. During drought conditions the fresh water flow was approximately 0.01 m s^{-1}. Near the end of the experiment it increased to about 0.1 m s^{-1} due to a storm. The amplitude of the tidal velocities were about 1 m s^{-1} during springs and 0.7 m s^{-1} during neaps. Salinity at the Battery remained near 25. The

150
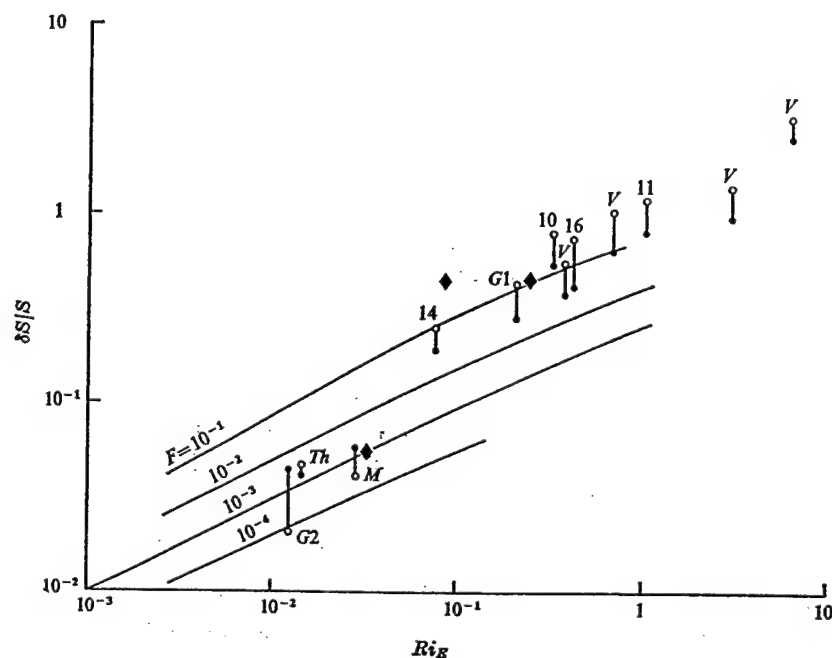
FIGURE 5. Relative stratification *vs.* estuarine Richardson number and Hansen & Rattray's Froude number. Lines of constant Froude number are as given by Hansen & Rattray (1966). ○, $\delta S/S$ *vs.* Ri_E as given by observed data; ♦, value of $\delta S/S$ corresponding to observed values of Ri_E and F according to the results of Hansen & Rattray. Numbers above points are run numbers of the WES experiments. Other points are identified as follows: G1, Gironde Estuary at point PK89 on 13 May 1969; G2, Gironde Estuary at point PK78 on 17 December 1968, both values from data given by Bonnefille (1970); Th, Thames Estuary, from data given by Inglis & Allen (1957); M, Mersey Estuary; V, Vellar Estuary from data given by Dyer & Ramamoorthy (1969).

Figure 1: Adapted from (Fischer, 1972). Diamonds indicate observations from the Hudson Estuary (Chapter 3).

151

depth was approximately 15 meters. Using these values, Ri_E for neap drought conditions is 0.08, for spring storm conditions, 0.28, and for spring drought conditions, 0.03. The Hudson Estuary was highly stratified during neap drought and spring storm conditions (≈ 10) and weakly-stratified during spring drought (≈ 1). The values cross the transition in Ri_E (Figure 1, diamonds indicate the Hudson points), in agreement with the variations of stratification observed in the estuary.

Appendix B:
Extrapolations and error estimates

B.1 Salt content uncertainty estimates

B.1.1 HUDMIX salinity surveys

The total salt content of the Hudson Estuary is estimated four times using hydrographic surveys along the center of the channel from the Battery to 1 psu salinity. The biases and errors associated with the tidal fluctuations of the salt content and channel geometry are assessed in this section.

The influence of the tidal fluctuations of the salt content are estimated from the tidal conditions during the survey. Three of the four surveys began at the Battery and progressed into the estuary with the tidal wave. The speed of the surveys is comparable to the velocity of the barotropic tidal wave, providing nearly synoptic pictures of the salinity distribution. The fluctuation of the salt content over the entire tidal cycle is estimated at $\approx 1.5 * 10^9$ kilograms, or about 10% of the drought salt content. The estimate is based on shifting the salinity intrusion 10 kilometers (the tidal excursion) further into the river and estimating the additional salt in the estuary. Velocity from the moored ADCP in the lower estuary indicates the phase of the tidal cycle during the first three surveys. The first survey (Days 231) was completed near slack ebb tide when the salt content is lowest. Half the total tidal fluctuation of salt content is added to compensate for the underestimate. The second survey (Day 240) was completed near maximum ebb when the salt content is near the tidal average. No correction is made to the salt content. The third survey (Day 288) was taken from the river towards the Battery over a range of tidal conditions from slack flood to slack ebb. A correction of half the tidal fluctuation of salt content was added to correct for sampling the lower estuary at the end of

ebb. The last survey (Day 297) was taken after the ADCP had been recovered and no correction is made to the salt content. An error is added to every survey equal to a quarter of the tidal fluctuation of the salt content.

The biases associated with sampling are also assessed. CTD casts in each survey were made in the deepest part of the channel. The depth-averaged salinity is assumed to be equal to that of the cross section average of salinity at that location and the salt content calculated. During spring tides this is a reasonable approximation since the water column is only weakly stratified. During the neap tide surveys the water column has more stratification. The depth-averaged salinity from a cast in the deepest part is an overestimate of the net salinity at the cross section. An estimate of the bias in the total salt content of the estuary during neap tide surveys is made by assuming that two-thirds of a cross section is at a depth of half the maximum and and one-third of a cross section is at a depth of the maximum. Assuming a linear salinity profile with a typical neap surface-bottom salinity difference of half the depth-average salinity, the cross-sectionally averaged salinity is 95% of the depth-averaged salinity in the center. Assuming a step in stratification at the mid-water depth with the same salinity difference, the cross section salinity is 75% of the central depth average. Using a value of 80%, the error bars have been extended by 20% towards lower total salt content to reflect a range of the overestimate.

B.1.2 USGS conductivity measurements

During the experiment, the USGS had deployed four sensors to measure conductivity in the Hudson Estuary at 34, 83.5, 116.5, 124.5 kilometers from the Battery (Figure 3.14). The sensors were located at the sides of the channel, three meters below the surface. Conductivity from the sensors is used to provide salt content estimates only during spring tides when stratification is weak and measurements at one location are likely to be representative of the salinity over the entire cross section. An estimate of the average conductivity over each period of spring tides is

154

converted to salinity with estimates of temperature from the hydrographic surveys. Errors in the measurements are estimated from the range of conductivity and temperature as ±1 psu, ±0.5 psu, and ±0.05 psu for sensors located at kilometers 34, 83.4, and 116.4, respectively. Estimates of salinity from the gauges agreed with the spring tide hydrographic survey on Day 240 and deviated little from those values over the drought period. Since the salinity values had little change, the structure of the salinity from the Day 240 survey is used to approximate the structure between the gauges. An error of 10% of the salt content is added to the estimates.

B.2 Extrapolations of salinity and velocity profiles at the central site

An estimate of salt transport at the mooring requires velocity and salinity profiles that extend to the surface and bottom. Extrapolations are based on the structure from shipboard CTD casts. In almost every cast, salinity is weakly stratified near the surface and bottom. The average depth of the weakly stratified near-surface layer is 1 ± 0.5 meters. No correlation could be found between the speed and direction of the wind and the depth of the layer. The near bottom layer is often thick enough that the moored salinity instruments were also in it. A thickness of 2 meters was used for the purposes of extrapolation.

Salinity profiles are extrapolated towards the surface by fitting a parabola between the uppermost observed salinity and the bottom of a mixed layer of one meter depth (see Figure A.1). A parabola is used because a second order polynomial matches both the values and the vertical gradients of the measured values and the mixed layer. The parabola was constrained by matching the stratification at the uppermost observed salinity and matching no stratification at the base of the mixed layer. The lower extrapolation is performed in the same manner using a parabola to fit between the bottommost salinity measurements and a two meter well-mixed

155
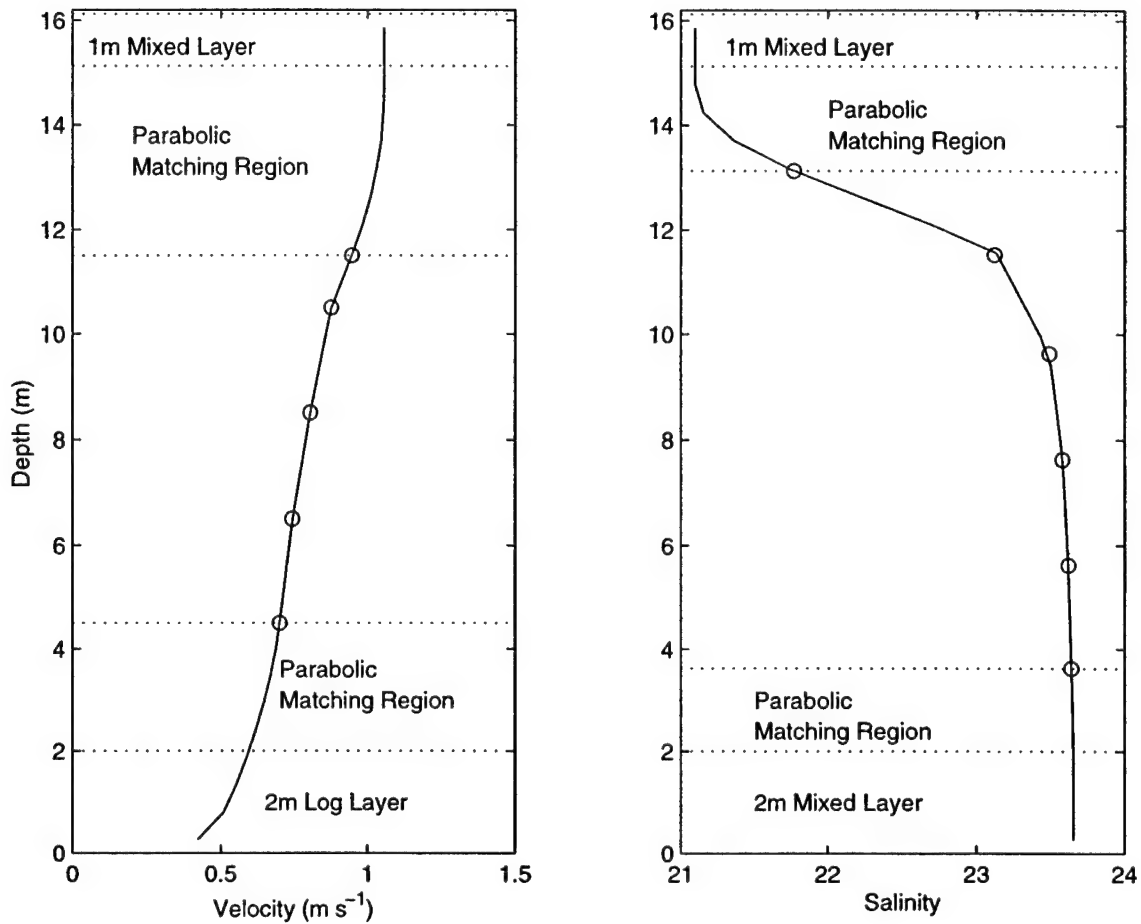
Figure 1: Extrapolations of velocity and salinity profiles are made using a one meter surface layer well-mixed in both salt and momentum. A two meter well-mixed layer is used to extrapolate salinity to the bottom. Velocity is extrapolated with a log layer in the lower two meters. Parabolas are used to join the mixed layers to the observations.

layer.

The estimates of upper and lower boundary layers from the CTD casts are also used to extrapolate the velocity profiles. Although shipboard ADCP profiles were taken, they do not measurements two meters from the surface or bottom. The estimates of upper and lower boundary layers from the CTD casts are used to extrapolate the velocity profiles. Velocity is assumed to be constant in an upper mixed layer of the same depth as salinity. A parabola is fit between a surface layer of constant

velocity of one meter thick and the uppermost velocity measurement. The parabola is constrained by matching the shear of the uppermost velocity measurements and no shear at the base of the surface layer.

Near-bottom velocity is assumed to have a log layer structure with the top of the log layer coinciding with the top of the salinity mixed layer two meters above bottom. A parabola is used to fit between the top of the log layer and the lowest velocity measurement. The parabola is constrained by matching the bottommost observed shear and the shear at the top of the log layer. A z_0 of 1 cm^{-1} is used to determine the log layer. The second free parameter, u_*, is found by iterating to match the the shear at the bottom of the parabolic layer. The iteration converges quickly to a high degree of accuracy.

B.3 Estimated uncertainty of salt transport at the central site

Error estimates for the estuarine and oscillatory salt transport are evaluated by using measurement errors, extrapolation errors, and the error due to the 150 meter separation between the velocity and salinity measurements. The greatest source of error in determining salt flux is from the surface extrapolations of the velocity and salinity profiles.

Errors are estimated for each velocity and salinity profile as follows. In the mid water column the error in each velocity measurement is estimated as 0.03m s^{-1} due to the zig-zag structure that appears to be an artifact of internal sampling in the ADCP (T. Chereskin, personal communication). Error on salinity estimates from observed conductivity and temperature is approximately 0.1 psu, primarily due to the conductivity fouling correction (as described in section 3.2.1). CTD casts show little salinity structure below the lowest temperature/conductivity sensor. In

many cases, the boundary layer extends above the lowest instrument. The error of the bottom extrapolated salinity is assumed to be equal to the error of the lowest salinity estimate. The zig-zag structure in the velocity estimates increases at the bottom of the profiles and modulates with the flow speed. The error of the velocity extrapolations is taken to be the larger of either 10% of the flow speed or 0.03 m s^{-1}.

Errors in the surface extrapolations of salinity are estimated by comparing near surface salinities from the extrapolations with those from shipboard CTD casts. From these comparisons, error is estimated at 0.5 psu during spring tides, 1 psu during the first apogean neap tides, and 1.5 psu during the second and third apogean neap tides when the uppermost conductivity sensor was fouled. Errors in the extrapolated velocities are estimated by examining the range of error produced by varying the upper mixed layer depth over the range of depths observed in the CTD casts. Near surface errors are approximately 0.1 m s^{-1} during both neaps and springs.

The error in estuarine salt transport is estimated from the error of the product of residual velocity and salinity. Residual velocity and salinity at each depth are assumed to have the same error as each profile. The error in the product of the residual velocity and salinity is estimated by propagating error, assuming that errors are uncorrelated everywhere except the upper water column. Complete correlation is assumed in the upper water column because the extrapolations use the same mixed layer depth for both salinity and velocity. The error in the depth-averaged estuarine salt transport is found assuming errors of the estuarine salt transport in the lower water column are uncorrelated and errors in the upper extrapolated region are completely correlated. Figure A.2 shows the depth-averaged estuarine salt transport at the mooring with the error. The estuarine salt transport is not significantly different from zero during spring tides when the residual circulation and stratification are small. Error is approximately 50% during neap tides.

The error in oscillatory salt transport is estimated by finding the error in the
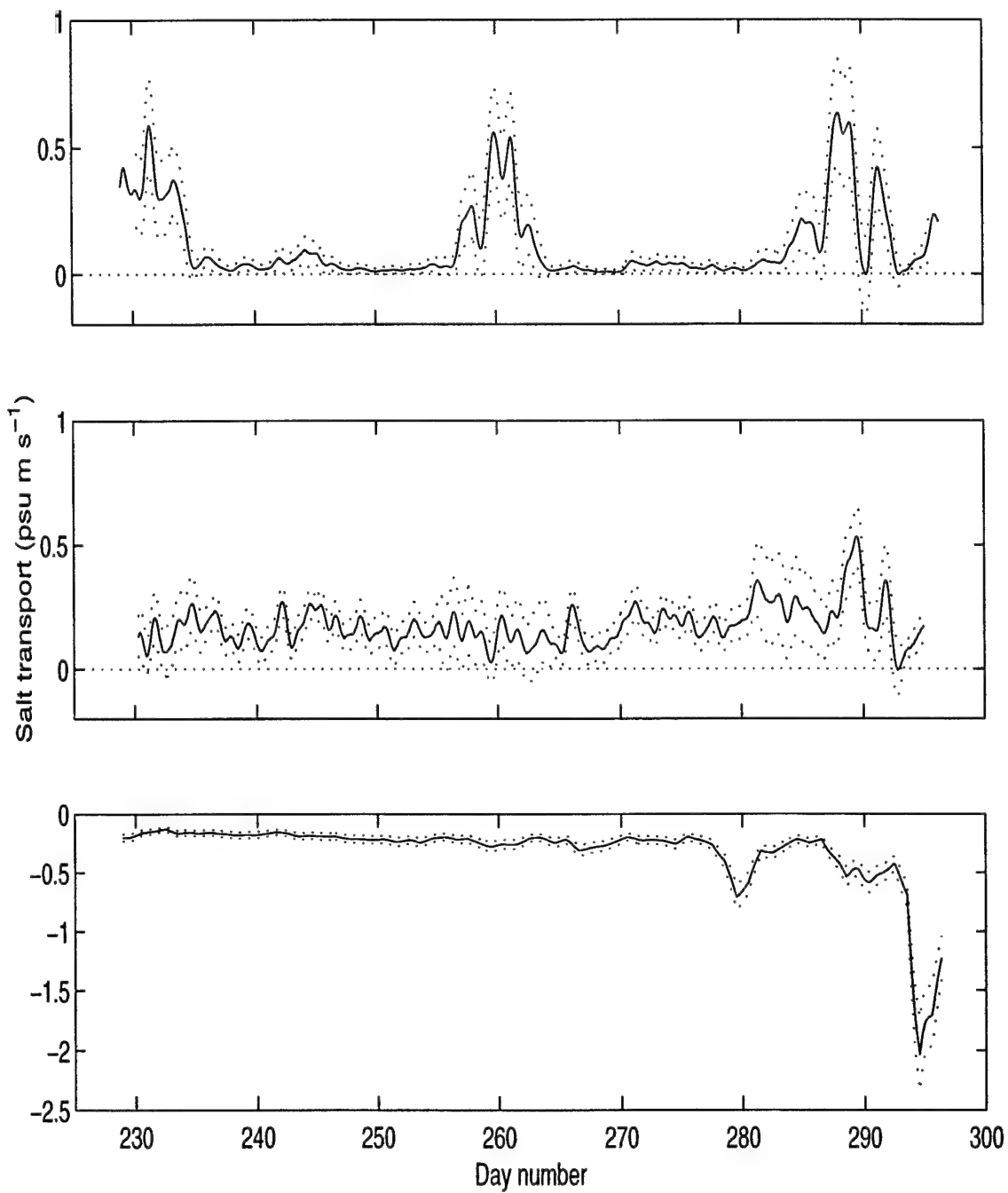
158

Figure 2: a. Depth-averaged estuarine salt transport at the central site and error. b. Depth-averaged oscillatory salt transport at the central site and error. c. Salt transport due to the net outflow at the central cross section and error.

covariance of the tidal velocity and salinity. Errors in the tidal fluctuations are assumed equal to the errors in the individual profiles. Error is propagated when multiplying the tidal fields and filtering over a tidal cycle, assuming complete correlation in the upper part of the water column.

An additional source of error comes from the separation of the moored ADCP and central mooring. Shipboard measurements showed that the magnitude of tidal velocity and salinity are comparable between the two sites. However, differences in tidal phase between the sites could not be measured accurately enough to provide an error estimate. A phase error of less than 2° was found from the spatial gradients of the tidal fields in a three-dimensional model of the Hudson Estuary [.Geyer Kineke.]. Figure A.2 shows the oscillatory salt transport and estimated error. Errors are largest during the second and third apogean neap tides when the salinity structure is less certain. Errors during spring tides are about 35%. Error during neap tides are considerably larger, about 80%-100%, due to the difficulties estimating tidal salinity in the upper part of the water column.

B.4 Estimated uncertainty of salt transport due to the net flow

Error estimating salt transport due to the net flow are from the estimate of cross sectional salinity and from the measurements of the net flow through the estuary. Salinity at the cross section is estimated assuming salinity at each depth is constant across the section. Shipboard estimates of the cross sectional average of salinity suggest that it is within 10% of the estimate from the mooring.

The errors in the measurements of net flow are made based on rough estimates of evaporation (2% of drought flow) and withdrawal and sewage discharge (5% of drought flow). Error was estimated at 15% of the salt transport with 5% from

salinity estimate and 10% from the discharge estimate. Figure A.2 shows the salt transport due to the net flow and estimated error.

Bibliography

Abood, K. A., 1974: Circulation in the Hudson Estuary. *Ann. N.Y. Acad. Sci.*, **250**, 39–111.

Blumberg, A. F., and G. L. Mellor, 1987: A description of a three-dimensional coastal ocean circulation model. *Three dimensional coastal ocean models*, N. S. Heaps, Ed., American Geophysical Union, Washington D.C., 1–16.

Chatwin, P. C., 1975: On the longitudinal dispersion of passive contaminant in oscillatory flows in tubes. *J. Fluid Mech.*, **71(3)**, 513–527.

Chatwin, P. C., 1976: Some remarks on the maintenance of the salinity distribution in estuaries. *Estuarine Coastal Mar. Sci.*, **4**, 555–566.

Coch, N. K., and H. J. Bokuniewicz, 1986: Oceanographic and geologicl framework of the Hudson system. *Northeastern Geology*, **8**, 96–108.

Dronkers, J., and J. van de Kreeke, 1986: Experimental determination of salt intrusion mechanisms in the Volkerak estuary. *Netherlands Journal of Sea Research*, **20(1)**, 1–19.

Dyer, K. R., 1973: *Estuaries: A Physical Introduction*. Wiley, London.

Festa, J. F., and D. V. Hansen, 1976: A two-dimensional numerical model of estuarine circulation: the effects of altering depth and river discharge. *Estuarine Coastal Mar. Sci.*, **4**, 309–323.

Fischer, H. B., 1974: Discussion of "Minimum length of the salinity intrusion in estuaries". *J. Hydraul. Div. Proc. ASCE*, **100**, 708–712.

Fischer, H. B., 1972: Mass transport mechanisms in partially mixed estuaries. *J. Fluid Mech.*, **53(4)**, 671–687.

Fischer, H. B., 1976: Mixing and dispersion in estuaries. *Annual review of Fluid Mechanics*, **8**, 107–133.

Fischer, H. B., E. J. List, R. C. Y. Koh, J. Imberger and N. H. Brooks, 1979: *Mixing in Inland and Coastal Waters*. Academic Press, San Diego.

Fredericks, J. J., J. H. Trowbridge, W. R. Geyer, A. J. Williams, M. Bowen and J. Woodruff, August, 1998: Stress, salt flux, and dynamics of a partially mixed estuary. Tech. Rept. WHOI-98-17, Woods Hole Oceanographic Institution.

Friedrichs, C. T., and J. M. Hamrick, 1996: Effects of channel geometry on cross sectional variations in along channel velocity in partially stratified estuaries. *Buoyancy Effects on Estuarine and Coastal Dynamics*, D. G. Aubrey, Ed., American Geophysical Union, Washington D.C.

Galperin, B., L. H. Kantha, S. Hassid and A. Rosati, 1988: A quasi-equilibrium turbulent energy model for geophysical flows. *J. Atmos. Sci.*, **45(1)**, 55–62.

Garvine, R. W., R. K. McCarthy and K-C. Wong, 1992: The axial salinity distribution in the Delaware Estuary and its weak response to river discharge. *Estuarine Coastal Shelf. Sci.*, **35**, 157–165.

Geyer, W. R., and G. A. Cannon, 1982: Sill processes related to deep water renewal. *J. Geophys. Res.*, **87**, 7985–7996.

Geyer, W. R., and H. M. Nepf, 1996: Tidal pumping of salt in a moderately stratified estuary. *Coastal and Estuarine Studies*, **53**, 213–226.

Geyer, W. R., and R. P. Signell, 1992: A reassessment of the role of tidal dispersion in estuaries and bays. *Estuaries*, **15(2)**, 97–108.

Geyer, W. R., R. P. Signell and G. C. Kineke, 1998: Lateral trapping of sediment in a partially mixed estuary. *8th International Biennial Conference on Physics of Estuaries and Coastal Seas, 1996*, A. A. Balkema, Rotterdam, 115–126.

Geyer, W. R., J. H. Trowbridge and M. M. Bowen, 1999: The dynamics of a partially mixed estuary. *J. Geophys. Res.*, In Press.

Godfrey, J. S., 1980: A numerical model of the James River Estuary, Virginia, U.S.A. . *Estuarine Coastal Mar. Sci.*, **11**, 295–310.

Haas, L. W., 1977: The effect of the spring-neap tidal cycle on the vertical structure of the James, York and Rappahannock Rivers, Virginia, U.S.A.. *Estuarine Coastal Mar. Sci.*, **5**, 485–496.

Hansen, D. V., and M. Rattray, 1965: Gravitational circulation in straits and estuaries. *J. Marine Res.*, **23(2)**, 104–122.

Hansen, D. V., and M. Rattray, 1966: New dimensions in estuary classification. *Limnology and Oceanography*, **11(3)**, 319–325.

Heathershaw, A. D., 1979: The turbulent structure of the bottom boundary layer in a tidal current. *Geophys. J. R. astr. Soc.*, **58**, 395–430.

Hunkins, K., 1981: Salt dispersion in the Hudson Estuary. *J. Phys. Oceanogr.*, **11**, 729–738.

Hyer, P. V., and E. P. Ruzecki, 1974: Changes in salinity structure of the James, York and Rappahannock estuaies resulting from the effects of Tropical Storm Agnes. *The effects of Tropical Storm Agnes on the Chesapeake Bay Estuarine System*, J. Davis, Ed., Johns Hopkins University Press, Baltimore, A39–A76.

Ianniello, J. P., 1979: Tidally induced residual currents in estuaries of variable breadth and depth. *J. Phys. Oceanogr.*, **9**, 962–974.

Jay, D. A., W. R. Geyer, R. J. Uncles, J. Vallino, J. Largier and W. R. Boynton, 1997: A review of recent developments in estuarine scalar flux estimation. *Estuaries*, **20**(2), 262–280.

Jay, D. A., and J. D. Musiak, 1996: Internal tidal asymmetry in channel flows: origins and consequences. *Mixing in Estuaries and Coastal Seas*, C. Pattiaratchi, Ed., American Geophysical Union, Washington D.C., 211–249.

Jay, D. A., and J. D. Smith, 1990: Circulation, density distribution and neap-spring transitions in the Columbia River Estuary. *Prog. Oceanog.*, **25**, 81–112.

Kennish, M. J., 1986: *Ecology of Estuaries*. CRC Press, Boca Raton.

Ketchum, B. J., Ed., 1983: *Estuaries and Enclosed Seas*. Elsevier Scientific, Amsterdam.

Knudsen, M., 1900: Ein hydrographische Lehrsatz. *Annalen der Hydr. und Mar. Met.*, **28**, 316–320.

Kranenburg, C., 1986: A time scale for long-term salt intrusion in well-mixed estuaries. *J. Phys. Oceanogr.*, **16**, 1329–1331.

van de Kreeke, J., 1990: Longitudinal dispersion of salt in the Volkerak Estuary. *Residual Currents and Lon-term Transport*, R. T. Cheng, Ed., Springer-Verlag, New York, 151–164.

Larsen, L. H., 1977: Dispersion of a passive contaminant in oscillatory fluid flows. *J. Phys. Oceanogr.*, **7**, 928–931.

Lewis, R. E., and J. O. Lewis, 1983: The principal factors contributing to the flux of salt in a narrow, partially stratified estuary. *Estuarine Coastal Mar. Sci.*, **16**, 599–626.

Limeburner, R., 1985: CODE-2: Moored array and large-scale data report. Tech. Rept. WHOI-85-35, Woods Hole Oceanographic Institution.

Linden, P. F., and J. E. Simpson, 1988: Modulated mixing and frontogenesis in shallow seas and estuaries. *Continental Shelf Research*, **8(10)**, 1107–1127.

MacCready, P., 1999: Estuarine adjustment to changes in river flow and tidal mixing. *J. Phys. Oceanogr.*, **29**, 708–726.

Mellor, G. L., and T. Yamada, 1982: Development of a turbulence closure model for geophysical fluid problems. *Reviews of Geophy. and Space Phys.*, **20**(4), 851–875.

Monismith, S., J. R. Burau and M. Stacey, 1996: Stratification dynamics and gravitational circulation in northern San Francisco Bay. *San Francisco Bay, the Ecosystem*, J. T. Hollibaugh, Ed., AAAS Press, Washington D.C., 123–153.

Neilson, B. J., and L. E. Cronin, Eds., 1981: *Estuaries and Nutrients*. Humana Press, Clifton.

Nepf, H. M., and W. R. Geyer, 1996: Intratidal variations in stratification and mixing in the Hudson Estuary. *J. Geophys. Res.*, **101**(C5), 12079–12086.

Nunes, R. A., and J. H. Simpson, 1985: Axial convergence in a well-mixed estuary. *Estuarine Coastal Shelf. Sci.*, **20**, 637–649.

Nunes, R. A., and G. W. Lennon, 1987: Episodic stratification and gravity currents in a marine environment of modulated turbulence. *J. Geophys. Res.*, **92(C5)**, 5465–5480.

Nunes Vaz, R., G. W. Lennon and J. R. deS. Samarasinghe, 1989: The negative role of turbulence in estuarine mass transport. *Estuarine Coastal Shelf. Sci.*, **28**, 361–377.

Nunes Vaz, R. A., 1990: Periodic stratification in coastal waters. *Modeling Marine Systems*, A. M. Davies, Ed., CRC Press, Boca Raton, 69–105.

Nunes Vaz, R. A., and J. H. Simpson, 1994: Turbulence closure modeling of estuarine stratification. *J. Geophys. Res.*, **99(C8)**, 16143–16160.

Oey, L. -Y., G. L. Mellor and R. I. Hires, 1985: A three-dimensional simulation of the Hudson-Raritan Estuary. Part III: Salt flux analyses. *J. Phys. Oceanogr.*, **15**, 1711–1720.

Officer, C. B., 1976: *Physical oceanography of estuaries and associated coastal waters*. John Wiley, New York.

Okubo, A., 1973: Effect of shoreline irregularities on streamwise dispersion in estuaries and other embayments. *Netherlands Journal of Sea Research*, **6**, 213–224.

Ou, H. W., C. Dong and D. Chen, 1999: Can property flux induced by tides be counter-gradient? . *J. Phys. Oceanogr.*, In Press.

Park, K., and A. Y. Kuo, 1996: Effect of variation in vertical mixing on residual circulation in narrow, weakly nonlinear estuaries. *Buoyancy Effects on Estuarine and Coastal Dynamics*, D. G. Aubrey, Ed., American Geophysical Union, Washington D.C., 301–317.

Peters, H., 1997: Observations of stratified turbulent mixing in an estuary. Neap-to-spring variations during high river flow. *Estuarine Coastal Shelf. Sci.*, **45**, 69–88.

Peters, H., and R. Bokhorst, 1999: Microstructure observations of turbulent mixing in a partially mixed estuary, I: Dissipation rate. In press.

Posmentier, E. S., and J. M. Raymont, 1979: Variations of longitudinal diffusivity in the Hudson Estuary. *Estuarine Coastal Shelf. Sci.*, **8**, 555–564.

Prandle, D., 1985: On salinity regimes and the vertical structure of residual flows in narrow tidal estuaries. *Estuarine Coastal Shelf. Sci.*, **20**, 615–635.

Pritchard, D. W., 1954: A study of teh salt balance in a coastal plain estuary. *J. Marine Res.*, **13(1)**, 133–144.

Pritchard, D. W., 1956: The dynamic structure of a coastal plain estuary. *J. Marine Res.*, **15(1)**, 22–42.

Rigter, B. P., 1973: Minimum length of the salinity intrusion in estuaries. *J. Hydraul. Div. Proc. ASCE*, **99**, 1475–1496.

Savenije, H. H. G., 1993: Predictive model for salt intrusion in estuaries. *Journal of Hydrology*, **148**, 203–218.

Schijf, J. B., and J. C. Schönfeld, 1953: Theoretical considerations on the motion of salt and fresh water. *Proc. Minnesota Int. Hydraul. Conf.* , Minneapolis, Minnesota, 321–333.

Scott, C. F., 1994: A numerical study of the interaction of tidal oscillations and non-linearities in an estuary. *Estuarine Coastal Shelf. Sci.*, **39**, 477–496.

Sharples, J., J. H. Simpson and J. M. Brubaker, 1994: Observations and modelling of periodic stratification in the Upper York River Estuary, Virginia. *Estuarine Coastal Shelf. Sci.*, **38**, 301–312.

Simpson, J. H., J. Brown, J. Matthews and G. Allen, 1990: Tidal straining, density currents, and stirring in control of estuarine stratification. *Estuaries*, **13**(2), 125–132.

Simpson, J. H., W. R. Crawford, T. P. Rippeth, A. R. Campbell and J. V. S. Cheok, 1996: The vertical structure of turbulent dissipation in shelf seas. *J. Phys. Oceanogr.*, **26**, 1579–1590.

Simpson, J. H., and J. Sharples, 1991: Dynamically-active models in the prediction of estuarine stratification. *Dynamics and Exchanges in Estuaries and the Coastal Zone*, D. Prandle, Ed., Springer-Verlag, New York, 101–113.

Smith, R., 1980: Buoyancy effects upon longitudinal dispersion in wide well-mixed estuaries. *Philosophical Transactions of the Royal Society of London Series A*, **296**, 467–496.

Stacey, M. T., 1996: Turbulent Mixing and Residual Circulation in a Partially Stratified Estuary. PhD Thesis, Stanford University Press.

Stacey, M. T., S. G. Monismith and J. R. Bureau, 1999: Observations of turbulence in a partially stratified estuary. *J. Geophys. Res.*, In press.

Stommel, H., and H. G. Farmer, 1952: On the nature of estuarine circulation. References Nos. 52–51, 52–63, 52–88 , Woods Hole Oceanographic Institution.

Taylor, G. I., 1954: The dispersion of matter in turbulent flow through a pipe. *Pro. R. Soc. London Ser. A*, **223**, 446–468.

Thatcher, M. L., and D. R. F. Harlemann, 1981: Long-term salinity calculation in Delaware Estuary. *Journal of the Environmental Engineering Division*, **107(EE1)**, 11–27.

Trowbridge, J. H., W. R. Geyer, M. Bowen and A. J. Williams, 1999: Near-bottom turbulence measurements in a partially-mixed estuary: turbulent energy balance, velocity structure, and along-channel momentum balance.. *J. Geophys. Res.*, In Press.

Uncles, R. J., A. J. Bale, R. J. M. Howland, A. W. Morris and R. C. A. Elliot, 1983: Salinity of surface water in a partially-mixed estuary, and its dispersion at low run-off. *Oceanol. Acta*, **6**, 289–296.

Uncles, R. J., J. E. Ong and W. K. Gong, 1990: Observations and analysis of a stratification-destratification event in a tropical estuary. *Estuarine Coastal Shelf. Sci.*, **31**, 651–665 .

Uncles, R. J., and P. J. Radford, 1980: Seasonal and spring-neap tidal dependence of axial dispersion coefficients in the Severn–a wide, vertically mixed estuary. *J. Fluid Mech.*, **89(4)**, 703–726.

Uncles, R. J., and J. A. Stephens, 1996: Salt intrusion in the Tweed Estuary. *Estuarine Coastal Shelf. Sci.*, **43**, 271–293.

Wang, D. -P., and A. J. Elliott, 1978: Non-tidal variability in the Chesapeake Bay and Potomac River: evidence for non-local forcing. *J. Phys. Oceanogr.*, **8**, 225–232.

170

Wells, A. W., and J. R. Young, 1992: Long-term variability and predictability of Hudson River physical and chemical characteristics. *Estuarine Research in the 1980s*, C. L. Smith, Ed., S.U.N.Y. Press, Albany, 29–58.

West, J. R., and J. S. Mangat, 1986: Determination and prediction of longitudinal dispersion coefficients in a narrow, shallow estuary. *Estuarine Coastal and Shelf Science*, **22(2)**, 161–181.

Wong, K-C., 1994: On the nature of transverse variability in a coastal plain estuary. *J. Geophys. Res.*, **99**(C7), 14209–14222.

Young, W. R., P. B. Rhines and C. J. R. Garrett, 1982: Shear-flow dispersion, internal waves and horizontal mixing in the ocean. *J. Phys. Oceanogr.*, **12**, 515–527.

Zimmerman, J. T. F., 1978a: Topographic generation of residual circulation by oscillatory tidal currents . *Geophys. Astrophys. Fluid Dynam.*, **11**, 35–47.

Zimmerman, J. T. F., 1978b: Dispersion by tide-induced residual current vortices. *Hydrodynamics of Estuaries and Fjords*, J. C. J. Nihoul, Ed., Elsevier Scientific, Amsterdam, 207–216.

University of California, San Diego
SIO Library 0175C
9500 Gilman Drive
La Jolla, CA 92093-0175

Hancock Library of Biology & Oceanography
Alan Hancock Laboratory
University of Southern California
University Park
Los Angeles, CA 90089-0371

Gifts & Exchanges
Library
Bedford Institute of Oceanography
P.O. Box 1006
Dartmouth, NS B2Y 4 A2
CANADA

NOAA/EDIS Miami Library Center
4301 Rickenbacker Causeway
Miami, FL 33149

Research Library
U.S. Army Corps of Engineers
Waterways Experiment Station
3909 Halls Ferry Road
Vicksburg, MS 39180-6199

Institute of Geophysics
University of Hawaii
Library Room 252
2525 Correa Road
Honolulu, HI 96822

Marine Resources Information Center
Building E38-320
MIT
Cambridge, MA 02139

Library
Lamont-Doherty Geological Observatory
Columbia University
Palisades, NY 10964

Library
Serials Department
Oregon State University
Corvallis, OR 97331

Pell Marine Science Library
University of Rhode Island
Narragansett Bay Campus
Narragansett, RI 02882

Working Collection
Texas A&M University
Dept. of Oceanography
College Station, TX 77843

Fisheries-Oceanography Library
151 Oceanography Teaching Bldg.
University of Washington
Seattle, WA 98195

Library
R.S.M.A.S.
University of Miami
4600 Rickenbacker Causeway
Miami, FL 33149

Maury Oceanographic Library
Naval Oceanographic Office
Building 1003 South
1002 Balch Blvd.
Stennis Space Center, MS 39522-5001

Library
Institute of Ocean Sciences
P.O. Box 6000
Sidney, B.C. V8L 4B2
CANADA

National Oceanographic Library
Southampton Oceanography Centre
European Way
Southampton SO14 3ZH
UK

The Librarian
CSIRO Marine Laboratories
G.P.O. Box 1538
Hobart, Tasmania
AUSTRALIA 7001

Library
Proudman Oceanographic Laboratory
Bidston Observatory
Birkenhead
Merseyside L43 7 RA
UK

IFREMER
Centre de Brest
Service Documentation–Publications
BP 70 29280 PLOUZANE
FRANCE

50272-101

REPORT DOCUMENTATION PAGE	1. REPORT NO. MIT/WHOI 00-04	2.	3. Recipient's Accession No.
4. Title and Subtitle Mechanisms and Variability of Salt Transport in Partially-Stratified Estuaries			5. Report Date February 2000
			6.
7. Author(s) Melissa Marie Bowen			8. Performing Organization Rept. No.
9. Performing Organization Name and Address MIT/WHOI Joint Program in Oceanography/Applied Ocean Science & Engineering			10. Project/Task/Work Unit No. MIT/WHOI 00-04
			11. Contract(C) or Grant(G) No. OCE 94-15617 (C) N00014-97-1-0134 (G) NA46RG0470 HRF 006/96A
12. Sponsoring Organization Name and Address National Science Foundation Office of Naval Research Hudson River Foundation NOAA Sea Grant			13. Type of Report & Period Covered Ph.D. Thesis
			14.

15. Supplementary Notes

This thesis should be cited as: Melissa Marie Bowen, 2000. Mechanisms and Variability of Salt Transport in Partially-Stratified Estuaries. Ph.D. Thesis. MIT/WHOI, 00-04.

16. Abstract (Limit: 200 words)

The variability of salt transport determines the variation of the length of the salinity intrusion and the large-scale density gradient in an estuary. This thesis contains three studies that address salt transport and the salt balance. The variation of salt transport with the depth, the along-channel salinity gradient, and the amplitude of the tidal velocity is investigated with analytic and numerical models. The results indicate that salt transport increases dramatically during stratified periods when vertical mixing is weak. Analysis of salt transport from observations in the Hudson Estuary show that stratified periods with elevated estuarine salt transport occur in five-day intervals once a month during apogean neap tides. Oscillatory salt transport, which is hypothesized to be primarily caused by lateral exchange and mixing of salt, appears to play a more minor role in the salt balance of the estuary. The salt balance of the estuary adjusts very little to the spring-neap modulation of salt transport but adjusts rapidly to pulses of freshwater flow. A simple model is used to investigate the process and time scales of adjustment of the salt balance by connecting variations of salt transport to the variations of freshwater flow and vertical mixing. The results show the length of the salinity intrusion adjust via advection to rapid and large increases in freshwater flow. The salinity intrusion adjusts more rapidly to the spring-neap cycle of tidal mixing the higher the freshwater flow.

17. Document Analysis   a. Descriptors

salt transport
salt balance
salinity intrusion

b. Identifiers/Open-Ended Terms

c. COSATI Field/Group

18. Availability Statement Approved for publication; distribution unlimited.	19. Security Class (This Report) UNCLASSIFIED	21. No. of Pages 172
	20. Security Class (This Page)	22. Price

(See ANSI-Z39.18)   *See Instructions on Reverse*   OPTIONAL FORM 272 (4-77)
(Formerly NTIS-35)
Department of Commerce